Fluid‐Rock Interaction and Formation of Granulites in the Gondwana Collisional Orogen

January 2017

Takahiro ENDO

Fluid‐Rock Interaction and Formation of Granulites in the Gondwana Collisional Orogen

A Dissertation Submitted to
the Graduate School of Life and Environmental Sciences,
the University of Tsukuba
in Partial Fulfillment of the Requirements
for the Degree of Doctor of Philosophy in Science
(Doctoral Program in Earth Evolution Sciences)

Takahiro ENDO

Contents

ABSTRACT

Granulite-facies rocks are regarded as one of the fundamental components of the lower crust. It is generally known that fluids associated with granulite formation probably control various lower-crustal processes such as progress of dehydration/hydration reactions, stability of mineral assemblages, partial melting, material circulation, and high-temperature metasomatism. Characterization of deep-crustal fluid and its interaction process with granulites is therefore a key to understand the evolution of continental crust in convergent plate margins. This study particularly focuses on petrogenesis of charnockites (orthopyroxene-bearing granitoids) in various localities because its petrogenesis is closely related to fluid-rock interaction in lower crust.

Dark brownish to grayish irregular patches and lenses of charnockite occur within orthopyroxene-free leucocratic biotite ± hornblende orthogneiss from Ginikarawa in the Wanni complex, Sri Lanka. The application of mineral equilibrium modeling to constrain the conditions of incipient-charnockite formation defines a *P–T* range of 3.0-3.7 kbar and 740-790°C at relatively low H_2O activity ($a(H_2O)$) condition of 0.46. The estimated *P–T* condition is lower than the available peak metamorphic condition of the Wanni Complex (~850°C and ~7 kbar), which confirmed that incipient-charnockite formation at Ginikarawa is a post-peak retrograde event possibly related to local infiltration of low-$a(H_2O)$ and CO_2-bearing fluid.

Incipient charnockite from Ambodin Ifandana area in the Ikalamavony Sub-domain of south-central Madagascar occurs as patches, lenses, and layers in migmatitic biotite gneiss. Lenses and layers of calc-silicate rocks are closely associated with the charnockite. The application of mineral equilibrium modeling and fluid inclusion study on charnockite to

constrain the conditions of incipient-charnockite formation defines a *P-T* range of 840°C/4.5 kbar to 880°C/10.5 kbar, which is nearly consistent with the inferred peak *P-T* condition of the Ikalamavony Sub-domain. The modeling also demonstrated that charnockite is stable under relatively low $a(H_2O)$ condition of 0.42-0.43 similar to that of Ginikarawa. The dominant occurrence of CO_2-rich fluid inclusions in the contact charnockite suggests that the dehydration was caused by decarbonation of calc-silicate rocks during the initial stage of decompression slightly after the peak metamorphism. The calc-silicate rocks might have also behaved as a cap rock that trapped CO_2 infiltrated from external sources. 'CO_2-rich fluid ponds' formed beneath calc-silicate rocks could have produced layers of charnockite.

The dominant lithologies of the studied locality near Nuliyam in the Trivandrum Block, southern India, are greenish to leucocratic quartzo-feldspathic rock, garnet-biotite gneiss, and incipient charnockite which are closely associated with calc-silicate rocks. The peak condition of ~900°C and the graphite precipitated at <400°C were obtained based on ternary-feldspar and graphite geothermometers, respectively. The petrographical and mineral chemical characters of clinopyroxenes and amphiboles suggest two-stage infiltrations of fluorine and chlorine-bearing hydrous fluids. The fluid inclusion study reveals the presence of various types of fluid composed of H_2O, CO_2, N_2, and CH_4, which also implies several different sources of the fluids. Various types of fluid inclusions and unaltered calc-silicate enclave confirmed the role of calc-silicate rocks as an impervious cap rock against CO_2. The results of this study therefore suggest that the incipient-charnockite formation of Nuliyam area is derived by infiltration of carbonic fluid from external sources.

The results of this study suggest metamorphic fluids played an important role on the stability of minerals during prograde to retrograde stages in all the studied localities from the Gondwana collisional orogeny, which is consistent with abundant occurrence of incipient

charnockite in this region. Such CO_2-bearing fluid might have derived from decarbonation of deeply-subducted carbonates during Gondwana amalgamation or degassing of sub-lithospheric mantle related post-peak slab break-off. The Gondwana collisional orogen is thus considered to have experienced significant effect of CO_2-bearing metamorphism and dehydration throughout burial and exhumation stage of the orogeny.

Keywords: incipient charnockite; pseudosection; fluid inclusion; CO_2 metasomatism; Gondwana

List of Figures

List of Tables

CHAPTER 1

General introduction

Granulite-facies metamorphism is known as the highest temperature classification in metamorphism (e.g., Spear, 1993). Today, over 90 granulite terranes or occurrences were reported in the world including reports of ultra high-temperature localities showing metamorphic temperatures over 900°C (see Harley et al. (1989), Kelsey (2008), and references therein). Such high-grade metamorphic rocks are important as one of the fundamental components of the lower crust, and its petrogenesis is often closely associated with metamorphic fluids (e.g., Newton et al., 1980). Recent development of the mineral equilibrium modeling in addition to conventional geothermobarometry and petrogenetic grid techniques, for example Perple_X (Connolly and Petrini, 2002), THERIAK-DOMINO (de Capitani and Petrakakis, 2010), and THERMOCALC (Holland and Powell, 1998a), contributes evaluation of integrated pressure, temperature, and chemical conditions and cross-checked *P*-*T* path for high-grade metamorphism.

This study particularly focuses on petrogenesis of charnockites (orthopyroxene-bearing granitoids) in various localities because the evolution of the rocks is closely related to fluid-rock interaction in lower crust (e.g., Janardhan et al., 1979; Newton et al., 1980; Rajesh and Santosh, 2012; Touret and Huizenga, 2011). Charnockite has been reported from many high-grade metamorphic terranes worldwide since its first discovery from Pallavaram Hills in the Madras Block of southern India by Holland (1900) (e.g., Rajesh and Santosh, 2012, and references therein). It commonly occurs as large massive bodies as “massive charnockite” probably formed by dry magmatism and/or regional high-grade metamorphism. On the other hand, Pichamuthu (1960) reported dark veins and irregular patches of charnockite within granitic amphibole-biotite gneiss from a quarry near Kabbal village, Karnataka State in the Archean Dharwar Craton of southern India, and attributed the presence of orthopyroxene to localized prograde metamorphism in granulite facies as “charnockite in the making”. Although some

earlier studies on this quarry argued that the charnockite patches are product of retrograde hydration from a widespread granulite (Devaraju and Sadashivaiah, 1969; Ray, 1972), many later studies confirmed that they are products of localized prograde metamorphism as inferred by Pichamuthu (1960) (e.g., Ramiengar et al., 1978; Janardhan et al., 1979, 1982; Srikantappa et al., 1985; Hansen et al., 1987; Stähle et al., 1987; Santosh et al., 1990, 1991, 1992; Raith and Srikantappa, 1993; Yoshida and Santosh, 1994; Endo et al., 2012, 2013, Newton and Tsunogae, 2014, among others). Such "incipient" or "arrested" charnockite patches have been found in many high-grade metamorphic terranes, particularly in southern India (e.g., Pichamuthu, 1960; Srikantappa et al., 1985; Hansen, et al. 1987; Santosh et al., 1990; Rajesh et al., 2011; Endo et al., 2012, 2013; Newton and Tsunogae, 2014, and many others), Sri Lanka (e.g., Hansen, et al. 1987; Hiroi et al., 1990; Milisenda et al., 1991; Perchuk et al., 2000), and Madagascar (Rakotondrazafy et al., 2007; Nédélec et al., 2014), which correspond to the central part of the East African – Antarctic Orogenic Belt formed by continent-continent collision related to the assembly of the Gondwana Supercontinent during Neoproterozoic to Cambrian (e.g., Meert and Voo, 1997; Jacobs and Thomas, 2004; Collins and Pisarevsky, 2005). Incipient charnockite is also reported from other granulite terranes such as SW Greenland (McGregor and Friend, 1992), the Lake Baikal region of Siberia (Hopgood and Bowes, 1990), North China Block (Yang et al., 2014), and the Limpopo Belt of South Africa (van Reenen et al., 1988), varying in age from Neoarchean to Paleoproterozoic. Detailed petrological investigations of incipient-charnockite patches and/or veins within amphibolite-facies gneiss/migmatite therefore provide important insights into formation of granulites in lower to middle crust.

The petrogenesis of incipient charnockite is still controversial, but many previous studies invoked the passage of low-H_2O activity (aH_2O) fluid along structural pathways within upper amphibolite-facies gneisses stabilized orthopyroxene through breakdown of biotite as

open-system metasomatic processes (e.g., Janardhan et al., 1982; Newton et al., 1980; Hansen et al., 1987; Santosh et al., 1990; Newton, 1992; among others). However, the origin of such anhydrous fluid and the mechanism of its infiltration are still not known. This study thus performs detailed investigations of incipient charnockite from three different localities in Gondwana fragments based on petrography, mineral chemistry, geothermobarometry, phase equilibrium modeling, and fluid inclusion microthermometry. The first locality in the Wanni complex, Sri Lanka, exposes typical patches of incipient charnockite in amphibolite-facies gneiss. The second locality in the Ikalamavony sub-domain, south-central Madagascar, is composed of incipient charnockite closely associated with calc-silicate rocks within migmatitic biotite gneiss. The last locality in the Trivandrum Block, southern India, is also composed of quartzo-feldspathic gneiss and calc-silicate rock, but the rocks probably underwent the influence of infiltration of several different metamorphic fluids. This study further compares the results of these examples and discusses granulite-formation processes related to fluid-rock interaction in the Gondwana collisional orogen.

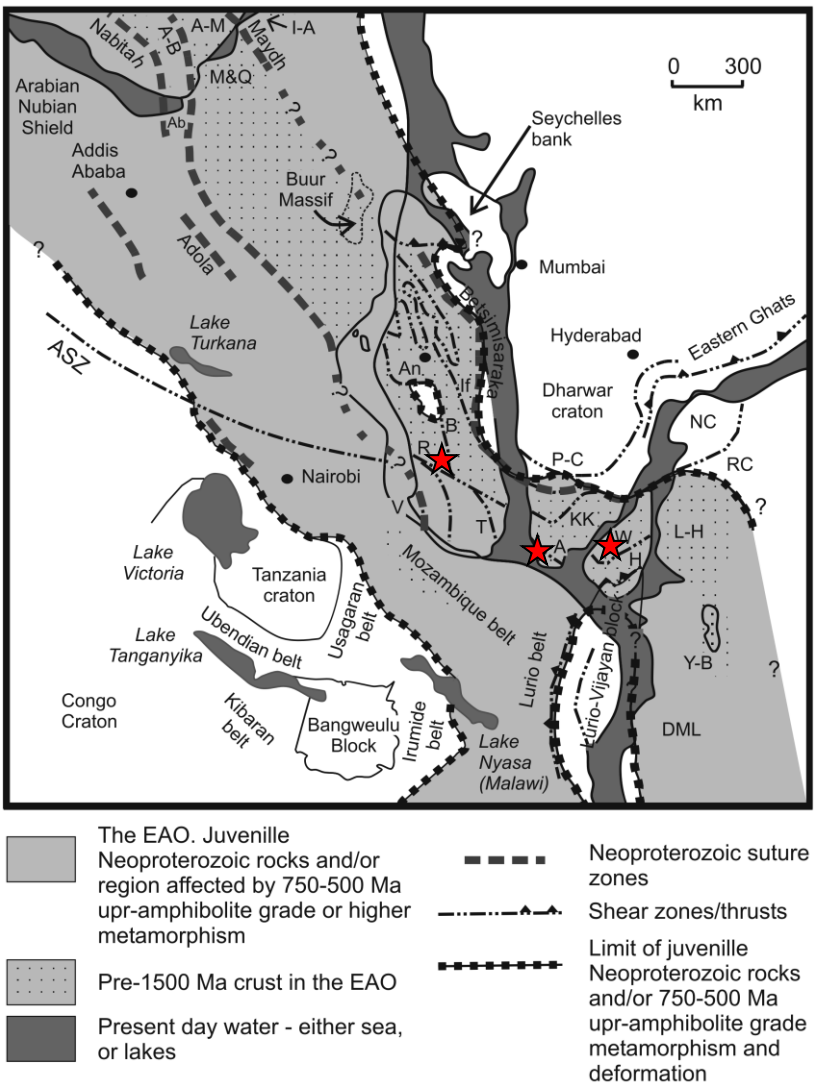

Fig. 1. Reconstruction of Gondwana supercontinent with the localities of samples (star) discussed in this study (after Collins and Windley, 2002). Ab = Abdulkadir terrane; A = Achankovil shear zone; A-B = Al-Bayda terrane; A-M = Al-Mahfid terrane; An = Antananarivo; ASZ = Aswa shear zone; DML = Dronning Maud Land; H = Highland Complex; I-A = Inda Ad Complex; If = Ifanadriana shear zone; KK = Karur-Kambam-Painavu-Trichur shear zone; L-H = Lützow-Holm Complex; M&Q = Mora and Qabri Bahar terrane; NC = Napier Complex; P-C = Palghat-Cauvery shear zone system; R = Ranotsara shear zone; RC = Rayner Complex; T = Tranomaro shear zone; V = Vohibory belt; W = Wanni Complex; Y-B = Yamato-Belgica complex; Betsimisaraka = Betsimisaraka suture.

CHAPTER 2

Formation of incipient charnockite from Ginikarawa in the Wanni Complex, Sri Lanka

2.1. Introduction

This chapter discusses petrogenesis of Kabbal-type orthocharnockite in the Wanni Complex, Sri Lanka. Hansen et al. (1987) divided incipient charnockites into two types based on mineralogy of host gneisses; "Kabbal type" in amphibole-biotite gneiss and "Ponmudi type" in garnet-biotite gneiss. Kabbal-type charnockite (or orthocharnockite) is tonalitic to granodioritic, and orthopyroxene in this type was formed by breakdown of calcic amphibole by dehydration reaction with biotite and quartz, whereas Ponmudi-type charnockite (or paracharnockite) is metapelitic, and its orthopyroxene formation involved the reaction of biotite, garnet, and quartz to orthopyroxene and K-feldspar. Newton and Tsunogae (2014) performed mass balance calculations for the two types, and concluded that the orthopyroxene formation in Kabbal type by breakdown reaction of hornblende with biotite accompanies loss of FeO, MgO, TiO_2, and CaO, as well as H_2O from the host rock, with concomitant gain of SiO_2. On the other hand, orthopyroxene in Ponmudi type derived through biotite breakdown with some involvement of garnet has been controlled by metasomatic alteration with loss of FeO and MgO and increase of SiO_2 and alkalis. Both the Kabbal- and Ponmudi-type alterations occurred at mid-crustal levels (5-6 kbar and 700-750°C).

The petrogenesis of incipient charnockite is still controversial, but many previous studies invoked the passage of low-H_2O activity (aH_2O) fluid along structural pathways within upper amphibolite-facies gneisses stabilized orthopyroxene through breakdown of biotite as open-system metasomatic processes (e.g., Janardhan et al., 1982; Newton et al., 1980; Hansen et al., 1987; Santosh et al., 1990; Newton, 1992; among others). In contrast, closed-system dehydration melting (Bhattacharya and Sen, 2000; Burton and O'Nions, 1990; Hiroi et al., 1990), open-system metasomatism and partial melting (Perchuk et al., 2000), and primary

bulk-chemical control (Endo et al., 2013) are also suggested for the origin of incipient charnockite. Previous fluid inclusion studies on incipient charnockite reported the occurrence of abundant CO_2-rich fluid inclusions (e.g., Hansen et al., 1984; Santosh et al., 1990; Perchuk et al., 2000; Tsunogae et al., 2008a, and many others), based on which they argued infiltration of CO_2-rich anhydrous fluids resulted in the lowering of water activity and stabilization of orthopyroxene-bearing dry assemblage in charnockite. Occurrence of abundant high-salinity aqueous fluid inclusions in orthopyroxene-bearing rocks could also play a role as charnockite-forming low-$a$$H_2O$ fluid (e.g., Knudsen and Lidwin, 1996; Perchuk et al., 2000).

Previous studies of incipient charnockites suggest that charnockite patches and host biotite gneisses have similar bulk-rock chemistry (e.g., Janardhan et al., 1982; Santosh et al., 1990; Endo et al., 2012), although some studies suggested decrease of FeO, CaO, MgO, TiO_2 and increase of SiO_2 from biotite gneiss to charnockite (e.g., Hansen et al., 1987; Stähle et al., 1987; Milisenda et al., 1991; Yoshida et al., 1991). Yoshida et al. (1991) reported that Ponmudi type is characterized by loss of Rb and Ba and enrichment of Ti, whereas Kabbal type shows marked LILE enrichment with gain of K_2O, Rb and Ba and loss of CaO. Stähle et al. (1987) and Endo et al. (2013) also reported elevated K_2O in charnockite. Several studies argued that the chemical variation is not a primary nature, but probably caused by fluid-rock interaction and metasomatism in granulite-facies condition (e.g., Perchuk et al., 2000; Newton and Tsunogae, 2014).

Recently Endo et al. (2013) applied phase equilibrium modeling technique to peak mineral assemblages in Ponmudi-type incipient charnockite and adjacent garnet-biotite gneiss from Mavadi in the Trivandrum Block of southern India in Na_2O-CaO-K_2O-FeO-MgO-Al_2O_3-SiO_2-H_2O-TiO_2-Fe_2O_3 (NCKFMASHTO) system. They confirmed that orthopyroxene-bearing mineral assemblage in the charnockite is stable at lower

molar H_2O ($M(H_2O)$) (<0.3 mol.%) than that of the host garnet-biotite gneiss (0.3 to 1.5 mol.%), which is consistent with the previous model of the formation of incipient charnockite. They also argued an alternative model that orthopyroxene is more stable than biotite in slightly K- and Fe-rich portion, suggesting that charnockitization is controlled by variations in local bulk-rock chemistry. Endo et al. (2012) also applied the technique on Ponmudi-type incipient charnockite from Rajapalaiyam in the Madurai Block, southern India, and inferred the infiltration of reduced fluid associated with incipient-charnockite formation.

This study reports new occurrence of incipient charnockites in a quarry near Kurunegala in the Wanni Complex, Sri Lanka, and present new mineralogical and petrological data on the incipient charnockite and surrounding orthopyroxene-free biotite gneiss. This study also applies mineral equilibrium modeling to evaluate the petrogenesis of the charnockite formation. This is the first attempt to apply this new technique on incipient charnockite in Sri Lanka, and the results evaluate the existing models on its petrogenesis.

2.2. Geological buckground

2.2.1. General geology of Sri Lanka

Sri Lanka is an integral component of the late Neoproterozoic Gondwana supercontinent where recent studies have revealed prominent Neoproterozoic tectono-thermal events (e.g., Santosh et al., 2012, 2014; He et al., 2016a,b). The basement rocks of Sri Lanka have been subdivided into four litho-tectonic units from west to east namely, Wanni Complex (WC), Kadugannawa Complex (KC), Highland Complex (HC) and Vijayan Complex (VC) mainly based on Nd-model ages (Cooray, 1994; Kröner et al., 1991; Milisenda et al., 1988, 1994;) (Fig. 2).

Among the four major tectonic units, the HC is regarded to be part of a supracrustal basin containing rocks metamorphosed under granulite grade including quartzites, marbles, calc-silicate rocks, pelitic gneisses, charnockites, meta-granitoids and granitic gneisses (Cooray, 1962, 1984, 1994; Mathavan and Fernando, 2001). The rocks in the WC were metamorphosed under upper amphibolite to granulite facies, the protoliths of which are mainly magmatic, with minor sedimentary units. Metamorphism under upper amphibolite-facies conditions is recorded in the VC and the dominant rock types include granitic gneisses, migmatites and hornblende-biotite gneisses with very limited metasediments (Kehelpannala, 1997; Mathavan et al., 1999; Kröner et al., 2013). The KC forms doubly plunging synforms containing rocks metamorphosed under upper amphibolite to granulite facies conditions (Kröner et al., 1991; Cooray, 1994) with hornblende-biotite gneisses and charnockites as the dominant rock types.

Classically, the HC has been interpreted as a tilted crustal section with a metamorphic gradient increasing from 4.5-6 kbar and 700-750°C in the southwest up to 8-9 kbar and 800-900°C in the east and southeast (Faulhaber and Raith, 1991; Schumacher and Faulhaber, 1994; Raase and Schenk, 1994; Mathavan et al., 1999; Kriegsman, 1995; Kriegsman and Schumacher, 1999; Braun and Kriegsman, 2003). In addition, rare UHT granulites that formed at extreme crustal conditions of T = 925-1150°C and P = 9-12.5 kbar have been reported from a few localities in the central and southwestern HC (e.g., Osanai, 1989; Osanai et al., 2000, Kriegsman and Schumacher, 1999; Osanai et al., 2006; Sajeev and Osanai, 2004a, 2004b; Sajeev et al., 2007; Dharmapriya et al., 2015).

The VC consists of microcline-bearing granitic gneisses, migmatites and hornblende-biotite gneisses with rare quartzites and calc-silicates (Kehelpannala, 1997; Mathavan et al., 1999; Kröner et al., 2013). The limited number of petrological studies on the VC revealed that the peak metamorphic temperature conditions are 750-850°C (Kleinschrodt et

al., 1991; Kleinschrodt, 1994).

The KC is interpreted as a layered intrusion within the WC (e.g., Kröner et al., 2003; Willbold et al., 2004) and is regarded as a part of the WC (e.g., Kehelpannala, 1997). However, Santosh et al. (2014) and He et al. (2016a) suggested that the KC is a disrupted huge magma chamber exposed at the eastern margin of the WC. In these models, it is proposed that the western suture between Wanni and Highland with Kadugannawa Complex to represent oceanic crust subduction westward (present co-ordinates) beneath the Wanni Complex (Santosh et al., 2014; He et al., 2016a). Lithological and geochronological equivalents of the Kadugannawa Complex have been found from the Lützow-Holm Bay in Antarctica implying that the KC is an extension of the Lützow-Holm Bay during the Gondwana (e.g., Tsunogae et al., 2015; He et al., 2016b).

2.2.2. Brief overview of geology of the Wanni Complex

The Wanni Complex (WC) occurs NW and W of the Highland Complex (HC) and is constituted of predominantly upper amphibolite- to granulite-facies meta-igneous gneisses and minor meta-sediments. The predominant meta-igneous rocks show a vast range of protolith chemistry from granitic, granodioritic, monzonitic, tonalitic, charnockitic and enderbitic compositions (e.g., Pohl and Emmermann, 1991). Garnet-sillimanite gneisses, cordierite gneisses, quartzites and calc-silicate rocks occur as minor meta-sediments, close to the inferred boundary with the HC and marble is absent in the WC. The western part of the WC is mainly composed of less-deformed granites, with an unmetamorphosed post-tectonic K-feldspar-rich granite at Tonigala (e.g., Hölzl et al., 1991, Cooray, 1994). Migmatization is also widely spread within the unit. The peak metamorphic conditions of the WC are estimated to be 700-830°C and 5-7 kbar

(Schenk et al., 1991; Raase and Schenk, 1994). The *P-T* conditions gradually increase towards the inferred tectonic contact with the HC. (Schenk et al., 1991; Faulhaber and Raith, 1991; Weerakoon et al., 2001; Santosh et al., 2014; He et al., 2016a).

Classical outcrops of in-situ/incipient charnockites (arrested charnockites) developed within the host amphibole-gneissic layering are found in the central regions of the WC. These in-situ charnockites show zones of amphibolite to granulite facies transition of foliated light gray hornblende-gneisses into dark, greenish-brown and coarse-grained charnockite along shear zones and foliation planes (e.g., Hansen et al. 1987; Burtton and O'Nions, 1990; Baur et al. 1991; Milisenda et al. 1991; Santosh et al. 1991; Kehelpannala, 1999; Perchuk et al. 2000). Further, the WC contains unmetamorphosed, post-tectonic (<500 Ma) granites at Tonigala and Galgamuwa (e.g., Cooray, 1984; Hölzl et al., 1991; Cooray, 1994) and carbonatite deposits at Eppawala and Kawisigamuwa (e.g., Weerakoon et al. 2001; Pitawala and Lottermose, 2012; Madugalla et al., 2014).

The WC is considered to represent a higher crustal level than that of the HC although there is no clear structural break between the rocks of the two complexes, and the contact between these two has been obliterated by later events (Voll and Kleinschrodt, 1991). Thus, the HC-WC boundary is merely an isotopic boundary (i.e. a boundary defined by contrasts in isotopic values) based on entirely a regional sampling set of Nd model ages, which is physically unrecognizable in the field. Lithologies along the most part and on either side of this so-called 'inferred boundary' are petrologically and structural geologically more or less comparable and therefore serves a poor guide to define an absolute crustal boundary.

2.2.3. Incipient charnockite in Sri Lanka

Hansen et al. (1987) reported Kabbal-type incipient charnockite patches within hornblende-biotite orthogneiss at Udadigana, Angangola, and Waraddana quarries in Kurunegala District, the Wanni Complex, and argued significant depletion in CaO, FeO, and MgO in charnockite compensated by SiO_2 and Na_2O enrichment. They also reported mixed CO_2-H_2O and CO_2 fluid inclusions most of which occur along planar arrays within quartz possibly as secondary inclusions.

Hiroi et al. (1990) examined field occurrence and petrography of incipient charnockite from quarries near Kurunegala and Kandy, and inferred the formation of charnockite through partial melting of original amphibolite-facies gneisses, although they did not provide direct evidence for partial melting. They further pointed out that charnockite formation is a post-peak event because of the occurrence of secondary andalusite associated with siderite and cordierite in other pelitic rocks, suggesting CO_2 infiltration and formation of orthopyroxene in charnockite is a later low-pressure event.

Milisenda et al. (1991) examined incipient charnockite at Angangala and showed lower bulk FeO, CaO, MgO and TiO_2 contents in charnockite than the host biotite-hornblende gneiss.

Yoshida and Santosh (1994) investigated incipient charnockites in southern India and Sri Lanka based on field occurrence, petrology, and fluid inclusions, and inferred infiltration of CO_2-rich fluids through faults and shears under brittle-quasi-brittle conditions gave rise to local desiccation and stabilization of orthopyroxene-bearing dry mineral assemblage in charnockite. They pointed out that incipient-charnockite formation postdates regional peak metamorphism, and the process can be correlated with the final stages of collisional orogens when the tectonic regime changed from compressional to extensional. They also inferred that post-tectonic alkaline intrusives could be a source of CO_2-rich fluid.

Perchuk et al. (2000) investigated reaction textures, fluid inclusions, and metasomatic zoning coupled with thermodynamic calculations of incipient charnockite in biotite–hornblende gneiss from Udadigana in Kurunegala. They reported brine and almost pure CO_2 fluid inclusions in charnockite, and inferred migration of such metasomatic fluid through the amphibolite-facies gneiss along shear zones under the peak metamorphic conditions of 700–750°C and 5–6 kbar with dry condition of $a(H_2O)$=0.52-0.59, which has given rise to the formation of incipient charnockite patches. They also reported several metasomatic zonation patterns around the patches, based on which they inferred partial melting in incipient-charnockite cores. The orthopyroxene-baring assemblage could have crystallized from a partial melt during cooling from 720 to 660°C at $a(H_2O)$=0.67 to 0.5, and formed late-stage minerals such as myrmekite, biotite, cummingtonite, and carbonates.

Newton and Tsunogae (2014) reported CO_2-rich fluid trapped as pseudosecondary inclusions within quartz in charnockite from Ginikarawa, the same sample discussed in this study. The inclusions show melting temperatures close to the triple point of pure CO_2 as −57.8 to −56.6°C, indicating lack of CH_4 and other miscible components, and homogenization temperatures of +29.6 to +30.9°C, suggesting entrapment of low-density near-pure CO_2 fluid.

3.3. Analytic methods

3.3.1. Petrology and mineral chemistry

Polished thin sections were prepared for petrographic study at the University of Tsukuba, Japan. Mineral chemical analyses were carried out using an electron microprobe analyzer (JEOL

JXA8530F) at the Chemical Analysis Division of the Research Facility Center for Science and Technology, the University of Tsukuba. The analyses were performed under conditions of 15 kV accelerating voltage and 10 nA sample current, and the data were regressed using an oxide-ZAF correction program supplied by JEOL. Representative compositions of minerals in the analyzed samples are given in Tables 2 and 3.

2.3.2. Mineral equilibrium modeling

Metamorphic *P-T* conditions of the stability of mineral assemblages in the charnockite and biotite gneiss from Kurunegala were constrained using THERMOCALC 3.33 (Powell and Holland, 1988, updated October 2009) with an updated version of the internally consistent data set of Holland and Powell (1998a; data set tcds55s, file created November 2003). Calculations were undertaken in the system Na_2O-CaO-K_2O-FeO-MgO-Al_2O_3-SiO_2-H_2O-TiO_2-Fe_2O_3 (NCKFMASHTO) (White et al., 2003, 2007), which provides a realistic approximation to model the examined rocks. The phases considered in the modeling and the corresponding *a-x* models used are garnet, biotite, and melt (White et al., 2007), plagioclase and K-feldspar (Holland and Powell, 2003), clinopyroxene (Green et al., 2007), amphibole (Diener and Powell, 2012), muscovite (Coggon and Holland, 2002), spinel and magnetite (White et al., 2002), ilmenite-hematite (White et al., 2000), cordierite, epidote, and fluid (Holland and Powell, 1998b), and dolomite (White et al., 2003). Quartz and H_2O are treated as pure end-member phases. For the analysis, slabs of relatively homogeneous part of the examined rocks were used for thin-section preparation, and the counterpart of the same slabs was used for chemical analysis. Bulk rock compositions for the rocks were determined by X-ray fluorescence spectroscopy at Activation Laboratories, Canada. Charnockite containing unaltered fresh

orthopyroxene (sample SL2-1D) is used for the modeling, and its chemical composition (in wt.%) is SiO_2 = 68.54, Al_2O_3 = 15.09, Fe_2O_3 = 0.53, FeO = 3.3, MgO = 0.96, MnO = 0.077, CaO = 2.42, Na_2O = 3.51, K_2O = 4.19, TiO_2 = 0.54, LOI = 0.69. The charnockite sample contains 0.18 wt.% P_2O_5, which is reflected in ~0.5 modal % of apatite. As this analysis neglects P_2O_5 from the system, the CaO content equivalent to apatite should be extracted from the calculation. The corrected CaO content (2.18 wt.%) is adopted for the pseudosection calculation.

2.4. Results

2.4.1. Petrography

The gneiss-incipient charnockite pairs examined in this study were collected from a previously unreported quarry near Ginikarawa (N07° 33' 40'', E80° 21' 08''), about 9 km north of Kurunegala. The locality exposes charnockites occurring within foliated orthopyroxene-free biotite ± hornblende orthogneiss (Fig. 3a). The host orthogneiss displays NNW-SSE-trending and sharply west-dipping foliation defined by alternation of leucocratic layers and biotite-rich gray layers (Fig. 3b). Irregular patches or lenses of dark grayish to brownish charnockite are present throughout the quarry (Fig. 3a). The size of the patches varies from 30 cm to up to 2 m. Although foliation is obvious in the host biotite-hornblende gneiss, it disappears while passing into the charnockite patches (Figs. 3c, d). Grain size of minerals is coarser in the charnockite than the host gneiss. These features are closely comparable with those displayed by many gneiss-incipient charnockite locations elsewhere in Sri Lanka (e.g., Hansen et al., 1987; Hiroi et al., 1990) and in southern India (e.g., Pichamuthu, 1960; Santosh et al., 1990; Raith and

Srikantappa, 1993; Endo et al., 2012, 2013). The charnockite patches in this quarry do not show any systematic distribution pattern, although a prominent structural control in incipient charnockite patches has been described in previous studies from other localities (e.g., Santosh et al., 1990; Raith and Srikantappa, 1993; Kehelpannala, 1999). Two representative samples (charnockite (sample SL2-1D) and biotite gneiss (sample SL2-1A)) collected from this quarry were examined in detail. A brief summary of the petrological features and mineral assemblages of the charnockite and biotite gneiss are given below. Mineral name abbreviations are after Kretz (1983).

2.4.1.1. Charnockite (sample SL2-1D)

The charnockite is composed mainly of quartz (30-40 %), K-feldspar (30-40 %), plagioclase (20-25 %), orthopyroxene (1-2 %) and biotite (1-2 %) with accessory apatite, zircon, magnetite and ilmenite (Figs. 4a and b). Ilmenite often contains thin lamellae of hematite, suggesting that hematite is a product of later exsolution. K-feldspar is subidioblastic, coarse grained (0.6-5.0 mm), and occurs mostly as perthite with thin exsolution lamellae of albite-rich plagioclase. Quartz (0.3-4.5 mm) and plagioclase (0.5-2.7 mm) are also coarse grained and scattered in the matrix. Plagioclase rarely shows antiperthitic texture. Orthopyroxene is coarse grained (3.0-6.0 mm), xenoblastic, and often weakly altered possibly due to later hydrothermal events or surface weathering, although unaltered fresh orthopyroxene is also present. Biotite is fine to medium grained (0.2-1.7 mm), xenoblastic, and often occurs as small flakes scattered in the matrix. Biotite also occurs as fine-grained aggregates with quartz along the grain boundaries of quartz and feldspars, or as biotite + quartz symplectite replacing orthopyroxene, which have been regarded as products of either retrograde hydration or as reactions with ferro-magnesian minerals and hydrous melt.

2.4.1.2. Biotite gneiss (sample SL2-1A)

The biotite gneiss is composed of quartz (30-40 %), K-feldspar (30-40 %), plagioclase (20-25 %), and biotite (4-5 %) with accessory apatite, zircon, magnetite and ilmenite (Figs. 4c and d). Ilmenite contains exsolution lamellae of hematite, similar to that in charnockite. Grain size of matrix subidioblastic quartz (0.3-2.0 mm) and plagioclase (0.8-1.9 mm) are smaller than those of charnockite, which is a common character of gneiss-incipient charnockite association, although the size of K-feldspar (1.1 mm-1.3 cm) and biotite (0.3-2.9 mm) in biotite gneiss is in turn coarser than those in charnockite. Biotite in the matrix occurs as subidioblastic and medium- to coarse-grained flakes associated with quartz and feldspars, and it is often rimed by symplectitic intergrowth of biotite + quartz ± plagioclase ± K-feldspar (Fig. 4e). This texture could have been formed by interaction of silicate melt and subsequent crystallization, or recrystallization through fluid infiltration. Charnockite also shows a similar texture of biotite + quartz, although it occurs only around orthopyroxene suggesting retrograde hydration. Calcic amphibole-bearing variety of biotite gneiss (Fig. 4f) principally shows the texture very similar to that of amphibole-free biotite gneiss.

2.4.2. Mineral chemistry

2.4.2.1. Orthopyroxene

Orthopyroxene in charnockite is Fe-rich as X_{Mg} = 0.43-0.44. Al content in the mineral is very low as 0.02-0.03 pfu (0.5-0.6 wt.%) (Table 2). These are common compositional characters of orthopyroxenes in Kabbal-type incipient charnockite (e.g., Perchuk et al., 2000).

2.4.2.2. Biotite

Biotite in charnockite is divided into two types; primary grains in matrix and secondary grains formed by hydration of orthopyroxene. The former is Fe-rich as X_{Mg} = 0.40-0.46 and its TiO_2 content is 2.6-5.1 wt.%, whereas the latter is more magnesian (X_{Mg} = 0.65-0.71) and its TiO_2 content is 3.1-3.8 wt.% (Table 2). Biotite in biotite gneiss is characterized by a homogeneous composition regardless of the occurrences as X_{Mg} = 0.44-0.46 and TiO_2 = 4.3-5.7 wt.%, which is nearly consistent with the composition of primary biotite in charnockite. Biotite in hornblende-bearing variety of biotite gneiss shows slightly higher X_{Mg} of 0.45-0.49 than that in hornblende-free biotite gneiss, although its TiO_2 content is similar (5.2-5.4 wt.%).

2.4.2.3. Feldspars

Plagioclase in charnockite shows nearly consistent albite-rich compositions of An_{25-26} without any core-rim variation (Table 2). That in biotite gneiss is slightly albite-rich as An_{17-23}. Composition of plagioclase in biotite-hornblende gneiss is nearly consistent with that in charnockite (An_{25-26}). K-feldspar in charnockite is orthoclase-rich as Or_{74-81}, whereas that in biotite gneiss and biotite-hornblende gneiss is more orthoclase-rich as Or_{88-91} and Or_{77-90}, respectively.

2.4.2.4. Calcic amphibole

Composition of calcic amphibole in biotite-hornblende gneiss is Fe-rich as X_{Mg} = 0.44-0.46 with Ti = 0.22-0.25 pfu, $(Na+K)_A$ = 0.48-0.67 pfu, and Si = 6.4-6.5 pfu (Table 3). It is classified mostly as ferro-edenite with minor ferro-pargasite and ferro-tschermakite components based on the classification of Leake et al. (1997).

2.4.3. Hornblende-plagioclase geothermometry

Petrographical observations of hornblende-bearing variety of matrix biotite gneiss suggest hornblende coexists with plagioclase; therefore we employ hornblende-plagioclase pair for geothermometry. Based on hornblende solid-solution models and well-constrained natural and experimental studies, two geothermometers were calibrated by Holland and Blundy (1994) for edenite-tremolite reaction, which is applicable to quartz-bearing rocks, and edenite-richterite reaction, which is applicable to both quartz-bearing and quartz-free rocks. As quartz is present in the gneiss sample, this study applied both the methods to calculate temperature of high-grade metamorphism. The calculated results are 740-790°C for edenite-tremolite reaction and 760-800°C for edenite-richterite reaction at a reference pressure of 7 kbar (which corresponds to approximate peak pressure of the Wanni Complex).

2.4.4. Mineral equilibrium modeling

Petrographical observations of the charnockite (sample SL2-1D) indicate that the stable mineral assemblage in the rock is biotite + orthopyroxene + K-feldspar + plagioclase + magnetite + ilmenite + quartz ± inferred melt, whereas that of biotite gneiss (sample SL2-1A) is biotite + K-feldspar + plagioclase + magnetite + ilmenite + quartz ± inferred melt. Although the rock does not indicate strong evidences to support the presence of melt phase during high-grade metamorphism, the occurrence of biotite + quartz symplectite (Fig. 4e) has been regarded as products of reaction between ferromagnesian minerals and melt. Figure 5 is a *P*-*T* pseudosection calculated based on an assumption that the analyzed LOI value is equivalent to H_2O content in the rock during high-grade metamorphism. As shown in the figure, the stability field of the

inferred peak mineral assemblage in the charnockite (Melt + Bt + Opx + Kfs + Pl + Mag + Ilm + Qtz in Fig. 5) occurs at 790-820°C and 3.0-4.5 kbar. However, the condition is not realistic because it is more than 100°C higher than the inferred solidus of the rock (melt-in line in Fig. 5, about 650-660°C at 4 kbar), suggesting about 9-19 mol.% of melt should be present in the rock. However, the examined thin section of charnockite shows no strong evidence of partial melting, due to which this study concluded the inferred H_2O content (2.465 mol.%) is too high. The overestimated H_2O content might be because orthopyroxene in charnockite is often partly hydrated possibly because of post-peak infiltration of H_2O-bearing fluid or later alteration. The evaluation of H_2O content during metamorphism is therefore needed.

Figures 6a and b are *P*-M(H_2O) (pressure versus mole H_2O content) and *P*-*a*(H_2O) (pressure versus H_2O activity) pseudosections, respectively, calculated at a fixed temperature of 750°C which corresponds to an approximate temperature condition of incipient charnockite-formation discussed in previous studies (e.g., Endo et al., 2012, 2013) and also the peak temperature range of estimated by hornblende-plagioclase geothermometry. The figure is useful for the evaluation of quantity of H_2O during incipient-charnockite formation. In Figure 6a, M(H_2O) content varies from 0 to 2.465 mol.% (calculated based on LOI value). The stability field of the peak mineral assemblage in charnockite (Bt + Opx + Kfs + Pl + Mag + Ilm + Qtz) appears in the figure as a narrow field around 3.2 kbar and H_2O content of about 55% of LOI value. Phase analyses in *P*-*a*(H_2O) pseudosection (Fig. 6b) indicate that the activity of water for the stability of the mineral assemblage in charnockite was about 0.46, which is consistent with approximate *a*(H_2O) condition of granulite-facies metamorphism (usually *a*(H_2O)<0.5; e.g., Newton et al., 1980).

Figure 7a is a *P*-*T* pseudosection recalculated using the inferred M(H_2O) value (M(H_2O)=1.356 mol.%, equivalent to 55% of LOI as shown in Fig. 6a). The stability field of the

assemblage in charnockite (Bt + Opx + Kfs + Pl + Mag + Ilm + Qtz) is estimated as 3.0-3.7 kbar and 740-790^{o}C in this diagram. The lower and upper pressure limits of the stability field were constrained by cordierite-out and garnet-out lines, whereas the upper temperature limit by the solidus line. Figure 7b is also a *P-T* pseudosection, but calculated based on the constant $a(H_2O)$ value (= 0.46) obtained in Fig. 6b. The phase relations in the figure are principally consistent with those in Fig. 7a, but showing much narrower stability field for the charnockite assemblage (ca. 750°C and 3.2 kbar).

Figure 8a, a *P*-$X(H_2O)$ pseudosection calculated at 750^{o}C, is probably useful for evaluating the effect of $H_2O/(H_2O+CO_2)$ ratio on the stability of orthopyroxene ($X(H_2O)$ = molar $H_2O/(H_2O+CO_2)$), because incipient-charnockite formation is always regarded to have a close relation with metamorphic fluid condition. The maximum H_2O content (M(H_2O=2.465) is estimated based on LOI value of the rock because the condition is suitable for amphibolite-facies metamorphism. A stability field of the charnockite assemblage in the pseudosection is around 3 kbar, which is well comparable with the pressure conditions inferred in Fig. 7a. $X(H_2O)$ is inferred as 0.71, which is higher than that of Santosh et al. (1990), but this is probably because of low metamorphic pressure inferred in this study. The *P*-$X(H_2O)$ pseudosection in Fig. 8a also display that the stability field of orthopyroxene expands to higher pressure with decreasing $X(H_2O)$. Figure 8b is a *P-T* pseudosection based on the $X(H_2O)$ value evaluated in the *P*-$X(H_2O)$ pseudosection (Fig. 8a). In this diagram, the stability field of charnockite assemblage is inferred as 3.0-3.5 kbar and 750-780°C, which is nearly consistent with the results argued in Fig. 7a.

2.5. Discussion

2.5.1. Petrology and phase equilibrium modeling

Incipient charnockite at Ginikarawa in the Wanni Complex of Sri Lanka contains a mineral assemblage of biotite + orthopyroxene + K-feldspar + plagioclase + magnetite + ilmenite + quartz, whereas the host biotite gneiss lacks orthopyroxene and contains a mineral assemblage of biotite + K-feldspar + plagioclase + magnetite + ilmenite + quartz ± ferro-edenite. Although calcic amphibole is absent in charnockite and absent or rare in matrix biotite gneiss, meta-igneous nature of the host gneiss as well as lack of garnet indicate that incipient charnockite at Ginikarawa is a Kabbal-type orthocharnockite with the formation of orthopyroxene through breakdown and possibly through consumption of calcic amphibole by reactions with biotite and quartz. Similar Kabbal-type incipient charnockites have been reported from nearby quarries at Udadigana, Angangala, and Waraddana in Kurunegala District (e.g., Hansen et al., 1987; Perchuk et al., 2000). Hansen et al. (1987) reported a thick incipient-charnockite stratum interlayered in a plunging syncline with quartzite and metasediments in this region, and the studied Ginikarawa area might correspond to the northern margin of this unit.

The application of phase equilibrium modeling in NCKFMASHTO system indicates that the orthopyroxene-bearing mineral assemblage in charnockite is stable at 3.0-3.5 kbar and 750-780°C (Fig. 8b), and under relatively low $a(H_2O)$ condition of 0.46. Metamorphic temperatures estimated using hornblende-plagioclase geothermometry for a calcic amphibole-bearing assemblage in the host biotite gneiss is 740–800°C, which is nearly consistent with the condition estimated by the modeling. The *P-T* condition is lower than the peak condition of the Wanni Complex (~830°C and ~7 kbar; Schenk et al., 1991; Raase and Schenk, 1994), but nearly consistent with the conditions obtained from Udadigana charnockite

(700–750°C, 5–6 kbar, and $a(H_2O)$=0.52-0.59; Perchuk et al., 2000), although pressure range and $a(H_2O)$ value obtained in this study are slightly low. The phase equilibrium modeling therefore confirmed that incipient-charnockite formation at Ginikarawa is a post-peak event as inferred from different localities reported in previous studies (e.g., Hansen et al., 1987; Perchuk et al., 2000; Newton and Tsunogae, 2014, and many others).

2.5.2. Fluid associated with incipient-charnockite formation

Newton and Tsunogae (2014) reported pseudosecondary fluid inclusions trapped within quartz in charnockite from this locality, with melting and homogenization temperature ranges of −57.8 to −56.6°C and +29.6 to +30.9°C, respectively, suggesting entrapment of low-density near-pure CO_2 fluid. This analysis also performed preliminary fluid inclusion study on the charnockite and identified near-pure CO_2 fluid inclusions of secondary generation trapped along healed cracks in quartz. Similar carbonic fluids have been reported from other incipient charnockite localities in southern India (e.g., Janardhan et al., 1982; Hansen et al., 1987; Santosh et al., 1990; Tsunogae et al., 2008a), Sri Lanka (e.g., Hansen et al., 1987; Perchuk et al., 2000), and Madagascar (e.g., Rakotondrazafy et al., 2007), suggesting CO_2 played an important role on the formation of charnockite in the Neoproterozoic collisional orogen. This study could not find high-salinity aqueous inclusions as reported by Hansen et al. (1987) and Perchuk et al. (2000) from Kabbal-type incipient charnockite in Sri Lanka, but this is probably because of higher propensity of the carbonic fluids to be captured and preserved in growing crystals, compared to the more reactive and grain-boundary-wetting saline solutions (e.g., Newton and Tsunogae, 2014). This study therefore infers that two immiscible fluids, high-salinity H_2O and almost pure CO_2, were present during incipient-charnockite formation at Ginikarawa. As summarized in

Newton and Manning (2010), the saline solution has greater capability for element transport because of its higher solubility for silicate minerals than pure CO_2. The systematic compositional variation between the charnockite patch and host gneiss reported in previous studies is probably related to the infiltration of such metasomatic fluid and local transport of some mobile elements.

The origin of immiscible fluids associated with incipient-charnockite formation at Ginikarawa is still unknown, and it will be a future research topic. The available carbon isotope data for incipient charnockite from the Trivandrum Block in southern India suggest deep-crustal granulite or primitive mantle source (e.g., Jackson et al., 1988; Santosh et al., 1993), whereas decarbonation of carbonates is also a possible source of CO_2. (e.g., Santosh and Omori, 2008).

2.5.3. Timing of incipient-charnockite formation

Phase equilibrium modeling in this study indicates that the incipient-charnockite formation at Ginikarawa is a post-peak retrograde event, which is consistent with the results from many incipient-charnockite localities in southern India and Madagascar (e.g., Santosh et al., 1990; Perchuk et al., 2000). Using the microthermometry data of carbonic fluid inclusions reported by Newton and Tsunogae (2014), this study estimated densities of the inclusions as 0.53-0.61 g/cm^3. The calculated CO_2 isochores using thermodynamic model are plotted at about 1.6-2.0 kbar at 750°C. The pressure range is even lower than that for the mineral assemblage of charnockite (3.0-3.7 kbar) discussed in this study, possibly suggesting partial leakage of the trapped fluid. Similar low-density carbonic fluid inclusions were also reported from Kurunegala (e.g., Hensen et al., 1987).

Hiroi et al. (1990) reported secondary andalusite associated with siderite and cordierite

in pelitic rocks from the Highland Complex, and suggested that CO_2 infiltration possibly related to lowering H_2O activity and stabilizing orthopyroxene by dehydration of biotite is a post peak later low-pressure event. Previous fluid inclusion study of incipient charnockite by Hansen et al. (1987) pointed out that CO_2-rich fluid inclusions occur along secondary healed cracks in quartz. Preliminary fluid inclusion data discussed in this study on the charnockite sample SL2-1D indicate the abundant occurrence of secondary CO_2-rich fluid inclusions trapped in quartz, whereas very little fluid inclusions were observed in other minerals. The available petrological data all suggest that CO_2-infiltration possibly triggered dehydration of biotite and formation of biotite is related to retrograde metamorphism.

The inferred incipient-charnockite formation at post-peak stage is consistent with the structure-control occurrence of some incipient-charnockite localities, for example Kottavattam quarry in southern India where incipient charnockite veins are showing spectacular rectilinear pattern along brittle fracturing of the host gneisses (e.g., Raith and Srikantappa, 1993; Kehelpannala, 1999), although ductile deformation should be dominant at high-grade metamorphic condition in lower crust. The estimated pressure for Ginikarawa incipient charnockite is 3.0-3.5 kbar, which corresponds to the depth of approximately 9 to 10 km. The depth is slightly shallower than the transition from ductile to brittle regime in quartzo-feldspathic continental rocks (13-18 km: Janecke and Evans, 1988), although the depth also depends on a number of factors, including ambient geothermal gradient, strain rate, mode of faulting, and pore-fluid pressure (e.g., Sibson, 1983). Such brittle deformation could have formed microcracks in quartz along which CO_2-rich fluid was trapped. Therefore, although fluids trapped in secondary arrays are generally thought as retrograde fluid (e.g., Van den Kerkhof and Hein, 2001; Touret, 2001), the CO_2 fluid in quartz discussed in this study might preserve the fluid associated with incipient-charnockite formation.

2.6. Conclusions

(1) Dark brownish to grayish irregular patches of incipient charnockite in Ginikarawa near Kurunegala in the Wanni Complex, Sri Lanka, contains mineral assemblage of biotite + orthopyroxene + K-feldspar + plagioclase + magnetite + ilmenite + quartz, whereas matrix orthopyroxene-free leucocratic biotite ± hornblende orthogneiss contains biotite + K-feldspar + plagioclase + magnetite + ilmenite + quartz ± ferro-edenite.

(2) Phase equilibrium modeling on the mineral assemblage within charnockite in NCKFMASHTO system constrained the conditions of incipient-charnockite formation at 3.0-3.7 kbar and 740-790°C under relatively low $a(H_2O)$ condition of 0.46. Orthopyroxene becomes unstable at higher $a(H_2O)$ condition of >0.46, which is consistent with the available model of incipient-charnockite formation that local decrease in $a(H_2O)$ within hydrous biotite gneiss gave rise to the progress of dehydration reaction and formation of orthopyroxene-bearing assemblage.

(3) The estimated *P–T* condition is lower than the available peak metamorphic conditions reported for typical granulites from the Wanni Complex (~850°C and ~7 kbar), which confirmed that incipient-charnockite formation is a post-peak retrograde event possibly related to local infiltration of low-$a(H_2O)$ and CO_2-bearing fluid.

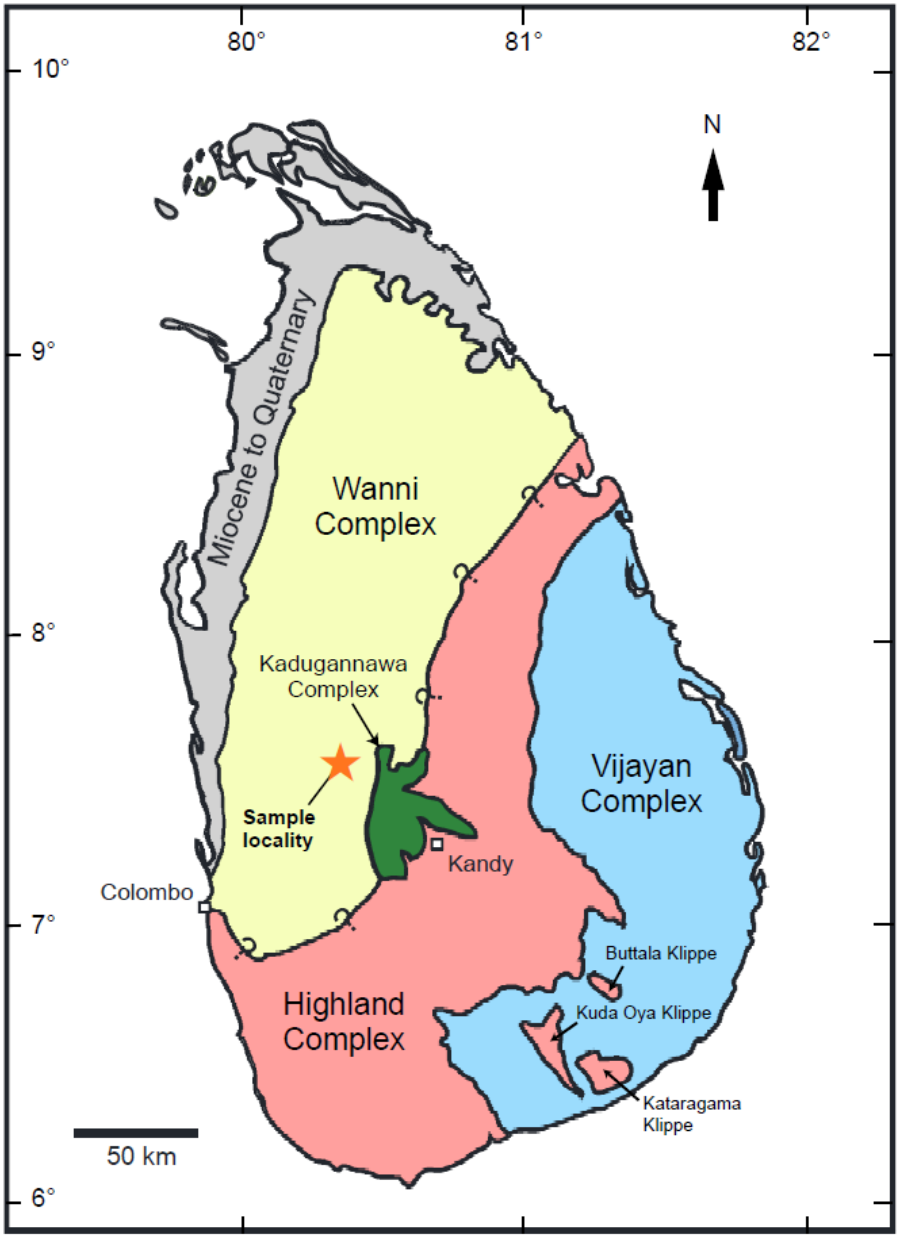

Fig. 2. Generalized geological and tectonic framework of Sri Lanka showing major crustal blocks and their boundaries with the locality of samples (star) discussed in this study (after Cooray, 1994).

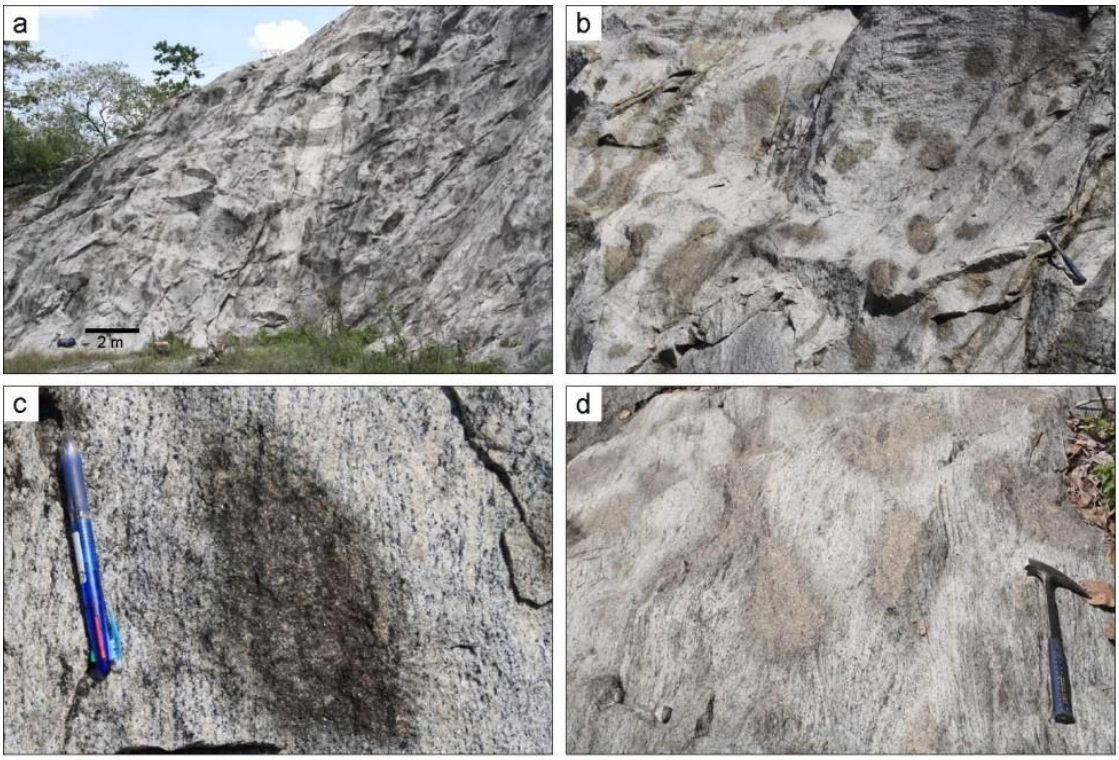

Fig. 3. Field photographs of incipient charnockite and host biotite gneiss discussed in this study. (a) Overview of incipient-charnockite quarry in Ginikarawa. (b) Irregular patches and veins of dark brownish charnockite in well-foliated biotite gneiss. (c) Enlarged photograph of charnockite patch in biotite gneiss. Foliation of the biotite gneiss is defined by alternation of quartzo-feldspathic and biotite-rich layers, which disappears in charnockite. (d) Incipient charnockite in the matrix of hornblende-bearing biotite gneiss from the same locality.

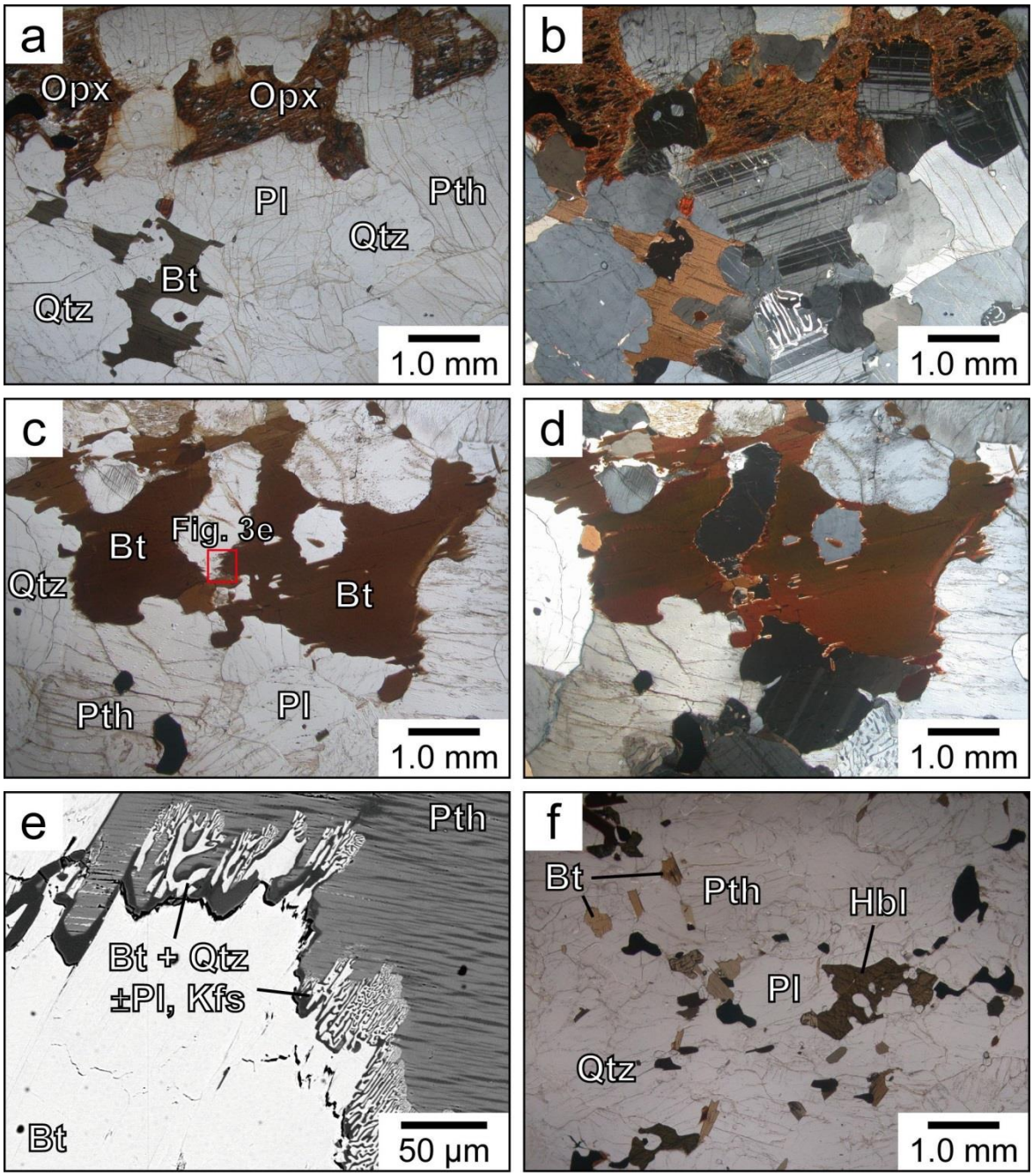

Fig. 4. Photomicrographs showing representative textures of charnockite and biotite gneiss at Ginikarawa in the WC. (a) and (b) Photomicrographs of charnockite (sample SL2-1D). (c) and (d) Photomicrographs of biotite gneiss (sample SL2-1A). (e) Symplectitic texture composed of biotite + quartz ± plagioclase ± K-feldspar in biotite gneiss (sample SL2-1A). (f) Calcic amphibole-bearing variety of biotite gneiss (sample SL2-1A-2).

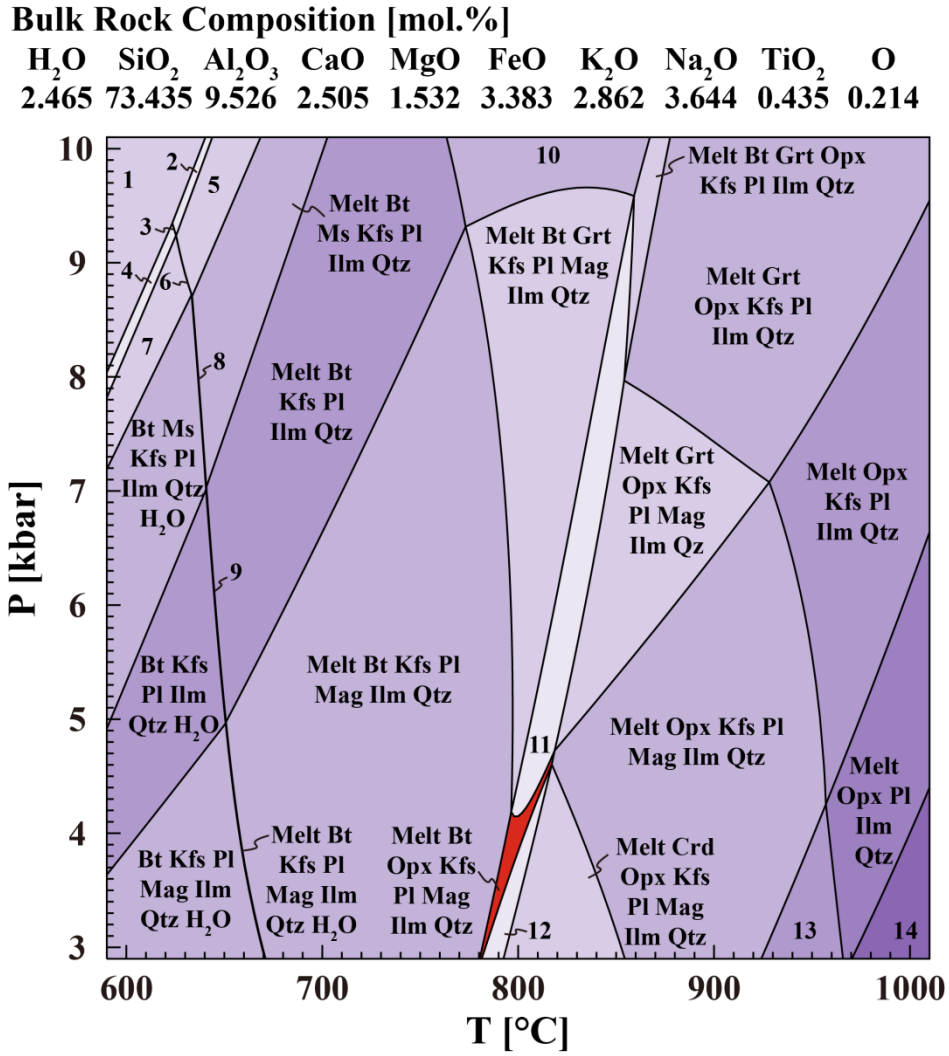

Fig. 5. *P-T* diagrams showing calculated pseudosections of mineral assemblage in charnockite (sample SL2-1D) at Ginikarawa in the WC. H_2O content of this diagram is calculated based on the assumption that LOI value is equivalent to the H_2O content during incipient-charnockite formation. The stability field of the orthopyroxene-bearing mineral assemblage in charnockite occurs at 790-820°C and 3.0-4.5 kbar, which is more than 100°C higher than the solidus of the rock.

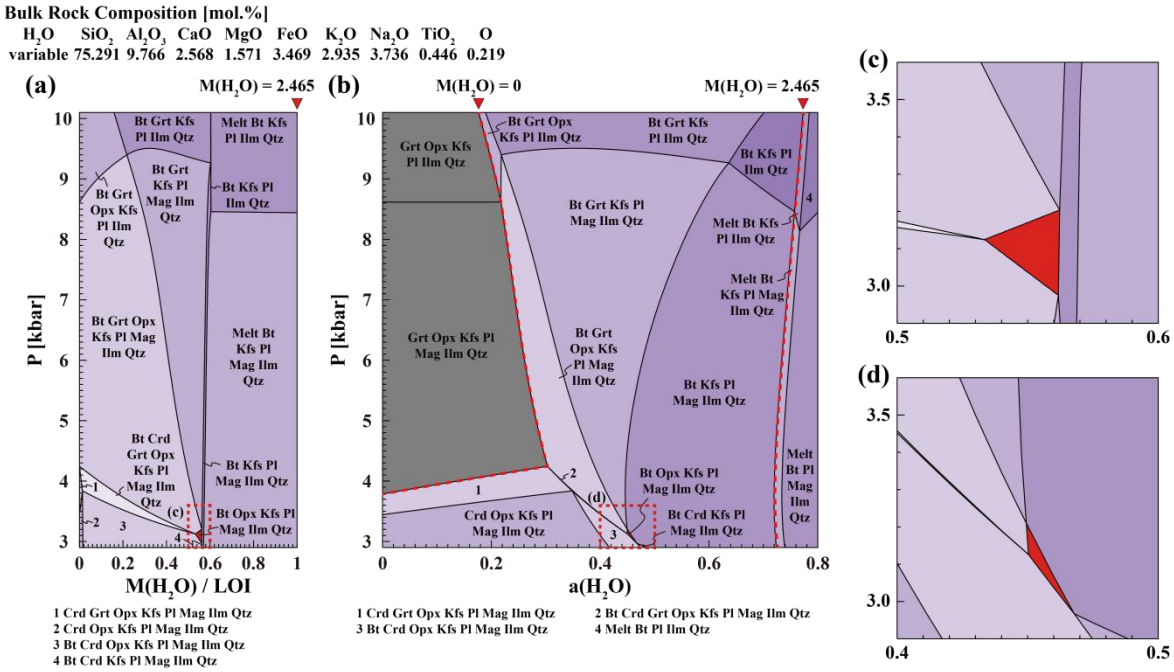

Fig. 6. *P*-M(H_2O) and *P*-*a*(H_2O) diagrams showing calculated pseudosections of mineral assemblage in charnockite (sample SL2-1D) from Ginikarawa in the WC. Hatched areas show the mineral assemblage of charnockite. (a) *P*-M(H_2O) pseudosection at *T* = 750°C. The maximum H_2O content is calculated from LOI. (b) *P*-*a*(H_2O) pseudosection at *T* = 750°C. Dashed lines indicate isopleths of M(H_2O) = 0 and 2.465 mol.% obtained from LOI value. (c) Enlarged drawing around the area of charnockite in *P*-M(H_2O) diagram (Fig. 6a). (d) Enlarged drawing around the area of charnockite in *P*-*a*(H_2O) diagram (Fig. 6b).

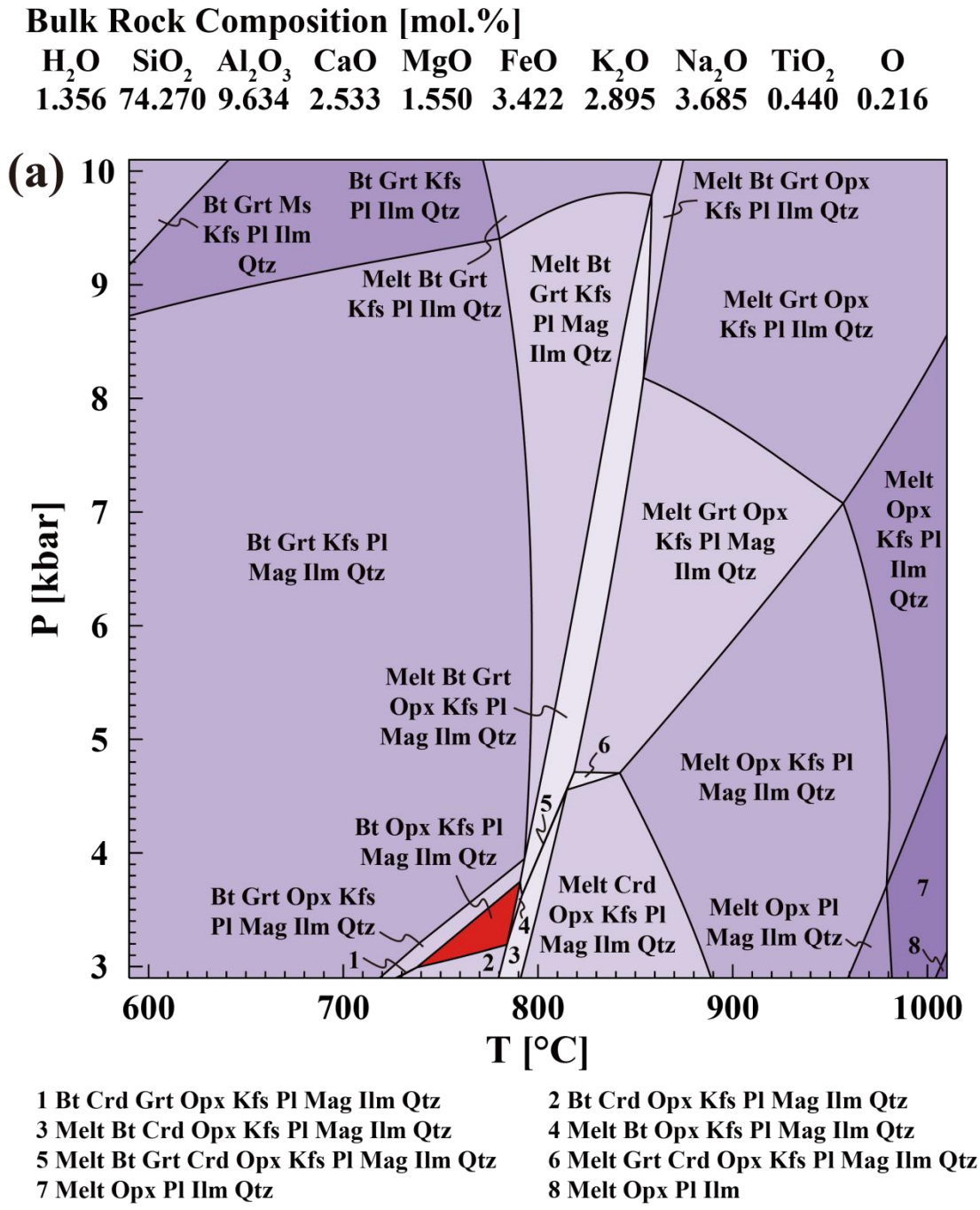

Fig. 7. *P-T* diagrams showing calculated pseudosections of mineral assemblage in charnockite (sample SL2-1D) from Ginikarawa in the WC using the calibrated H_2O content. Hatched areas show the mineral assemblage of charnockite. (a) *P-T* pseudosection at M(H_2O) = 1.356 mol.%, which is equivalent to H_2O (wt.%) = 0.55 x LOI (see Fig. 6a). (b) *P-T* pseudosection at *a*(H_2O) = 0.46 (see Fig. 6b). (c) Enlarged drawing around the area of charnockite in *P-T* pseudosection at *a*(H_2O) = 0.46 (Fig. 7b). (d) Enlarged drawing in *P-T* pseudosection at *a*(H_2O) = 0.46 (Fig. 7b).

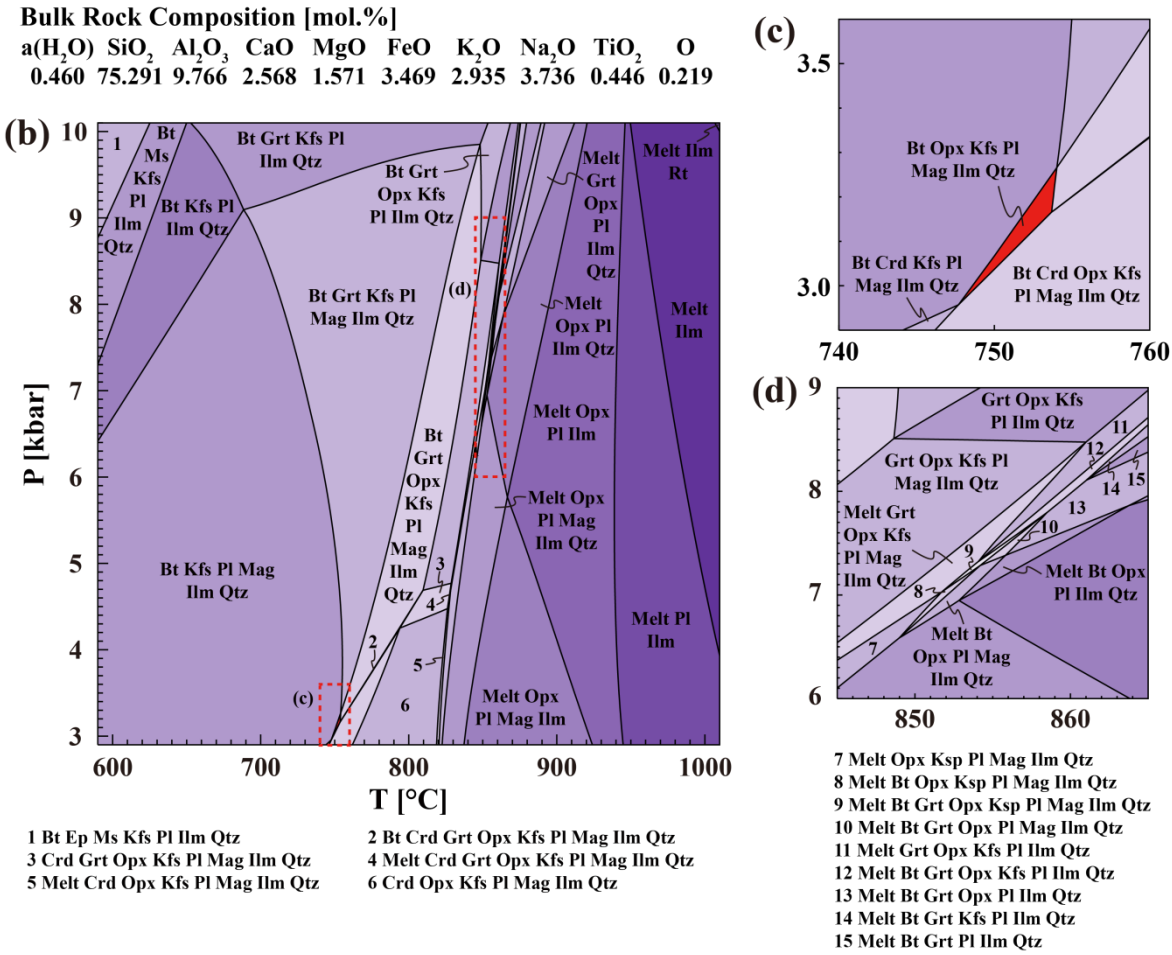

Fig. 7. *P-T* diagrams showing calculated pseudosections of mineral assemblage in charnockite (sample SL2-1D) from Ginikarawa in the WC using the calibrated H_2O content. Hatched areas show the mineral assemblage of charnockite. (a) *P-T* pseudosection at M(H_2O) = 1.356 mol.%, which is equivalent to H_2O (wt.%) = 0.55 x LOI (see Fig. 6a). (b) *P-T* pseudosection at *a*(H_2O) = 0.46 (see Fig. 6b). (c) Enlarged drawing around the area of charnockite in *P-T* pseudosection at *a*(H_2O) = 0.46 (Fig. 7b). (d) Enlarged drawing in *P-T* pseudosection at *a*(H_2O) = 0.46 (Fig. 7b).

Bulk Rock Composition [mol.%]

	H_2O	CO_2	SiO_2	Al_2O_3	CaO	MgO	FeO	K_2O	Na_2O	TiO_2	O
0	0.0001	2.465	73.435	9.526	2.505	1.532	3.383	2.862	3.644	0.435	0.214
1	2.465	0.0001	73.435	9.526	2.505	1.532	3.383	2.862	3.644	0.435	0.214

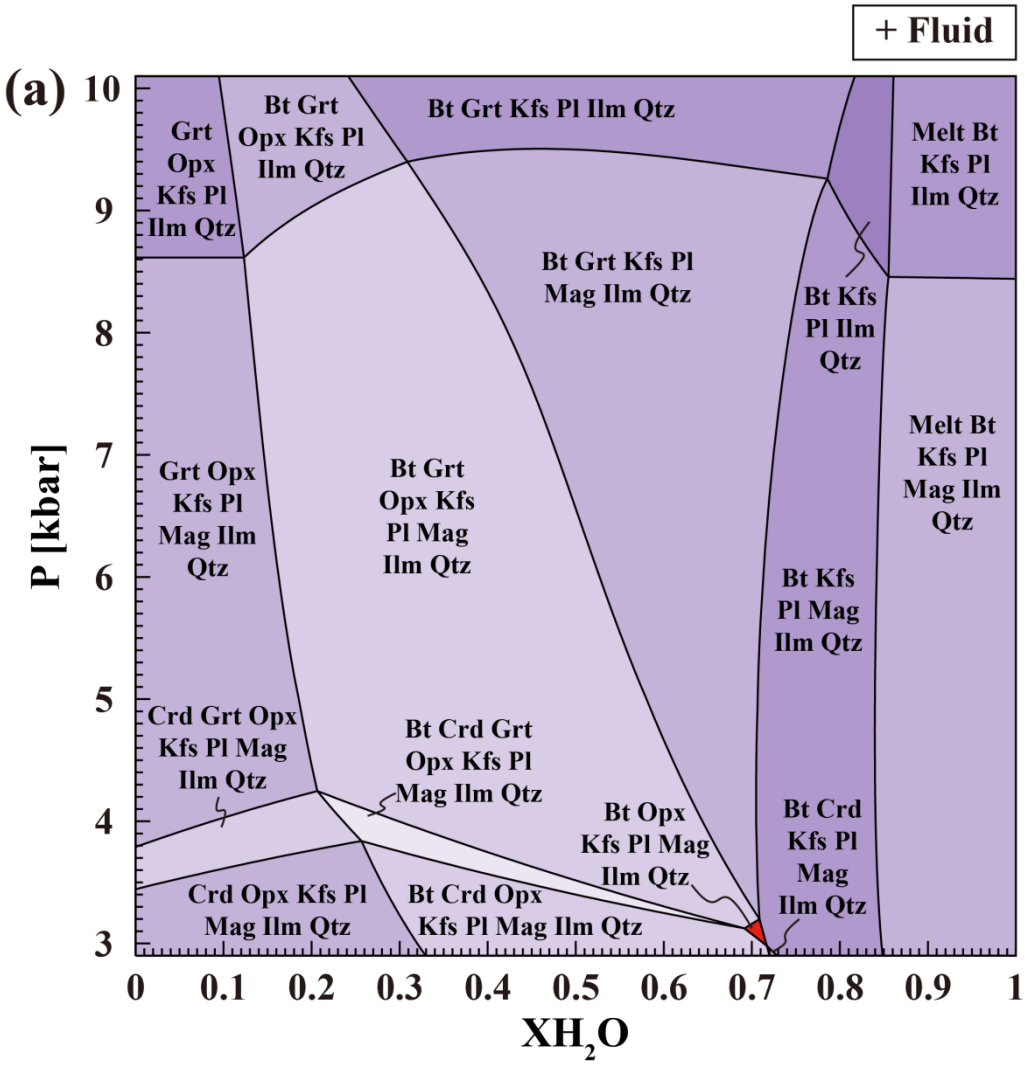

Fig. 8. *P*-*X*(H_2O) and *P*-*T* pseudosections of charnockite (sample SL2-1D) from Ginikarawa in the WC. In all domains of the diagrams, fluid phase composed of H_2O and CO_2 is present. Hatched areas show the mineral assemblage of charnockite. (a) *P*-*X*(H_2O) pseudosection at 750°C. (b) *P*-*T* pseudosection calculated at calibrated H_2O and CO_2 content.

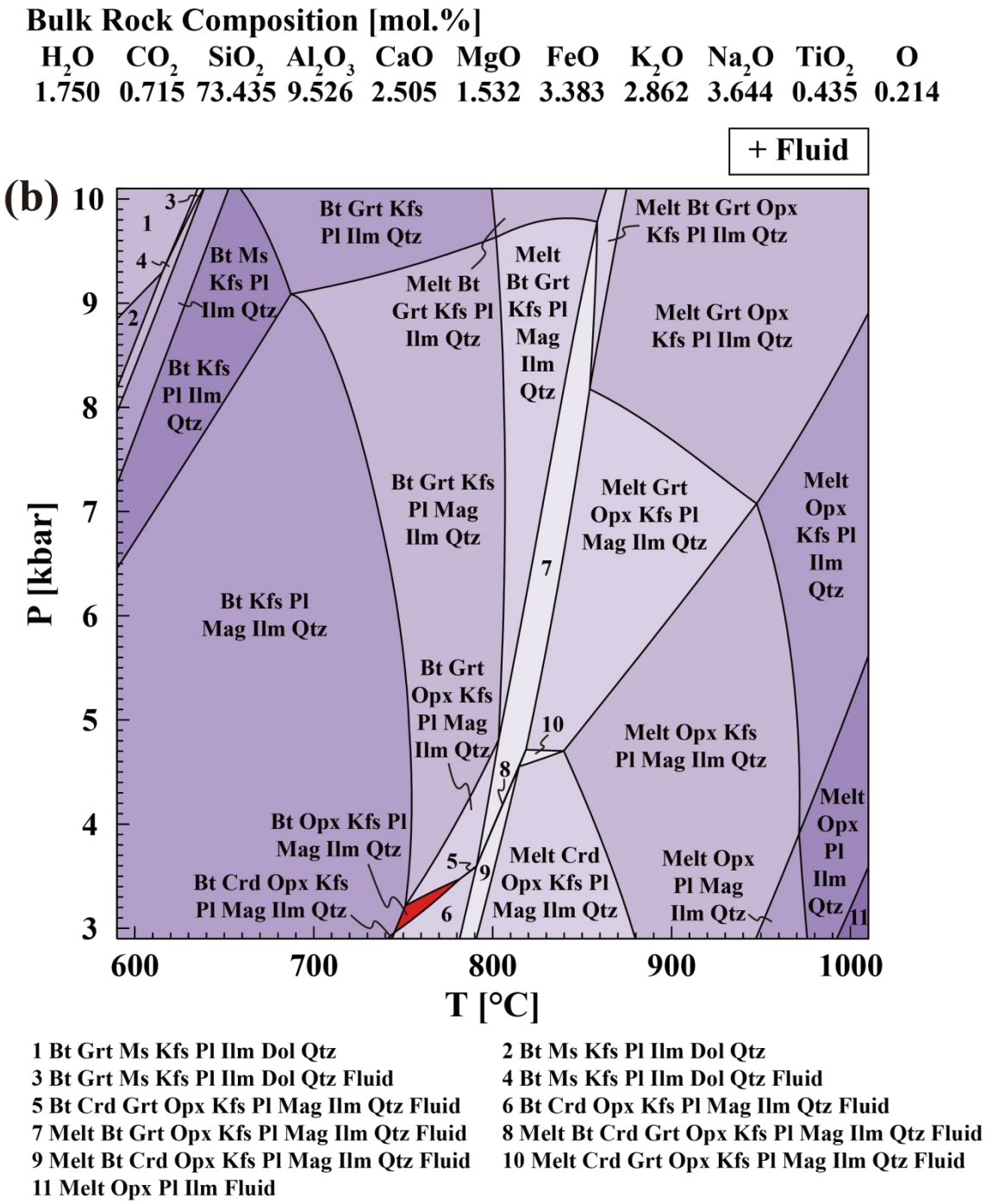

Fig. 8. *P*-*X*(H_2O) and *P*-*T* pseudosections of charnockite (sample SL2-1D) from Ginikarawa in the WC. In all domains of the diagrams, fluid phase composed of H_2O and CO_2 is present. Hatched areas show the mineral assemblage of charnockite. (a) *P*-*X*(H_2O) pseudosection at 750°C. (b) *P*-*T* pseudosection calculated at calibrated H_2O and CO_2 content.

Table 1. Mineral name abbreviations.

Mineral	Abbreviation
Amph	amphibole
Ap	apatite
Bt	biotite
Cal	calcite
Cpx	clinopyroxene
Gr	graphite
Grt	garnet
Hbl	hornblende
Ilm	ilmenite
Kfs	K-feldspar
Opx	orthopyroxene
Pl	plagioclase
Pth	perthite
Qtz	quartz
Scp	scapolite
Ttn	titanite
Wo	wollastonite

Table 2. Representative electron microprobe analyses of orthopyroxene, biotite, plagioclase, and K-feldspar from Ginikarawa in the WC.

Lithology*	CH	CH	CH	CH	BG	BG	HBG	CH	BG	HBG	CH	CH	BG	BG	HBG
Mineral Name	Opx	Opx	Bt	Bt	Bt	Bt	Bt	Pl	Pl	Pl	Kfs	Kfs	Kfs	Kfs	Kfs
Number of O	6	6	22	22	22	22	22	8	8	8	8	8	8	8	8
Remarks			Core	Rim	Matrix	Symp.	Matrix	Matrix	Matrix	Matrix	Perthite, Core	Perthite, Rim	Symp.	Perthite	Perthite
SiO_2	50.37	50.25	35.92	36.07	36.01	36.58	36.68	62.81	62.56	62.33	66.00	65.78	65.73	65.05	64.58
Al_2O_3	0.60	0.50	12.69	12.94	12.97	13.44	13.11	23.95	23.37	24.04	19.16	19.01	18.64	18.43	18.91
TiO_2	0.12	0.17	5.09	4.80	4.65	4.25	5.44	0.05	0.00	0.01	0.00	0.05	0.03	0.00	0.12
Cr_2O_3	0.03	0.00	0.00	0.00	0.00	0.00	0.00	0.00	0.00	0.03	0.00	0.04	0.00	0.01	0.01
FeO**	32.26	31.87	21.11	21.32	22.19	21.22	20.90	0.15	0.14	0.09	0.07	0.06	0.40	0.05	0.06
MnO	2.09	2.01	0.24	0.25	0.32	0.26	0.22	0.00	0.00	0.00	0.00	0.01	0.01	0.00	0.00
NiO	0.00	0.03	0.00	0.00	0.01	0.02	0.00	0.00	0.00	0.01	0.00	0.00	0.00	0.04	0.00
MgO	13.55	13.83	10.16	9.91	9.76	9.97	10.62	0.00	0.01	0.00	0.00	0.00	0.00	0.00	0.01
CaO	0.91	0.81	0.00	0.01	0.00	0.01	0.02	5.31	4.92	5.46	0.18	0.12	0.03	0.03	0.19
Na_2O	0.03	0.00	0.07	0.04	0.10	0.06	0.13	8.59	8.72	8.54	2.89	2.04	1.25	0.95	2.44
K_2O	0.01	0.01	9.50	9.59	9.17	9.14	9.60	0.47	0.34	0.30	12.70	14.07	14.24	15.30	13.17
Total	99.97	99.48	94.77	94.93	95.17	94.95	96.77	101.32	100.06	100.82	101.00	101.17	100.33	99.86	99.50
Si	1.989	1.990	5.604	5.621	5.608	5.666	5.585	2.754	2.773	2.746	2.983	2.983	3.003	3.000	2.972
Al	0.028	0.024	2.333	2.376	2.380	2.453	2.351	1.237	1.221	1.248	1.020	1.016	1.003	1.002	1.026
Ti	0.004	0.005	0.597	0.562	0.545	0.495	0.622	0.002	0.000	0.000	0.000	0.002	0.001	0.000	0.004
Cr	0.001	0.000	0.000	0.000	0.000	0.000	0.000	0.000	0.000	0.001	0.000	0.001	0.000	0.000	0.000
Fe^{2+}	1.065	1.055	2.753	2.778	2.889	2.748	2.660	0.005	0.005	0.003	0.003	0.002	0.015	0.002	0.002
Mn	0.070	0.067	0.031	0.032	0.042	0.035	0.029	0.000	0.000	0.000	0.000	0.000	0.001	0.000	0.000
Ni	0.000	0.001	0.000	0.000	0.001	0.002	0.000	0.000	0.000	0.000	0.000	0.000	0.000	0.001	0.000
Mg	0.797	0.816	2.360	2.300	2.265	2.299	2.408	0.000	0.001	0.000	0.000	0.000	0.000	0.000	0.001
Ca	0.038	0.035	0.000	0.002	0.000	0.001	0.003	0.249	0.234	0.258	0.009	0.006	0.001	0.001	0.010
Na	0.002	0.000	0.020	0.011	0.030	0.017	0.040	0.729	0.749	0.729	0.253	0.179	0.111	0.085	0.218
K	0.001	0.000	1.890	1.906	1.821	1.806	1.863	0.026	0.019	0.017	0.732	0.814	0.830	0.900	0.773
Total	3.994	3.993	15.588	15.588	15.582	15.523	15.568	5.003	5.001	5.002	4.999	5.003	4.964	4.991	5.006
Mg/(Fe+Mg)	0.43	0.44	0.46	0.45	0.44	0.46	0.48								
An								0.25	0.23	0.26	0.01	0.01	0.00	0.00	0.01
Ab								0.73	0.75	0.73	0.25	0.18	0.12	0.09	0.22
Or								0.03	0.02	0.02	0.74	0.81	0.88	0.91	0.77

* CH: charnockite (sample SL2-1D), BG: biotite gneiss (sample SL2-1A), BHG: biotite-hornblende gneiss (sample SL2-1A2)

** Total Fe as FeO

Table 3. Representative electron microprobe analyses of calcic amphibole from Ginikarawa in the WC.

Lithology*	HBG	HBG
Mineral Name	Hbl	Hbl
Number of O	23	23
Remarks	Core	Rim
SiO_2	42.69	43.16
Al_2O_3	10.18	9.88
TiO_2	2.17	2.04
Cr_2O_3	0.01	0.00
FeO**	20.25	19.81
MnO	0.52	0.59
MgO	9.13	9.20
CaO	11.17	11.24
Na_2O	1.98	1.82
K_2O	1.46	1.31
Total	99.55	99.06
Si	6.442	6.520
Al^{iv}	1.558	1.480
Sum T	8.000	8.000
Al^{vi}	0.251	0.279
Ti	0.246	0.232
Cr	0.001	0.000
Fe^{2+}	2.555	2.502
Mn	0.066	0.075
Mg	2.052	2.070
Sum C	5.172	5.158
Ca	1.805	1.819
Na(B)	0.195	0.181
Sum(B)	2.000	2.000
Na(A)	0.383	0.351
K	0.282	0.252
Sum(A)	0.665	0.603
Total	15.837	15.761
Mg/(Fe+Mg)	0.45	0.45

* BHG: biotite-hornblende gneiss (sample SL2-1A2)

** Total Fe as FeO

CHAPTER 3

Formation of incipient charnockite associated with calc-silicate rock from Ambodin Ifandana in Ikalamavony Sub-domain, south-central Madagascar

3.1. Introduction

The central and southern Madagascar domains are dominantly composed of migmatitic orthogneiss, metavolcanic and metasedimentary rocks, and granitic to granodioritic intrusives (e.g., Collins, 2006, and references therein), which were metamorphosed at amphibolite- to granulite-facies grade during Late Neoproterozoic to Cambrian (e.g., Kröner et al., 1996). Among the high-grade lithologies in the domains, charnockite occupies a significant part of the basement gneisses and occurs as large massive bodies (magmatic charnockite). However, occurrence of incipient charnockite in the Late Neoproterozoic to Cambrian high-grade terranes in Madagascar is rare, and only two examples has been reported from central Madagascar (Rakotondrazafy et al., 2007; Nédélec et al., 2014) and one from south-central Madagascar (Tsunogae et al., 2013). This study reports detailed petrological data of incipient charnockite from south-central Madagascar, and discuss the origin of the charnockite patches and layers within biotite gneisses. The incipient charnockite in this locality is unique among other examples in Madagascar because of its close association with calc-silicate rocks. This study employed phase equilibrium modeling technique to quantitatively evaluate the petrogenesis of the incipient-charnockite formation which was possibly triggered by decreasing H_2O activity related to CO_2 introduction during high-grade metamorphism. The results of this study are compared with similar investigations from elsewhere in order to discuss petrogenesis of incipient charnockite and fluid processes associated with the collisional assembly of Gondwana.

3.2. Geological setting

3.2.1. General geology

The basement rocks in Madagascar are subdivided into several crustal blocks (e.g., Antongil Block, Antananarivo Block, Betroka Belt, and Tsaratanana Sheet), which are dissected by several shear/suture zones (e.g., Ranotsara shear zone, Betsimisaraka Suture Zone; Kröner et al., 2000; Collins and Windley, 2002, and references therein). The Antananarivo Block forms the largest Precambrian tectonic unit of Madagascar and occupies the central and southern part of Madagascar (Fig. 9). The main rock units in the block are orthogneiss, migmatite, charnockite, metapelite, dolomitic marble, quartzite, amphibolite, and younger intrusive rocks (Collins, 2006, and references therein). The Itremo–Ikalamavony Domain, which is composed mainly of metasediments, migmatites, and older gneisses, are located southwest of the Antananarivo Block (Fig. 9). It is subdivided into the Itremo Sub-domain (mainly composed of quartzite, and metapelite, marble) and the Ikalamavony Sub-domain (mainly composed of metasediments, leucogneiss, amphibolite, and migmatitic gneiss) (Tucker et al., 2011). The orthogneisses discussed in this study were collected from the Dabolava Suite of the Ikalamavony Sub-domain. That shows 1035–982 Ma magmatic ages (e.g., Tucker et al., 2007, 2011). Tucker et al. (2011) examined SHRIMP zircon geochronology of a trondhjemitic gneiss from Zazafotsy, about 30 km NE from Ihosy, and obtained upper and lower intercept ages of 1035±30 Ma and 399±130 Ma, respectively, the former age corresponding to the magmatic emplacement time of the protolith.

The southern margin of the Antananarivo Block and the Itremo–Ikalamavony Domain is defined by NW-SE-trending Ranotsara shear zone (e.g., Hottin,1976; Kröner et al., 2000; Collins and Windley, 2002) which probably continues to the Achankovil Suture Zone of southern India (Windley et al., 1994; Collins, 2006). The Southern Madagascar, south of the

Ranotsara shear zone, is subdivision into six N–S striking tectonic belts (termed from west to east as Vohibory, Ampanihy, Bekily, Betroka, Tranomaro, and Fort Dauphin-Anosyan belts; Windley et al., 1994) separated by N–S-trending major shear zones (e.g., Ejeda, Ampanihy, and Beraketa shear zones). The rocks in southern Madagascar underwent granulite-facies metamorphism during the Late Neoproterozoic to Early Cambrian orogeny between 560 and 530 Ma (Andriamarofahatra et al., 1990; Paquette et al., 1994; Montel et al., 1996; Kröner et al.,1996 ; Nicollet et al., 1997; Jöns and Schenk, 2011).

3.2.2. Incipient charnockite in Madagascar

Incipient charnockite was first reported from Madagascar by Rakotondrazafy et al. (2007) from the area northwest from Antananarivo in the Antananarivo Block, central Madagascar. They described patches of dark incipient charnockites (plagioclase + K-feldspar + quartz + orthopyroxene) within migmatitic gneiss (plagioclase + K-feldspar + quartz + biotite) and dominant CO_2-rich fluid inclusions within plagioclase in the charnockite. Nédélec et al. (2014) reported geochemical and fluid inclusion characters of structurally-controlled charnockite patches in A-type granite from the Antananarivo Block, central Madagascar, and noted higher magnetic susceptibility in charnockite and mobility of Ti, Fe, Zn, Ca, F and REE during charnockitization. They also reported abundant CO_2-rich fluid inclusions in charnockites compared to surrounding granitic gneisses, and suggested a rather long history of fluid percolation, leading to prograde and then retrograde transformations from gneiss to charnockite. Tsunogae et al. (2013) reported patches of incipient charnockite (plagioclase + quartz + K-feldspar + biotite + garnet + orthopyroxene + ilmenite + magnetite) within orthopyroxene-free garnet-biotite gneiss for the first time from the southern margin of the

Ikalamavony Sub-domain in south-central Madagascar, immediately north of the Ranotsara shear zone. Their application of mineral equilibrium modeling technique on charnockite assemblage in NCKFMASHTO system constrained the condition of incipient-charnockite formation at 8.0-10.5 kbar and 820-880°C, which is broadly consistent with the results of conventional geothermobarometry (820-880°C at 9 kbar) of the host garnet-biotite gneiss. They argued that orthopyroxene-free hydrous assemblage in the garnet-biotite gneiss is stable at higher molar H_2O content ($M(H_2O)$) of >0.1 mol.%, whereas orthopyroxene in charnockite is stable at very low $M(H_2O)$ condition of <0.1 mol.%, which is consistent with the available petrogenetic model of incipient charnockite related to the lowering of water activity and stability of orthopyroxene through dehydration reaction/melting of biotite. They also reported dominant CO_2-rich fluid inclusions in charnockite compared to the host garnet-biotite gneiss, suggesting that the dehydration and incipient-charnockite formation could have been caused by infiltration of CO_2-rich fluid from external sources.

3.2.3. Field occurrence of incipient charnockite at Ambodin Ifandana

The studied incipient-charnockite locality at Ambodin Ifandana (S22°0'37", E46°23'18"), about 48 km north of Ihosy, is a fresh quarry composed mainly of dark grayish, coarse-grained, and weakly to strongly foliated migmatitic gneiss of the Ikalamavony Sub-domain of Itremo-Ikalamavony Domain in south-central Madagascar (Tucker et al., 2011). The foliation of the rock is defined by thin alternation of leucocratic (quartzo-feldspathic) and melanocratic (biotite-rich) layers (Fig. 10a) probably formed by partial melting and melt segregation during high-grade metamorphism. Irregular patches, lenses, or veins of light to dark brownish charnockite are present throughout the quarry (Figs. 10b-e). The size of the patches varies from

5 cm to up to 30 m (Figs. 10b, c), and the veins are about 5-20 cm in thickness and ~2 m long (Fig. 10d). Weak to strong foliation can be seen in the host biotite gneiss, but it disappears while passing into the charnockite patches (Fig. 10c), suggesting that, although migmatization of the host rock probably took place during prograde or peak stage, the incipient-charnockite formation postdated the event. The vein charnockites are sometimes folded together with the host migmatite (Fig. 10e), which implies ductile deformation after the incipient-charnockite formation. The charnockite patches and veins in this quarry do not show any systematic distribution pattern, although a prominent structural control in incipient charnockite patches has been described in previous studies from other localities (e.g., Santosh et al., 1990; Raith and Srikantappa, 1993). However, they are closely associated with layers or lenses of calc-silicate rocks (Fig. 10f). The calc-silicate rocks are dark greenish in color, medium-grained, and distributed nearly parallel to the foliation of the matrix biotite gneiss. It is interesting to note that, as shown in Fig. 10f, both patches and a layer of brownish charnockite are present adjacent to a calc-silicate layer, which is a common occurrence of patchy and layered charnockites in this quarry.

Previous petrological studies of many incipient charnockite locations in southern India (e.g., Pichamuthu, 1960; Santosh et al., 1990; Raith and Srikantappa, 1993; Endo et al., 2012, 2013) and Sri Lanka (e.g., Hansen et al., 1987; Hiroi et al., 1990) suggest that grain size of rock-forming minerals is coarser in charnockite than that of host hydrous gneiss. As discussed in the next chapter, there is no obvious difference in grain size between the two lithologies in the present case. However, the charnockite near the contact with a calc-silicate rock is slightly light brownish and coarser in grain size than other part of charnockite and biotite gneiss (Fig. 10g). As discussed later, the contact charnockitic rock contains abundant CO_2-rich fluid inclusions, based on which this study will argue in a later chapter decarbonation of calc silicate

rocks and formation of incipient charnockite by CO_2 infiltration.

Four representative samples collected from this quarry were examined in detail; charnockite (sample MGK2-1F1), biotite gneiss (sample MGK2-1F2), calc-silicate rock (sample MGK2-1A), and charnockite – calc-silicate contact rock (sample MGK2-1N). A brief summary of the petrological features and mineral assemblages of the four lithologies are given below. Mineral name abbreviations are after Kretz (1983).

3.3. Petrography

3.3.1. Charnockite

The charnockite (sample MGK2-1F1) is composed of quartz (40-50 %), plagioclase (20-30 %), K-feldspar (10-15 %), orthopyroxene (3-4 %), Fe-Ti oxide (3-4 %), and biotite (2-3%) (Fig. 11a). Accessory minerals are apatite and zircon. The rock shows massive texture without any obvious foliation, although orthopyroxene grains are sometimes distributed along the lithological boundaries between charnockite and calc-silicate rock, generating orthopyroxene-rich layers in charnockite (Fig. 10f). Fe-Ti oxide (magnetite and ilmenite) is medium-grained (0.2-1.1 mm) and irregular in shape. Ilmenite contains numerous thin lamellae of hematite formed by later exsolution. Fine- to medium-grained (0.3-2.0 mm) quartz is the most dominant mineral in the sample. Plagioclase is also fine to medium grained (0.3-1.0 mm), subidioblastic, free from inclusion, and scattered in the matrix. K-feldspar is also fine to medium grained (0.1-0.7 mm) and occurs either as subidioblastic grains in the matrix or as thin films filling grain boundaries of quartz and plagioclase. Such occurrence of K-feldspar films has

been regarded as an evidence of the presence of melt phase (e.g., Touret and Huizenga, 2012) or high-temperature metasomatism by infiltration of low H_2O-activity fluid (e.g., Harlov et al., 1998; Rajesh and Santosh, 2012; Tsunogae and van Reenen, 2014). Orthopyroxene is fine to medium grained (0.1-1.5 mm), xenoblastic, slightly pleochroic, and present along grain boundaries of quartz and feldspars. Ferromagnesian minerals (orthopyroxene and biotite) in charnockite occur as mottled aggregates with Fe-Ti oxide, forming dark spots of ~1 cm in diameter (Figs. 10b,c). The ferromagnesian spots are surrounded by light brownish quartz and feldspars. Orthopyroxene is sometimes replaced by fine-grained aggregates of biotite and quartz, which is considered to have been formed either by retrograde hydration reactions or reactions with hydrous melt.

3.3.2. Biotite gneiss

The migmatitic biotite gneiss (sample MGK2-1F) is composed mainly of quartz (45-55 %), plagioclase (20-30 %), K-feldspar (10-15 %), biotite (5-6%), and Fe-Ti oxide (3-4 %), with accessory apatite and zircon (Fig. 11b). The mineralogy is very similar to that of charnockite except for the absence of orthopyroxene. The rock shows obvious foliation defined by alternation of quartz- and feldspar-rich leucocratic layers and biotite-rich grayish layers. Fe-Ti oxide, mainly ilmenite and minor magnetite, is medium grained (0.2-1.4 mm) and irregular in shape. The ilmenite contains thin exsolution lamellae of hematite, similar to the ilmenite grains in charnockite. Textural characters, shape, and grain size of matrix quartz (0.3-2.1 mm), plagioclase (0.2-0.8 mm), and K-feldspar (0.3-1.0 mm) are similar to those in charnockite. Strongly pleochroic (dark to light brownish) biotite is more abundant in this sample than in the charnockite and it is obviously aligned along the rock foliation (Fig. 11b), but it is shape and

grain size (0.2-1.8 mm) are almost equivalent to that in charnockite.

3.3.3. Calc-silicate rock

The calc-silicate rock (sample MGK2-1A) is composed of quartz (40-50 %), plagioclase (25-35 %), clinopyroxene (15-20 %), garnet (3-4 %), and titanite (1-2 %). The dominant occurrences of Ca-bearing minerals as well as accessory calcite suggest that the protolith of this rock could be a limestone which was highly metasomatized during high-grade metamorphism. Quartz (0.5-2.2 mm) and plagioclase (0.4-1.1 mm) are semi-equigranular, granoblastic, and scattered in matrix. Clinopyroxene (0.1-1.3 mm) is pleochroic (greenish to greenish brown in color), subidioblastic to xenoblastic in shape, and often surrounding quartz and plagioclase grains. Titanite (0.1-0.3 mm) is brownish in color, subidioblastic to rounded, and associated with clinopyroxene. Garnet (0.3-1.2 mm) is also brownish, subidioblastic to rounded, and often coexisting with clinopyroxene.

3.3.4. Charnockite – calc-silicate contact rock

Sample MGK2-1N is a charnockite collected near the contact with a calc-silicate rock (Fig. 10g). It is composed of quartz (50-60 %), plagioclase (20-30 %), K-feldspar (10-15 %), orthopyroxene (2-3 %), biotite (2-3%), and Fe-Ti oxide (2-3 %) with accessory apatite and zircon (Fig. 11d). The mineral assemblage and textures of this rock are similar to those of charnockite, but this sample is more quartzo-feldspathic than charnockite, and grain size of quartz (0.8-5.2 mm), plagioclase (0.7-2.1 mm), K-feldspar (0.5-2.2 mm), and biotite (0.2-3.0 mm) is coarser than charnockite and host biotite gneiss. On the other hand, size of

orthopyroxene (0.2-1.2 mm) and Fe-Ti oxide (0.3-1.0 mm) grains is similar to those in charnockite. Orthopyroxene does not occur as aggregates with biotite and Fe-Ti oxide, which is common only in other parts of charnockite.

3.4. Mineral chemistry

Mineral chemical analyses were carried out using an electron microprobe analyzer (JEOL JXA8530F) at the Chemical Analysis Division of the Research Facility Center for Science and Technology, the University of Tsukuba. The analyses were performed under conditions of 15 kV accelerating voltage and 10 nA sample current, and the data were regressed using an oxide-ZAF correction program supplied by JEOL. Representative compositions of minerals in the analyzed samples are given in Tables 4 to 6.

3.4.1. Orthopyroxene

Orthopyroxene in the charnockite (sample MGK2-1F1) and contact rock (sample MGK2-1N) shows similar Mg-rich compositions of X_{Mg} = 0.76-0.80 (Table 6). Al content in the mineral is low, Al_2O_3 = 1.9-3.1 wt.%, which correspond to 0.08-0.13 pfu. It contains small amount of Fe^{3+} as $Fe^{3+}/(Fe^{2+}+Fe^{3+})$ = 0.01-0.16. Such compositional characters are consistent with those of Kabbal-type incipient charnockite (orthocharnockite) reported from granulite terranes in Southern India and Sri Lanka (e.g., Hansen et al., 1987; Perchuk et al., 2000).

3.4.2. Biotite

Composition of biotite varies depending on lithologies and occurrences (Table 5). Biotite in charnockite (sample MGK2-1F1) is texturally classified into two types; primary grains in matrix and secondary grains possibly formed during a retrograde hydration event. They are both Mg-rich as X_{Mg} = Mg/(Fe+Mg) = 0.77-0.80, but the former contains higher TiO_2 (3.2-3.5 wt.%) and fluorine (F = 0.37-0.58 wt.%) than the latter (TiO_2 <3.1 wt.%, F <0.21 wt.%). Chlorine contents of the two types are low, Cl <0.01 wt.%. Biotite in biotite gneiss (sample MGK2-1F2) shows slightly Mg-depleted composition of X_{Mg} = 0.72-0.74, although its TiO_2 content (3.1-3.4 wt.%) is similar to that of charnockite. Its fluorine content (0.19-0.31 wt.%) is slightly lower than the matrix biotite in charnockite, although its chlorine content is slightly higher (~0.3 wt.%).

Biotite in the contact rock (sample MGK2-1N) shows slight compositional variations depending on coexisting minerals. Biotite coexisting with orthopyroxene is depleted in Mg (X_{Mg} = 0.74-0.77) and F (0.34-0.58 wt.%) than that apart from orthopyroxene (X_{Mg} = 0.77-0.79 and F = 0.15-0.30 wt.%), although their TiO_2 (2.5-2.8 and 2.5-3.3 wt.%, respectively) and Cl (0-0.2 wt.%) contents are consistent. Such high F content in the biotite associated with orthopyroxene might suggest the progress of orthopyroxene-forming dehydration reaction, and the remaining biotite became enriched in fluorine as the mineral decreases in modal amount (e.g., Tsunogae et al., 2003a).

3.4.3. Feldspars

Plagioclase in the charnockite (sample MGK2-1F) and biotite gneiss (sample MGK2-1F2) shows similar albite-rich compositions of $An_{38-40}Ab_{60-62}$ (Table 6). In contrast, plagioclase in

calc-silicate rock (sample MGK2-1A) is highly anorthite-rich as $An_{92-94}Ab_{6-8}$. Plagioclase in the contact rock (sample MGK2-1N) shows intermediate albite component as $An_{39-44}Ab_{56-61}$, reflecting its close association with calc-silicate rocks. K-feldspar in charnockite is orthoclase-rich as Or_{88-89} and its BaO content is 0.61-0.78 wt.%. That in biotite gneiss shows similar orthoclase-rich compositions of Or_{86-89}, and it is slightly depleted in BaO (0.47-0.63 wt.%). K-feldspar in the contact rock is also orthoclase-rich as Or_{87-89}, but its BaO content (0.83-1.3 wt.%) is slightly higher than that of charnockite and biotite gneiss. Such high BaO content of K-feldspar and high anorthite content of plagioclase in the contact rocks might suggest metasomatism and transport of barium and calcium by fluid migration.

3.4.4. Other minerals

Clinopyroxene in calc-silicate rock (sample MGK2-1A) shows slightly Mg-rich rim (X_{Mg} = 0.63-0.64) than core (X_{Mg} = 0.57-0.59). It contains minor esseneite component as $Fe^{3+}/(Fe^{2+}+Fe^{3+})$ = 0.39-0.46, although compositional zoning in $Fe^{3+}/(Fe^{2+}+Fe^{3+})$ ratio is absent. Garnet in calc-silicate is essentially a solid solution of andradite and grossular components as $Adr_{66-69}Grs_{18-20}Sps_5Prp_1$. It shows no compositional zoning.

3.5. Mineral equilibrium modeling

3.5.1. Method of investigation

Metamorphic *P-T* conditions of the stability of mineral assemblages in the charnockite from the study area were constrained using THERMOCALC 3.33 (Powell and Holland, 1988, updated

October 2009) with an updated version of the internally consistent data set of Holland and Powell (1998a; data set tcds55s, file created November 2003). Calculations were undertaken in the system Na_2O-CaO-K_2O-FeO-MgO-Al_2O_3-SiO_2-H_2O-TiO_2-Fe_2O_3 (NCKFMASHTO) (White et al., 2003, 2007), which provides a realistic approximation to model the examined rocks. The phases considered in the modeling and the corresponding *a-X* models used are garnet, biotite, and melt (White et al., 2007), plagioclase and K-feldspar (Holland and Powell, 2003), clinopyroxene and amphibole (Diener and Powell, 2012), muscovite (Coggon and Holland, 2002), spinel and magnetite (White et al., 2002), ilmenite-hematite (White et al., 2000), cordierite (Holland and Powell, 1998b), and osumilite (Holland et al., 1996). Quartz, titanite, and H_2O are treated as pure end-member phases. For the analysis, slabs of relatively homogeneous part of the examined rocks were used for thin-section preparation, and the counterpart of the same slabs was used for chemical analysis. Bulk-rock compositions for the rocks were determined by X-ray fluorescence spectroscopy at Activation Laboratories, Canada. Charnockite containing unaltered fresh orthopyroxene (sample MGK2-1F1) is used for the modeling, and its chemical composition (in wt.%) is SiO_2 = 73.66, Al_2O_3 = 9.68, Fe_2O_3 = 2.34, FeO = 3.09, MgO = 1.91, CaO = 2.28, Na_2O = 1.90, K_2O = 2.13, TiO_2 = 0.67. FeO/Fe_2O_3 ratio was determined by titration. The charnockite sample contains ~0.1 wt.% P_2O_5, which is reflected in ~0.5 modal % of apatite. As P_2O_5 is neglect from the system, the CaO content equivalent to apatite should be extracted from the calculation. The corrected CaO content (2.14 wt.%) is adopted for the pseudosection calculation. Mn content is neglected because of the little amount (MnO ~0.1 wt.%).

3.5.2. Results

Petrographic observations of the charnockite (sample MGK2-1F1) indicate that the stable mineral assemblage in the rock is biotite + orthopyroxene + K-feldspar + plagioclase + magnetite + ilmenite + quartz + inferred melt. The presence of melt phase is inferred from the occurrence of thin K-feldspar film around plagioclase, possibly suggesting the presence of very small amount of liquid. As H_2O content of the rock during high-grade metamorphism is not known, this study first adopted LOI value of chemical analyses (0.3 wt.%) as the maximum H_2O content. The calculated molar H_2O content ($M(H_2O)$) is more than 1 mol.%, which is extremely higher than the inferred $M(H_2O)$ of granulite-facies rocks (Endo et al., 2012, 2013). The analysis therefore adopted $M(H_2O)$ of 0.5 mol.% based on the results of previous analyses (Endo et al., 2012, 2013). Figure 12 is a *P-T* pseudosection calculated based on $M(H_2O)$ = 0.5 mol.%. The stability field of the peak mineral assemblage in charnockite (biotite + orthopyroxene + K-feldspar + plagioclase + magnetite + ilmenite + quartz + inferred melt) occurs in the diagram as a narrow field of 810°C/2.2 kbar to 880°C/10.5 kbar. The upper-pressure limit of the field is defined by garnet- and clinopyroxene-out lines, whereas the lower-pressure limit by cordierite-out line. The higher- and lower-temperature limits are constrained by biotite-out and melt-out lines, respectively. Although the results show a wide *P-T* range, the condition is consistent with the available peak *P-T* condition of garnet-bearing charnockite from Zazafotsy in the Ikalamavony Sub-domain (8-10.5 kbar and 820-880°C, Tsunogae et al., 2013).

Figure 13 shows *T*-$a(H_2O)$ (temperature versus H_2O activity) pseudosections calculated at a fixed pressure of 9 kbar which is inferred from the peak *P-T* condition of Zazafotsy charnockite (Tsunogae et al., 2013). Figures 13a and 13b suggest that the mineral assemblage of charnockite is stable at $a(H_2O)$ = 0.42-0.45 (shaded area in Fig. 13b), which is consistent with the approximate $a(H_2O)$ condition of granulite-facies rocks (< 0.5; e.g., Newton et al., 1980).

Figures 13c and 13d are revised diagrams of Figure 13a and 13b, respectively, with isopleth lines of M(H_2O) (0, 0.5, 1, and 2 mol.%). Although Figure 13d suggest that the orthopyroxene-bearing mineral assemblage in charnockite can be stable at extremely high-M(H_2O) condition of >2 mol.% (even at 4 mol.%), the calculated modal abundance of inferred melt is ~35 mol.% (isopleth not shown in the figure). Such a high modal abundance of melt phase is not consistent with the petrographic observations of this study that suggest the amount of possible melt phase in charnockite is probably less than a few wt.%, which corresponds to M(H_2O) condition of 0-0.5 mol.%. The a(H_2O) condition of 0.42-0.43 is therefore inferred as a reasonable fluid condition during the formation of orthopyroxene-bearing assemblage in charnockite.

3.6. Fluid inclusions

3.6.1. Fluid-inclusion petrography

This study performed petrographic and microthermometric studies of fluid inclusions within the charnockite and biotite gneiss in order to verify the argument that incipient-charnockite formation in many granulite terranes was triggered by infiltration of CO_2-rich fluids, with the charnockite is usually rich in carbonic fluid inclusions than the adjacent hydrous gneiss (e.g., Janardhan et al., 1979; Newton et al., 1980; Santosh et al., 1990). Fluid inclusions are generally classified into three categories based on their occurrences and trapped stages (primary, pseudosecondary, and secondary; e.g., Roedder, 1984). Fluid inclusion petrography reveals that primary and pseudosecondary fluid inclusions, which were probably trapped during the growth

of host minerals, are very rare or absent in the analyzed samples. This study also examined fluid inclusions in the contact rock (MGK2-1N), and found abundant secondary inclusions that occur along healed fractures within quartz and plagioclase. Charnockite (sample MGK2-1F1) also contains very fine-grained secondary fluid inclusions, but they are too small for microthermometric study. Biotite gneiss (sample MGK2-1F2) contains only very few fluid inclusions. This study thus focused on fluid inclusions in the contact sample for microthermometry.

Fluid inclusions in the contact rock vary in size from 3 to 15 microns. Photomicrographs of representative fluid inclusions are shown in Fig. 14. They are aligned along healed cracks that continue to the edge of the host mineral, therefore inferred as secondary inclusions trapped during post-peak exhumation stage. Fluid inclusions in plagioclase are rectangular in shape (Fig. 14a), while those in quartz are vermicular or irregular (Fig. 14b).

3.6.2. Microthermometry

The heating and cooling experiments of fluid inclusions were performed using an optical microscope and a Linkam heating/freezing system at the University of Tsukuba following the technique described in Ohyama et al. (2008) and Tsunogae et al. (2008a). The analyzed fluid inclusions display melting temperature (*Tm*) between –56.7 and –56.6°C (Fig. 15a), indicating that the dominant fluid component present in plagioclase and quartz is CO_2 as the temperature range is close to the triple point of pure CO_2 (–56.6°C). This study also performed laser Raman spectroscopic study of some of the inclusions and confirmed there is no obvious peak of minor fluid components such as N_2 and CH_4 (Fig. 16), although the analysis could not evaluate the presence of minor H_2O because the experiment has been done at room temperature (Berkesi et

al., 2009). The inclusions homogenize into the liquid phase at a temperature (*Th*) range of +8.4 to +11.2°C (Fig. 15b; which corresponds to low CO_2 densities of 0.85-0.87 g/cm^3). A prominent peak of the *Th* data is around +9 to +10°C. The fluid densities were calculated using the computer program ‘‘MacFlinCor’’ developed by Brown and Hagemann (1994). Although this study could not obtain any microthermometry data for fluid inclusions in charnockite because of their very small grain size, lack of gas phase within minor coarser fluid inclusion cavities at room temperature might suggest that the trapped fluid phase is also CO_2-rich.

3.7. Discussion

3.7.1. Petrology and phase equilibrium modeling

This is the first report of detailed petrologic, mineralogical, and fluid inclusion data of incipient charnockite at Ambodin Ifandana in the Ikalamavony Sub-domain of south-central Madagascar. Charnockite in this locality occurs as irregular patches, lenses, or veins in migmatitic biotite gneiss (Fig. 10b-e), and it is often associated with lenses or layers of calc-silicate rock (Fig. 10f). The charnockite shows an assemblage of biotite + orthopyroxene + K-feldspar + plagioclase + quartz + magnetite + ilmenite, whereas the host biotite gneiss lacks orthopyroxene and contains a mineral assemblage of biotite + K-feldspar + plagioclase + magnetite + quartz + ilmenite. The calc-silicate rocks associated with charnockite contain clinopyroxene + garnet + plagioclase + quartz + titanite. The charnockite near the contact with a calc-silicate rock principally shows mineral assemblage and textures similar to those of charnockite, although it is more quartzo-feldspathic and grain size of quartz, feldspars, and biotite is coarser in the contact

sample. Incipient charnockites from central and south-central Madagascar reported in previous studies occur as patches or lenses within hydrous orthogneisses (e.g., Rakotondrazafy et al., 2007; Nédélec et al., 2014; Tsunogae et al., 2013), similar to the relations in many typical incipient-charnockite localities in southern India and Sri Lanka (e.g., Pichamuthu, 1960; Newton et al., 1980; Hansen et al., 1987; Santosh et al., 1990; Rajesh and Santosh, 2012; Newton and Tsunogae, 2014, and many others). However, the layered occurrence of incipient charnockite and its close association with calc-silicate rocks in this locality are obviously different from other occurrences of incipient charnockite in Madagascar.

The application of phase equilibrium modeling in NCKFMASHTO system indicates that the orthopyroxene-bearing mineral assemblage in charnockite was stable at a wide *P*-*T* range of 810°C/2.2 kbar to 880°C/10.5 kbar, which was further constrained as 840°C/4.4 kbar to 880°C/10.5 kbar based on fluid inclusion isochores as discussed later (Fig. 12). The *P*-*T* condition is nearly consistent with the peak metamorphic condition of garnet-bearing charnockite from Zazafotsy area in the southern margin of the Ikalamavony Sub-domain (8.0-10.5 kbar and 820-880°C; Tsunogae et al., 2013), suggesting that the incipient-charnockite formation in this locality took place around the peak of metamorphism. The results are in contrast with previous studies of incipient charnockite, where the formation of incipient charnockite mostly took place during retrograde stage (e.g., Hansen et al., 1987; Perchuk et al., 2000; Newton and Tsunogae, 2014, and many others). The low $a(H_2O)$ condition of 0.42-0.43 estimated for the stability of orthopyroxene-bearing assemblage in charnockite is consistent with the results of previous studies. Perchuk et al. (2000) inferred *P*-*T*-$a(H_2O)$ condition of 5–6 kbar, 700–750°C, and $a(H_2O)$=0.52-0.59 for the rock at Udadigana in the Wanni Complex of Sri Lanka. As discussed in Chapter 2, this study calculated based on phase equilibrium modeling that low $a(H_2O)$ condition of <0.46 is necessary for the stability of charnockitic assemblage at

Ginikarawa in Sri Lanka. The $a(H_2O)$ condition of 0.42-0.43 reported in this study is therefore comparable with available report of fluid condition associated with incipient-charnockite formation.

3.7.2. Role of carbonic fluid on the formation of charnockite

Fluid inclusion study of the contact rock (sample MGK2-1N) confirmed the occurrence of low-density (*Th* = +8.4 to +11.2°C; *d* =0.85-0.87 g/cm^3) CO_2-rich fluid inclusions (*Tm* = –56.7 to –56.6°C) trapped as a secondary phase within plagioclase and quartz. Fluid inclusions in charnockite (sample MGK2-1F1) also suggest the presence of secondary CO_2-rich fluid. The composition and density of the fluid phase can be represented through 'isochores' (line of constant volume) in *P-T* space (Fig. 12). Isochores for the carbonic inclusions were calculated using the equation and thermodynamic data of Brown and Lamb (1989). As shown in the *P-T* diagram, the calculated isochores intersect the stability field of charnockite at 4.4-4.7 kbar and 840-850°C. Tsunogae and Santosh (2011) evaluated CO_2 densities in granulites from several high-grade metamorphic terranes and reported significantly lower-pressure estimates of calculated isochores than the peak *P-T* conditions of the rocks, which is explained as a reflection of significant density decrease due to partial leakage of trapped fluid during post-peak decompression. Such CO_2 isochores significantly lower that the peak conditions have also been reported from many granulite terranes (e.g., Tsunogae and Santosh, 2011; Tsunogae et al., 2003b, 2008a,b; Tsunogae and van Reenen, 2007; Nishimiya et al., 2008). Therefore, the *P-T* condition obtained from the isochores is regarded as the minimum pressure condition of the incipient-charnockite formation. Similar carbonic fluid inclusions have been reported from other

incipient charnockite localities in southern India (e.g., Janardhan et al., 1982; Hansen et al., 1987; Santosh et al., 1990; Tsunogae et al., 2008a), Sri Lanka (e.g., Hansen et al., 1987; Perchuk et al., 2000; Newton and Tsunogae, 2014), and Madagascar (e.g., Rakotondrazafy et al., 2007), although some of them are primary and pseudosecondary inclusions. Fluid inclusion data discussed in this study therefore confirmed that CO_2 probably played an important role on the formation of incipient charnockite.

3.7.3. *Source of CO_2-rich fluid*

Origin of CO_2-rich fluids associated with incipient-charnockite formation at Ambodin Ifandana remains equivocal. Previous carbon isotope studies on charnockite suggest several different sources for CO_2-rich fluid such as deep-crustal granulite, mantle, or carbonate. Jackson et al. (1988) carried out systematic carbon isotopic study of CO_2-rich fluid inclusions in incipient charnockite and adjacent orthopyroxene-free gneiss from seven localities in the Southern Granulite Terrane, India, and reported isotopically heavier CO_2 than that in associated gneiss. For example fluid inclusions in charnockite from Ponmudi in the Achankovil Shear Zone have higher $\delta^{13}C$ value (–9.1 to –10.4 ‰) than that in gneiss (–11.2 to –12.6 ‰). They considered the heavy$\delta^{13}C$ value for carbonic fluids in charnockite to indicate mantle source. Santosh et al. (1990) performed a carbon isotope traverse across a typical gneiss-incipient charnockite reaction front in southern India and found that the carbon isotopic composition of CO_2 trapped within minerals that grew during charnockite formation has a ‘juvenile’ magmatic (mantle) signature ($\delta^{13}C$ = –8 ‰). In contrast, decarbonation of carbonates is also a possible source of CO_2 (e.g., Santosh and Omori, 2008). Jackson and Santosh (1992) examined

amphibolite-granulite transition in a charnockite quarry at Nuliyam in the Trivandrum Block, South India, and illustrated dehydration of an amphibolite-facies gneiss to granulite-facies charnockite resulted from the advective infiltration of CO_2-rich fluids generated from a local carbonate source. Santosh et al. (2003) reported detailed carbon isotope study of graphites from a calc-silicate rock–charnockite association and showed that multiple sources of CO_2 (decarbonation of carbonates and infiltration from external 'juvenile' sources) were involved in the growth of the graphite crystal. One of the unique features of incipient charnockite discussed in this study is its close association with calc-silicate rocks. The examined quarry contains numerous layers, lenses, and lenses of dark greenish calc-silicate rocks distributed parallel to the foliation of matrix biotite gneiss (Fig. 10a). As shown in Fig. 10f, several patches of incipient charnockite (about 10-15 cm) are scattered along the calc-silicate layer, whereas a layered charnockite is also present adjacent to the same calc-silicate layer. The boundary between the charnockite and calc-silicate rock is defined as light-brownish and coarse-grained contact rock with abundant quartz, feldspars, and CO_2-rich fluid inclusions. Although this study has no carbon isotope data of the fluid inclusions, the field occurrence and petrographic data clearly suggest that the incipient charnockite was formed by introduction of CO_2-rich fluid derived from decarbonation of calc-silicate rocks, which lowered $a(H_2O)$ of adjacent rocks and stabilized orthopyroxene instead of biotite.

An alternative model is also possible. Harley and Santosh (1995) investigated an association of calc-silicate rock and charnockite at Nuliyam studied by Jackson and Santosh (1992) based on field occurrence and petrology, and pointed out that the calc-silicate rocks were not the source for CO_2. They proposed that the calc-silicate rocks behaved as an impermeable barrier to fluid transport, and acted as impervious cap rocks structurally above the charnockites causing the ponding of externally-derived CO_2-rich fluids beneath the calc-silicate layer,

generating massive-type charnockite adjacent to the layers. Such a "structural trap" model of incipient-charnockite formation can be applied to incipient charnockite in this study. It is generally known that incipient charnockite occurs as patches or tubes because of higher wetting angle of CO_2 than H_2O (e.g., Watson and Brenan, 1987). The layered occurrence of charnockite can therefore be explained by infiltration of highly penetrative fluid such as brine (Safonov et al., 2012), although this study could not find any saline fluid inclusions in the contact rock. Therefore, infiltration of CO_2-rich fluid from an external source and formation of 'CO_2-rich fluid ponds' beneath calc-silicate layers might have enhanced dehydration of biotite to orthopyroxene, and produced layers of charnockite adjacent to calc-silicate layers (Figs. 10f, 17). On the other hand, charnockite patches, possibly located structurally above the calc-silicate layer, could have been formed by infiltrated CO_2 derived by decarbonation of calc-silicate rocks.

3.8. Conclusion

(1) Incipient charnockite from Ambodin Ifandana area in the Ikalamavony Sub-domain of south-central Madagascar occurs as patches, lenses, and layers in migmatitic biotite gneiss. Lenses and layers of calc-silicate rocks are closely associated with the charnockite. Coarse-grained charnockite occurs along the contact between the layered charnockite and calc-silicate rock.

(2) The application of mineral equilibrium modeling on the charnockite assemblage in NCKFMASHTO system as well as fluid inclusion study on charnockite to constrain the conditions of incipient-charnockite formation defines a *P-T* range of 840°C/4.4 kbar to 880°C/10.5 kbar, which is nearly consistent with the inferred *P-T* condition of the Ikalamavony

Sub-domain. The result of *T* versus H_2O activity ($a(H_2O)$) modeling demonstrated that orthopyroxene-bearing assemblage in charnockite is stable under relatively low $a(H_2O)$ condition of 0.42-0.43, which is consistent with the available model of incipient-charnockite formation related to the lowering of water activity and stabilization of orthopyroxene through dehydration of biotite.

(3) The dominant occurrence of CO_2-rich fluid inclusions in the contact charnockite suggests that the dehydration was caused by decarbonation of calc-silicate rocks during the initial stage of decompression slightly after the peak metamorphism. The calc-silicate rocks might have also behaved as a cap rock that trapped CO_2 infiltrated from an external source. 'CO_2-rich fluid ponds' formed beneath calc-silicate layers could have enhanced dehydration of biotite to orthopyroxene, and produced layers of coarse-grained charnockite adjacent to calc-silicate layers.

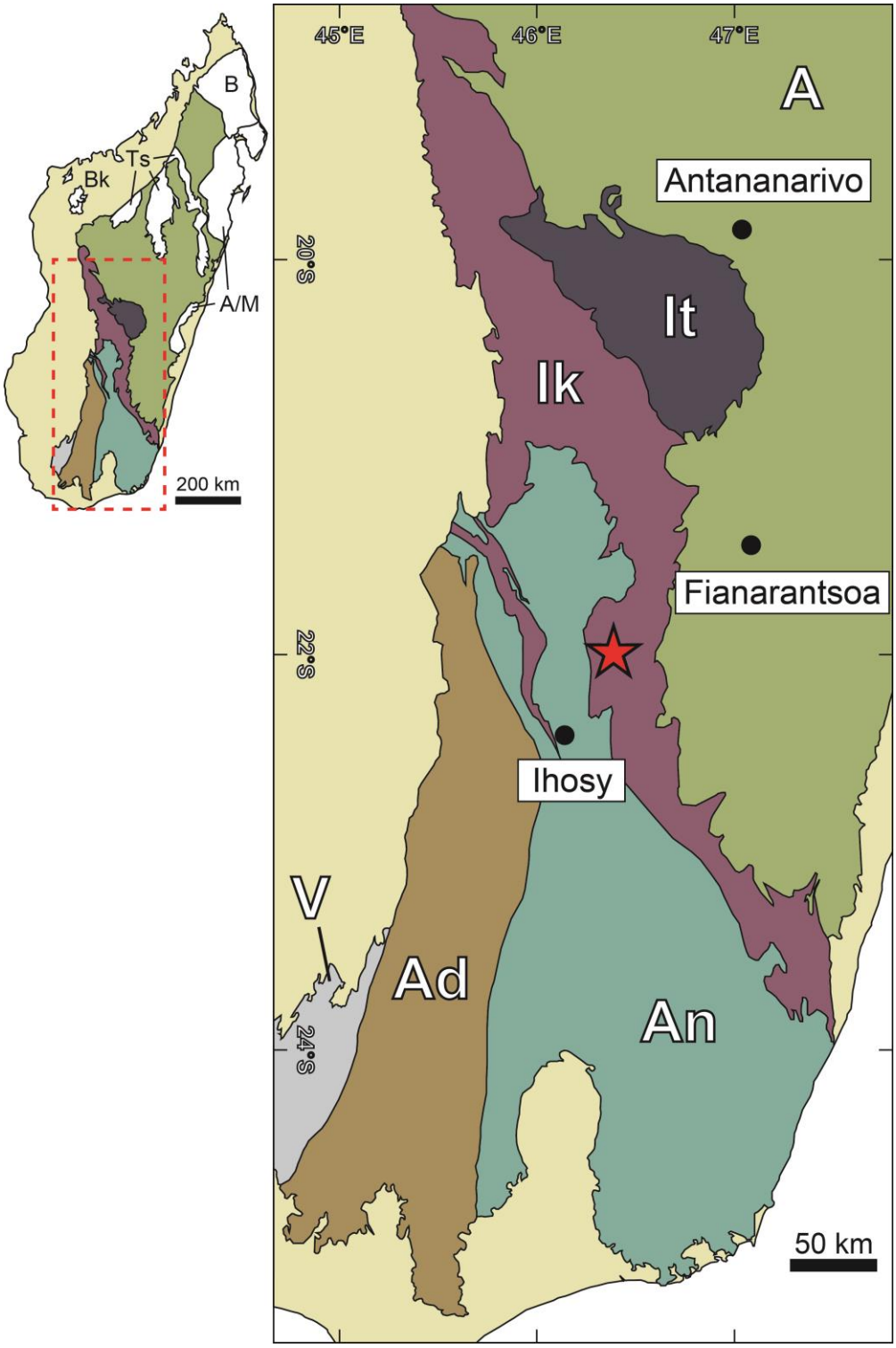

Fig. 9. Generalized geological map of south-central Madagascar showing major crustal blocks with the locality of samples (star) discussed in this study (after Tucker et al., 2011). A: Antananarivo Domain, It: Itremo Sub-domain, Ik: Ikalamavony Sub-domain, An: Anoysen Domain, Ad: Androyen Domain, V: Vohibory Domain.

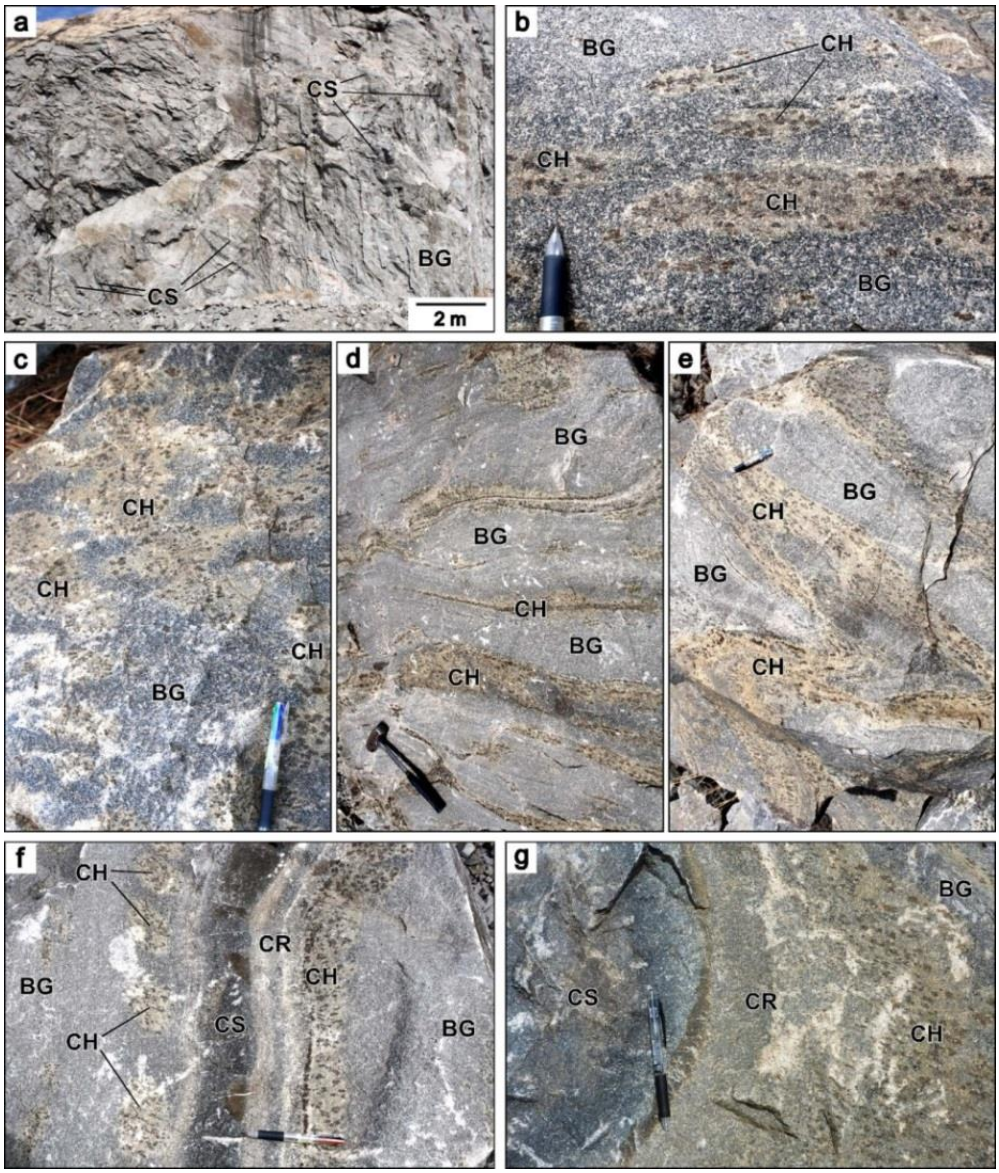

Fig. 10. Field photographs of charnockite and associated rocks from Ambodin Ifandana in the Ikalamavony Sub-domain. (a) An overview of charnockite quarry with numerous layers of calc-silicate rocks (CS) distributed along the foliation of host migmatitic biotite gneiss (BG). (b) and (c) Lenses and patches of brownish charnockite (CH) in biotite gneiss. Aggregates of orthopyroxene occur as black spots in the charnockite. (d) Layers of brownish charnockite distributed parallel to the foliation of host biotite gneiss. (e) Folded charnockite layers in biotite gneiss. (f) Close association of charnockite and calc silicate rocks. Note that charnockite occurs as patches in the left-hand side of calc silicate rock, whereas as a layer in the right-hand side of the rock. (g) Close-up photograph of the boundary between calc-silicate rock and layered charnockite. Coarse-grained and quartzo-feldspathic charnockite (CR) occurs along the contact of the two lithologies.

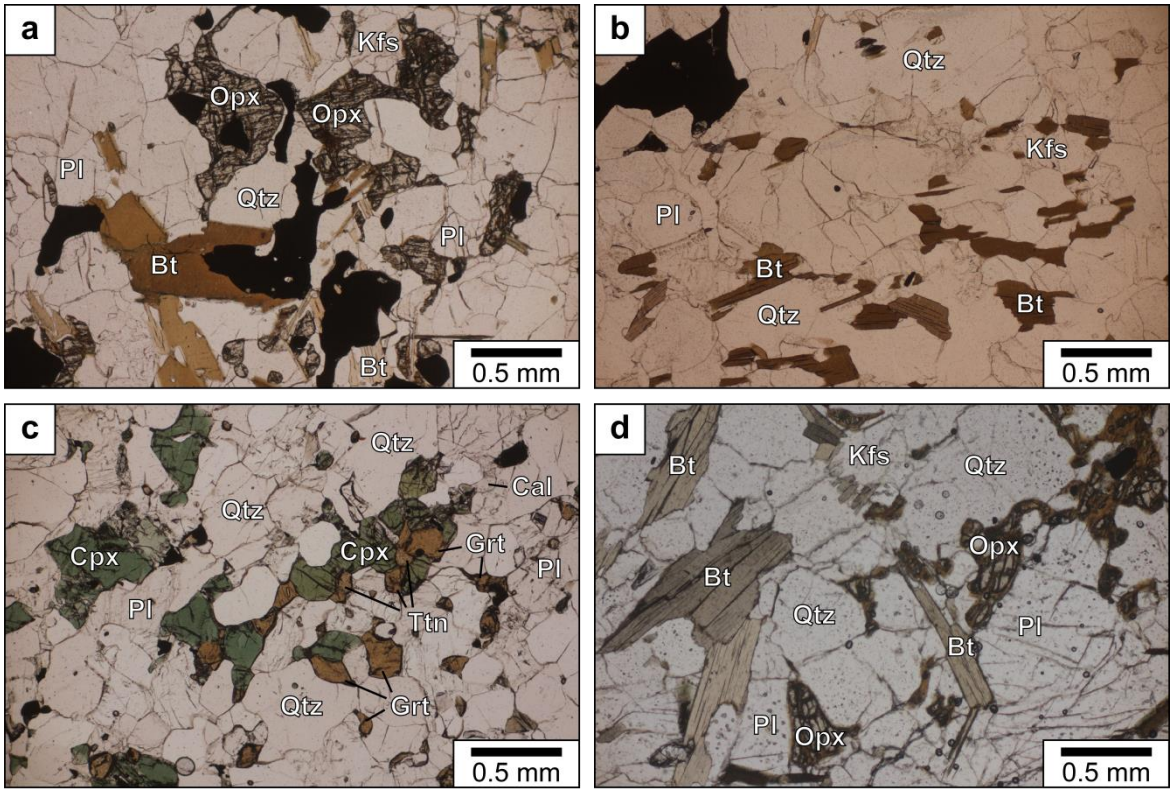

Fig. 11. Photomicrographs showing representative textures of samples from Ambodin Ifandana in the Ikalamavony Sub-domain. (a) Xenoblastic orthopyroxene associated with biotite, quartz, and feldspars in charnockite (sample MGK2-1F1). (b) Biotite flakes distributed along the foliation in biotite gneiss (sample MGK2-1F2). (c) Clinopyroxene + titanite + garnet + plagioclase + quartz assemblage in calc-silicate rock (sample MGK2-1A). (d) Coarse grained biotite + feldspars + quartz + orthopyroxene assemblage in the contact rock (sample MGK2-1N).

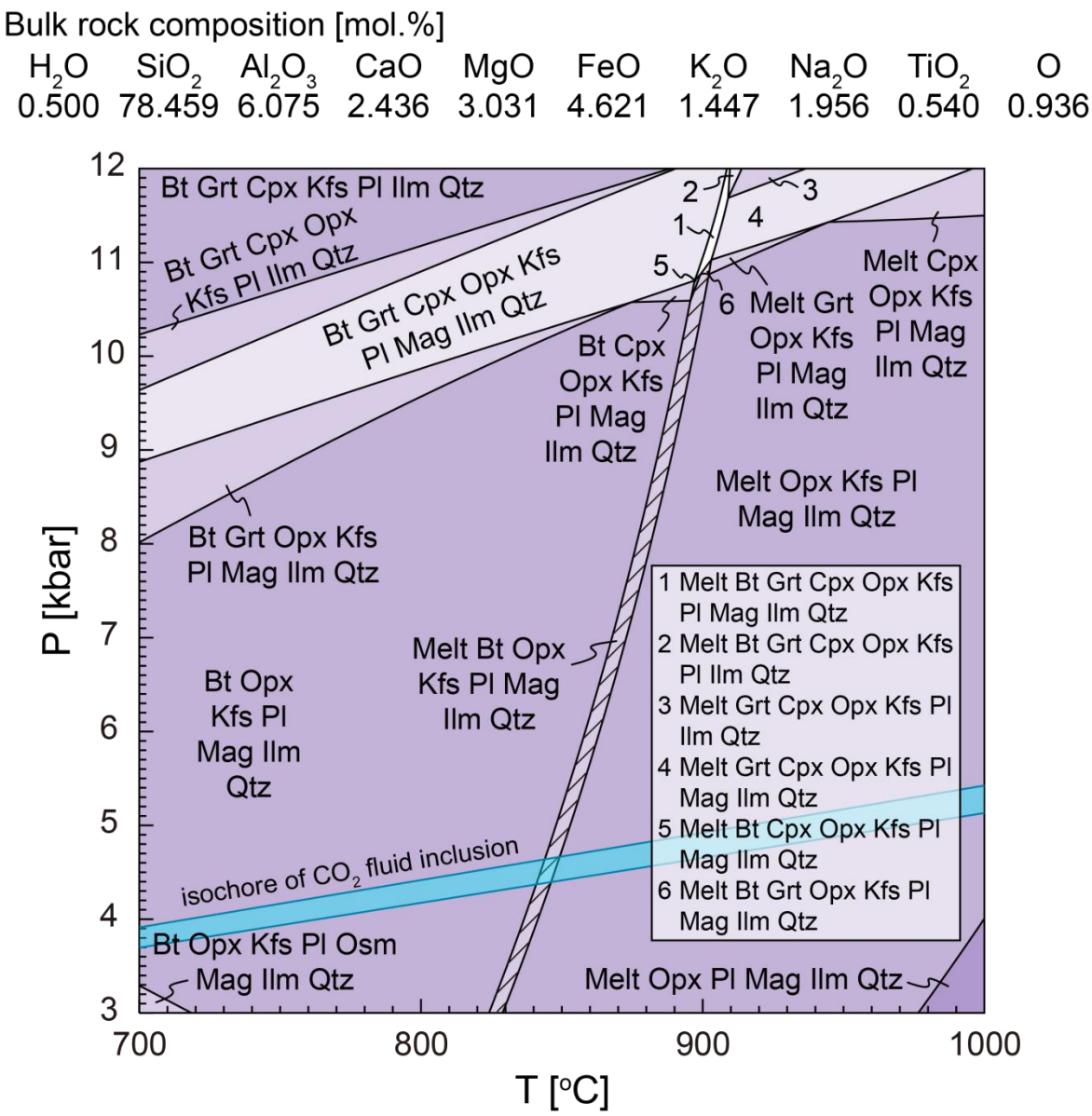

Fig. 12. *P-T* diagram showing a calculated pseudosection of mineral assemblage in incipient charnockite (sample MGK2-1F1) at Ambodin Ifandana in the Ikalamavony Sub-domain of south-central Madagascar. The stability field of the orthopyroxene-bearing mineral assemblage in charnockite is shown as a shaded area. Isochores for carbonic fluid inclusions in sample MGK2-1N is also shown in the diagram.

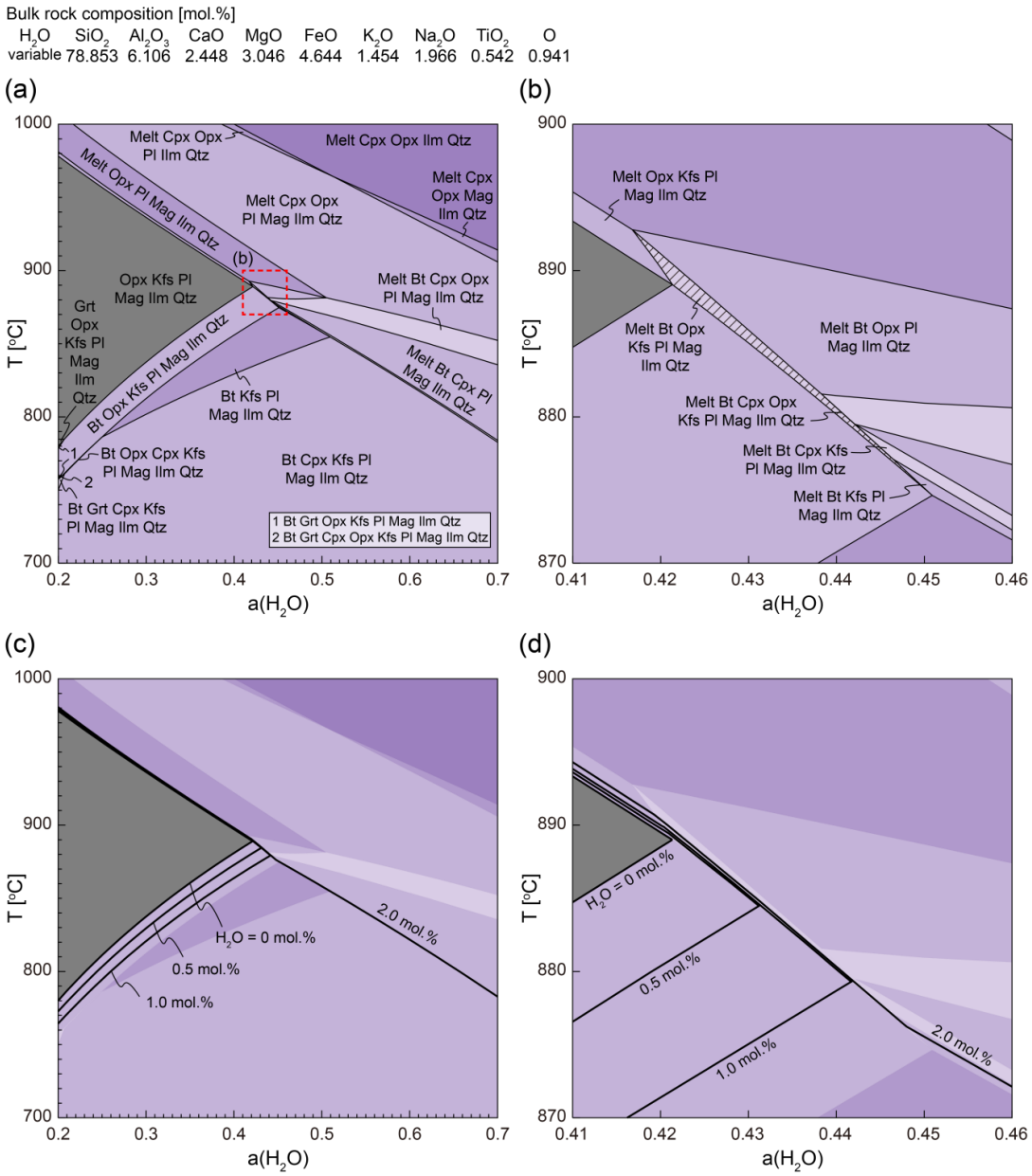

Fig. 13. *T*-*a*(H_2O) diagrams showing calculated pseudosections of mineral assemblage in charnockite (sample MGK2-1F1) from Ambodin Ifandana in the Ikalamavony Sub-domain of south-central Madagascar. Hatched areas show the mineral assemblage of charnockite. (a) *T*-*a*(H_2O) pseudosection at P = 9 kbar. (b) An enlarged *T*-*a*(H_2O) diagram around the area shown in Fig. 13a. (c) *T*-*a*(H_2O) pseudosection with isopleths of molar H_2O content. (d) An enlarged *T*-*a*(H_2O) diagram with isopleths of molar H_2O content around the area shown in Fig. 13a.

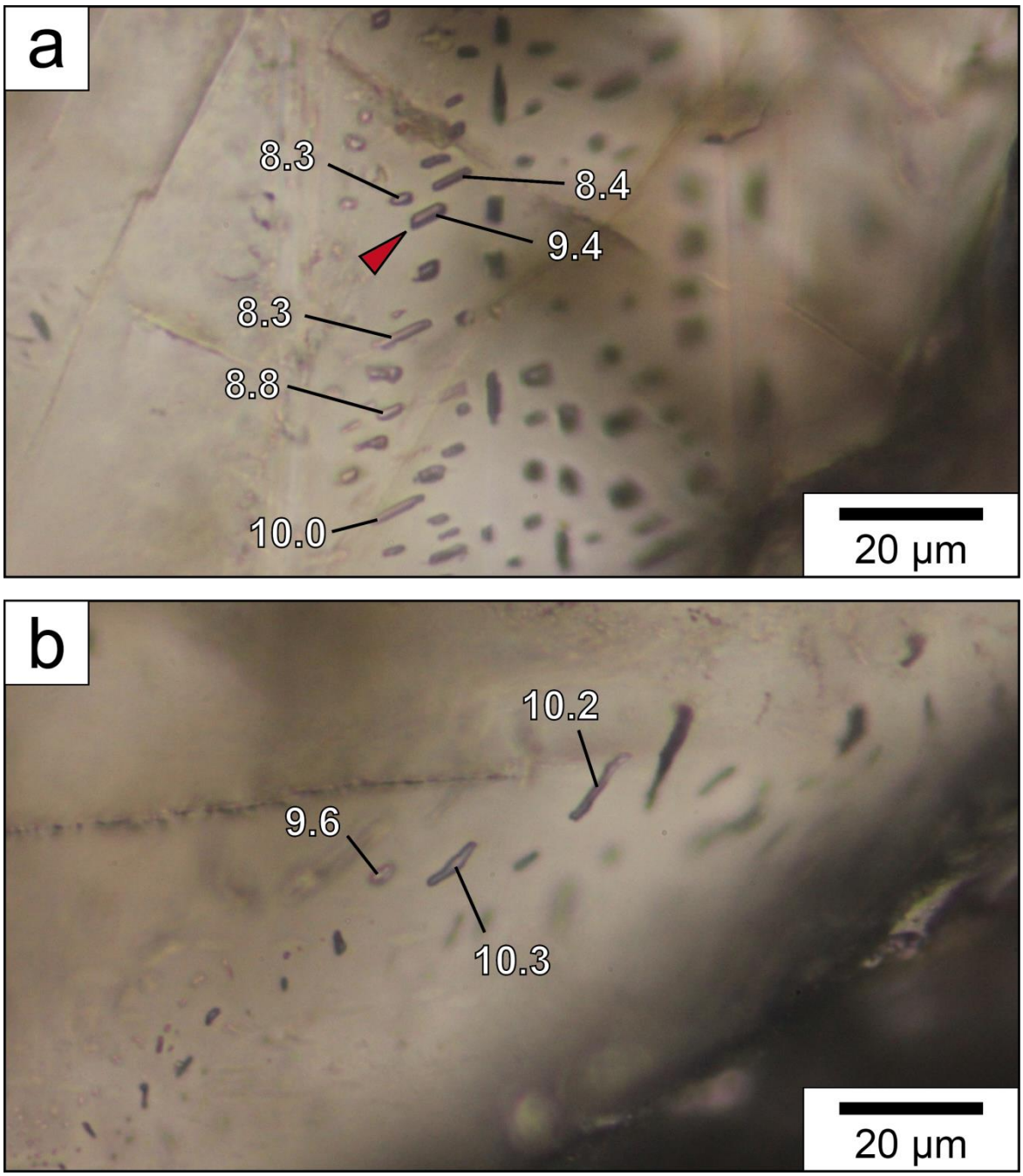

Fig. 14. Photomicrograph of representative fluid inclusions in plagioclase (a) and quartz (b) in coarse-grained charnockite (sample MGK2-1N) from Ambodin Ifandana. Numbers indicate homogenization temperatures (in °C). An arrow in Fig. 14a indicates a grain analyzed for laser Raman spectroscopy (Fig. 16).

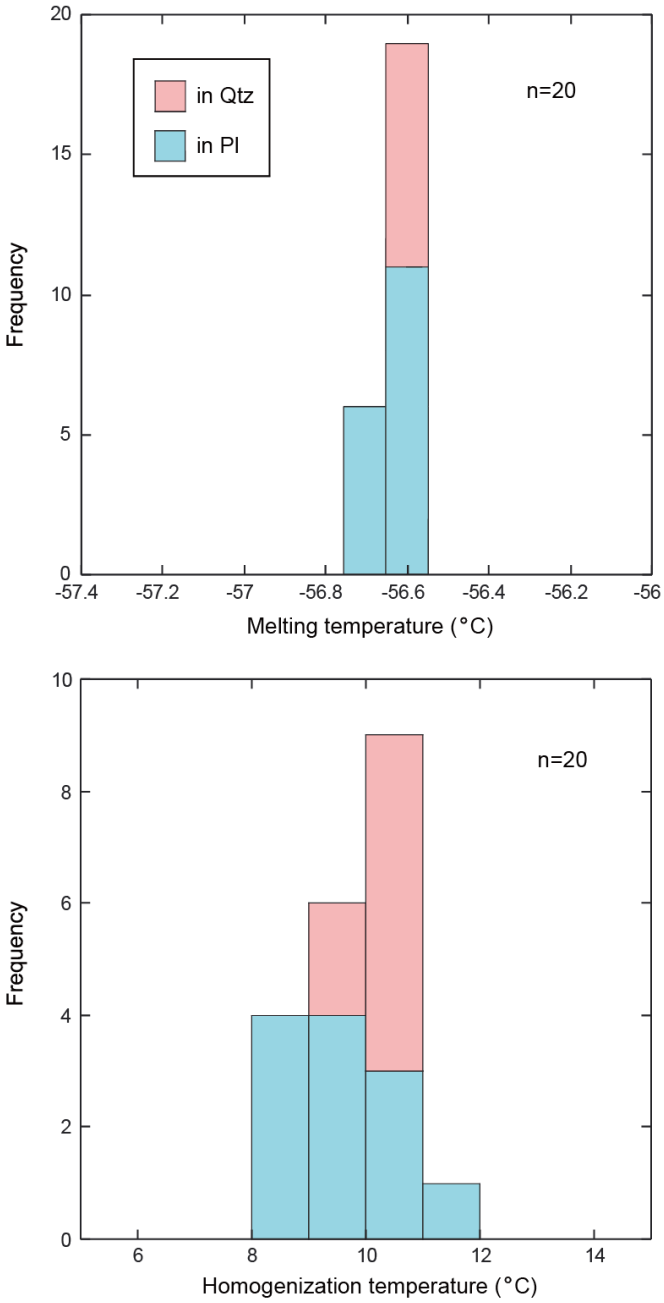

Fig. 15. Histograms showing the distribution of melting (a) and homogenization (b) temperatures of carbonic fluid inclusions in the coarse-grained charnockite (sample MGK2-1N).

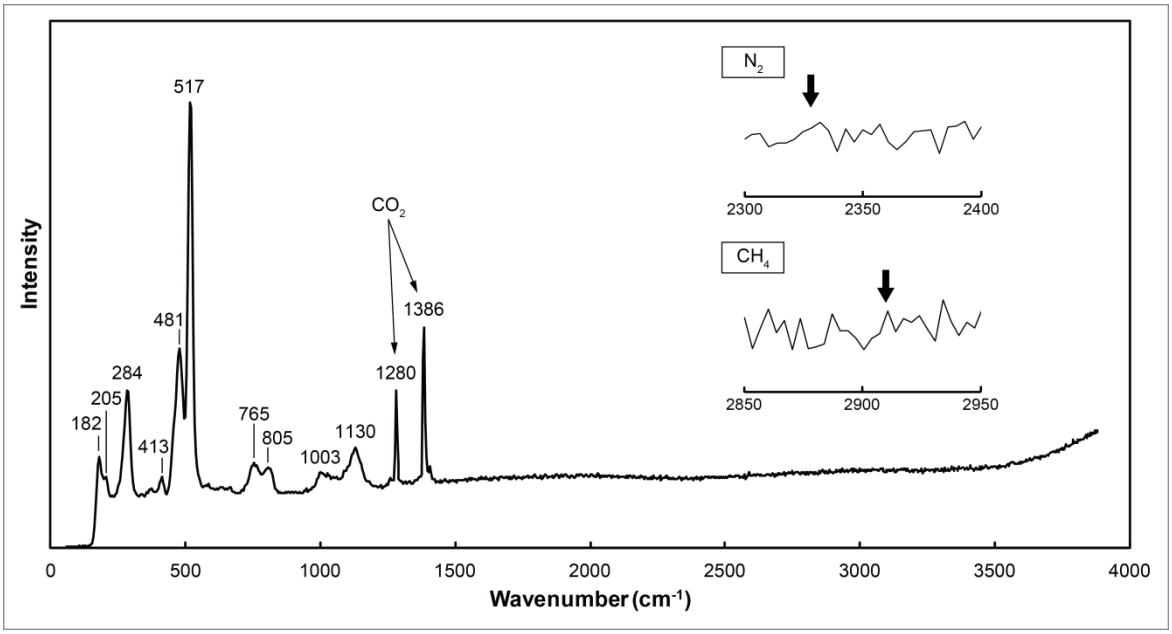

Fig. 16. Raman spectra of a representative fluid inclusion in sample MGK2-1N (coarse-grained charnockite). Peaks of 1280 cm^{-1} and 1386 cm^{-1} correspond to CO_2. Other peaks are derived from host plagioclase.

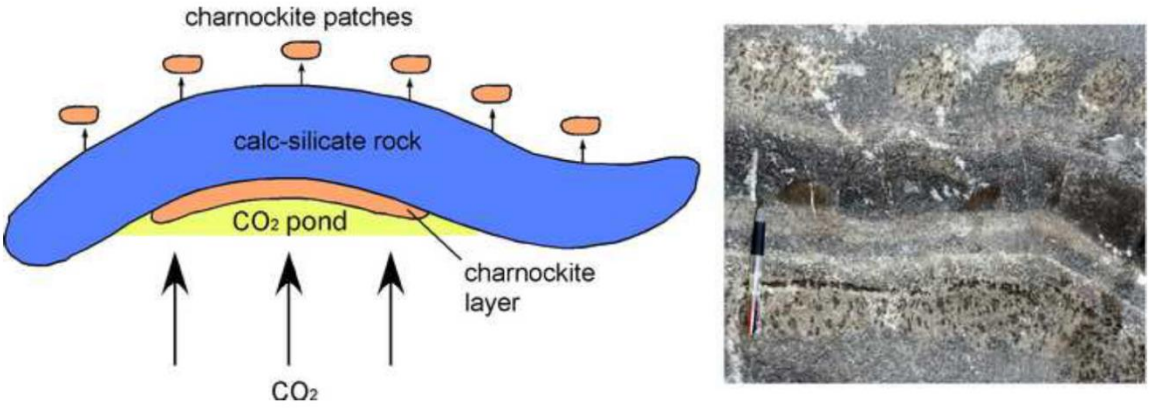

Fig. 17. A schematic model illustrating processes of incipient-charnockite formation at Ambodin Ifandana. Layered charnockite was formed in CO_2 pond, whereas patch charnockite was formed by decarbonation from calc-silicate rock.

Table 4. Representative electron microprobe analyses of pyroxenes (O=6) and garnet (O=12) from Ambodin Ifandana in the Ikalamavony Sub-domain.

Mineral Name	Orthopyroxene				Clinopyroxene		Garnet	
Sample No.	MGK2-1F1	MGK2-1F1	MGK2-1N	MGK2-1N	MGK2-1A	MGK2-1A	MGK2-1A	MGK2-1A
Lithology	CH	CH	CR	CR	CS	CS	CS	CS
Remarks	core	rim	core	rim	core	rim	core	rim
SiO_2	53.34	53.02	52.71	53.76	46.11	46.19	35.84	35.44
Al_2O_3	3.03	2.92	2.91	2.68	5.34	5.19	5.73	5.42
TiO_2	0.05	0.05	0.03	0.00	0.35	0.31	0.94	1.05
Cr_2O_3	0.06	0.04	0.01	0.00	0.04	0.04	0.06	0.03
Fe_2O_3	0.95	1.43	1.76	0.16	7.73	7.46	22.88	22.21
FeO	13.97	13.24	13.66	14.98	9.97	8.46	3.16	3.61
MnO	2.15	2.34	2.02	2.15	1.06	1.13	2.34	2.25
MgO	26.58	26.65	26.41	26.24	7.45	8.12	0.37	0.30
CaO	0.18	0.15	0.25	0.22	22.84	23.06	30.29	29.83
Na_2O	0.02	0.04	0.00	0.03	0.44	0.44	0.02	0.00
K_2O	0.00	0.00	0.00	0.00	0.00	0.00	0.00	0.00
Total	100.35	99.86	99.75	100.21	101.33	100.41	101.61	100.12
Si	1.921	1.918	1.913	1.942	1.771	1.779	2.920	2.933
Al	0.129	0.124	0.124	0.114	0.242	0.235	0.550	0.528
Ti	0.001	0.001	0.001	0.000	0.010	0.009	0.057	0.065
Cr	0.002	0.001	0.000	0.000	0.001	0.001	0.004	0.002
Fe^{3+}	0.026	0.039	0.048	0.004	0.223	0.216	1.402	1.383
Fe^{2+}	0.421	0.400	0.414	0.452	0.320	0.272	0.215	0.250
Mn	0.066	0.072	0.062	0.066	0.034	0.037	0.162	0.157
Mg	1.426	1.436	1.428	1.411	0.426	0.466	0.045	0.037
Ca	0.007	0.006	0.010	0.009	0.939	0.951	2.643	2.645
Na	0.001	0.003	0.000	0.002	0.032	0.033	0.002	0.000
K	0.000	0.000	0.000	0.000	0.000	0.000	0.000	0.000
Total	4	4	4	4	4	4	8	8
X_{Mg}	0.77	0.78	0.78	0.76	0.57	0.63	0.17	0.13
$Fe^{3+}/(Fe^{3+}+Fe^{2+})$	0.06	0.09	0.10	0.01	0.41	0.44	0.87	0.85
Adr (mol.%)							68.6	67.2
Grs (mol.%)							17.6	18.5
Alm (mol.%)							7.0	8.1
Sps (mol.%)							5.3	5.1
Prp (mol.%)							1.5	1.2

Table 5. Representative electron microprobe analyses of biotite (O=22) from Ambodin Ifandana in the Ikalamavony Sub-domain.

Sample No.	MGK2-1F1	MGK2-1F1	MGK2-1F1	MGK2-1F2	MGK2-1F2	MGK2-1N	MGK2-1N
Lithology	CH	CH	CH	BG	BG	CR	CR
Remarks	core	rim	with Qtz	core	rim	with Opx	without Opx
SiO_2	37.36	37.32	37.32	37.20	37.61	37.52	38.12
Al_2O_3	15.72	15.98	15.68	15.91	16.60	15.53	15.25
TiO_2	3.37	3.21	3.11	3.13	3.06	2.49	2.49
Cr_2O_3	0.02	0.01	0.01	0.02	0.04	0.07	0.02
FeO*	8.66	8.54	8.86	10.54	10.30	10.20	9.42
MnO	0.26	0.29	0.22	0.23	0.22	0.21	0.44
MgO	18.59	18.57	18.54	17.25	16.63	18.96	19.16
CaO	0.06	0.08	0.00	0.02	0.03	0.12	0.00
Na_2O	0.08	0.07	0.03	0.08	0.08	0.09	0.03
K_2O	9.49	9.46	9.59	9.29	8.76	9.22	9.58
F	0.53	0.58	0.21	0.31	0.26	0.58	0.24
-O	-0.22	-0.25	-0.09	-0.13	-0.11	-0.24	-0.10
Cl	0.01	0.00	0.00	0.00	0.00	0.00	0.01
-O	0.00	0.00	0.00	0.00	0.00	0.00	0.00
Total	93.92	93.87	93.47	93.84	93.49	94.73	94.66
Si	5.518	5.512	5.534	5.531	5.573	5.527	5.595
Al	2.736	2.781	2.739	2.787	2.898	2.696	2.637
Ti	0.374	0.357	0.347	0.350	0.341	0.276	0.275
Cr	0.003	0.001	0.001	0.002	0.005	0.008	0.003
Fe^{2+}	1.069	1.054	1.098	1.311	1.276	1.257	1.156
Mn	0.033	0.036	0.028	0.029	0.028	0.026	0.055
Mg	4.090	4.085	4.094	3.821	3.670	4.160	4.189
Ca	0.010	0.012	0.000	0.003	0.005	0.018	0.000
Na	0.021	0.020	0.009	0.023	0.022	0.024	0.009
K	1.787	1.782	1.813	1.760	1.656	1.731	1.793
Total	15.643	15.641	15.661	15.616	15.474	15.724	15.711
X_{Mg}	0.79	0.79	0.79	0.74	0.74	0.77	0.78

*: Total Fe as FeO

Table 6. Representative electron microprobe analyses of feldspars (O=8) from Ambodin Ifandana in the Ikalamavony Sub-domain.

Analysis No.	Plagioclase				K-feldspar		
Sample No.	MGK2-1F1	MGK2-1F2	MGK2-1N	MGK2-1A	MGK2-1F1	MGK2-1F2	MGK2-1N
Lithology	CH	BG	CR	CS	CH	BG	CR
Remarks	core	rim	rim	rim			core
SiO_2	58.53	59.10	59.03	45.26	64.54	64.81	64.79
Al_2O_3	25.66	25.68	26.37	35.41	18.65	18.39	18.77
TiO_2	0.00	0.00	0.00	0.05	0.08	0.00	0.00
FeO*	0.04	0.02	0.09	0.47	0.00	0.00	0.05
MgO	0.02	0.01	0.00	0.00	0.00	0.00	0.00
CaO	7.62	7.63	8.29	19.03	0.07	0.10	0.09
Na_2O	6.97	7.21	6.87	0.71	1.04	1.23	1.11
K_2O	0.40	0.22	0.25	0.02	15.03	14.71	14.97
BaO	0.08	0.08	0.00	0.03	0.78	0.47	0.96
Total	99.32	99.96	100.89	100.73	100.18	99.71	100.74
Si	2.635	2.642	2.617	2.073	2.982	2.997	2.981
Al	1.361	1.353	1.378	1.911	1.016	1.002	1.017
Ti	0.000	0.000	0.000	0.002	0.003	0.000	0.000
Fe^{2+}	0.002	0.001	0.003	0.018	0.000	0.000	0.002
Mg	0.001	0.001	0.000	0.000	0.000	0.000	0.000
Ca	0.368	0.365	0.394	0.933	0.004	0.005	0.004
Na	0.608	0.625	0.590	0.063	0.093	0.110	0.099
K	0.023	0.013	0.014	0.001	0.885	0.867	0.878
Ba	0.001	0.001	0.000	0.001	0.014	0.009	0.017
Total	4.999	5.000	4.996	5.002	4.996	4.991	4.999
An (mol.%)	36.8	36.4	39.5	93.6	0.4	0.5	0.4
Ab (mol.%)	60.9	62.3	59.2	6.4	9.3	11.1	9.9
Or (mol.%)	2.3	1.3	1.4	0.1	88.9	87.5	87.9
Cls (mol.%)					1.4	0.9	1.7

*: Total Fe as FeO

CHAPTER 4

Petrogenesis and fluid history of Nuliyam area in the Trivandrum Block, southern India

4.1. Introduction

This study reports the effect of various types of metamorphic fluids associated with an active quarry near the village of Nuliyam from southern India. It is composed of amphibolite-facies gneiss and incipient charnockite closely associated with calc-silicate rock, and shows remarkable precipitation of graphite. Nuliyam area has been studied by Jackson and Santosh (1992) and Harley and Santosh (1995), however, the previous studies leaded different conclusions. Jackson and Santosh (1992) focused on the field relation and carbon isotope study of carbonic fluid inclusion and graphite, and proposed incipient charnockite is formed by decarbonation of adjacent calc-silicate rock. On the other hand, Harley and Santosh (1995) suggested the infiltrated fluid triggering the charnockitization was derived from external sources based on isotopic data and stability field of wollastonite-bearing assemblage of calc-silicate rock and charnockite. In addition, some orthopyroxenes in charnockite are intensely altered and calc-silicate rock shows reaction texture possibly formed by infiltration of fluid. Hence, in this study, petrography and fluid inclusion study of quartzo-feldspathic rocks and calc-silicate rock from the locality were discussed to evaluate the petrogenesis of incipient charnockite in order to understand the detailed fluid history of Nuliyam area.

4.2. Geological setting

The Southern Granulite Terrane (SGT) in India is known for its classic exposures of regionally metamorphosed granulite-facies rocks formed during the collisional orogeny in Late Neoproterozoic to Early Cambrian (~0.55 Ga, e.g. Braun et al., 1998; Santosh et al., 2003, 2006a,b; Collins et al., 2007a,b) related to the amalgamation of Gondwana supercontinent. The

SGT is composed of a collage of Proterozoic crustal blocks exposing mid and lower levels of the continental crust, and is dissected by large Late Neoproterozoic shear/suture zones (Fig. 18). The Trivandrum Granulite Block (TGB), also known as the Kerala Khondalite Belt, is a vast accretionary belt developed during the Neoproteorzoic-Cambrian subduction-collision history associated with the final amalgamation of Gondwana (Santosh et al., 2009), and comprises dominantly metasedimentary sequence with khondalites (granulite facies metapelites), leptynites (metamorphosed psammpelitic rocks) and charnockites (garnet and orthopyroxene-bearing felsic granulites). Quartzite, mafic granulite, calc-silicate rocks, and fragments of meta-ultramafic rocks are also present subordinately.

The TGB is also known as one of the classic examples for the spectacular development of 'incipient charnockites' within orthopyroxene-free felsic gneisses as exposed in several quarry sections in the states of Kerala and Tamil Nadu. The charnockite-forming process in the TGB is considered to have been triggered by the infiltration of CO_2-rich anhydrous fluids along structural pathways within upper amphibolite-facies gneisses, resulting in the lowering of water activity and stabilization of orthopyroxene through the breakdown of biotite (e.g. Janardhan et al., 1979; Hansen et al., 1987; Santosh et al., 1990; Newton, 1992). The metamorphic *P-T* condition estimated for garnet-bearing charnockite is 700-870ºC and 7-8 kbar (e.g. Santosh, 1986; Chacko et al., 1987; Santosh et al., 1990; Tsunogae and Santosh, 2003), although ultrahigh-temperature (UHT) conditions of T >900°C (e.g. Chacko et al., 1996; Nandakumar and Harley, 2000) have also been reported particularly from garnet + spinel + quartz + sillimanite assemblages in khondalite (Morimoto et al., 2004; Tadokoro et al., 2008).

The studied locality is an active quarry near Nuiliyam village approximately 50 km southeast

from Trivandrum city. The quarry is composed of felsic orthogneisses and calc-silicate rocks. The felsic orthogneisses, which is very coarse-grained and massive, are mostly leucocratic, although the rock around coarse-grained amphibole (~1 cm) and clinopyroxene are characteristically greenish in color. The width of the green-color rock is about 20 cm to 2 m. The calc-silicate rocks occur as minor enclaves of several tens of centimeters. It is important to note that coarse-grained (~1 cm) graphite occurs in the felsic gneiss and charnockite. Detailed petrological and fluid inclusion studies have been done by Jackson and Santosh (1992) and Harley and Santosh (1995) for dominant lithologies in this locality. Jackson and Santosh (1992) reveals reaction front and isotope front based on the gap of isotopic data of the inclusions between charnockite (-13.3 ‰) and gneiss (-15.9 ‰), and indicates that the heaviest carbon of graphite in charnockite adjacent to calc-silicate rock (~10 ‰) implies decarbonation of calc-silicate as a possible source of carbonic fluid. In contrast, Harley and Santosh (1995) reexamined petrogenesis of the quarry based on detailed field association of particularly wollastonite-bearing assemblage in calc-silicate rock, which suggested the wollastonite-bearing assemblage is not stable under high $X\mathrm{CO_2}$ condition (> 0.85) forming incipient chanockite at an inferred *P-T* condition (5 kbar, 725°C). Therefore, they proposed the infiltrated fluid is considered to be derived from external source rather than decarbonation of calc-silicate rock. They further argued that calc-silicate rocks played an important role and acted as a relatively unreactive and impermeable barrier to fluid transport and caused fluid ponding as antiformal cap rock. They proposed a fluid-pond model to explain isotopically heaviest carbon of graphite from charnockite beneath calc-silicate rock. Although the above two studies worked on the same materials, their conclusions are completely different from each other, and still controversial.

4.3. Petrography

4.3.1. Greenish quartzo-feldspathic rock

This quarry is mainly composed of quartzo-feldspathic rocks, which can be subdivided into two types; a small-scale greenish quartzo-feldspathic rock around coarse-grained amphibole and clinopyroxene, and a large-scale leucocratic quartzo-feldspathic rock.

The greenish quartzo-feldspathic rock (sample KR22-1B) is composed mainly of clinopyroxene, amphibole, perthite, plagioclase, quartz, and ilmenite with accessory apatite and zircon. Clinopyroxene (0.2-0.7 mm) is rounded in shape and its rim is sometimes modified to amphibole (Fig. 20a). Coarse-grained perthite (0.5-7.9 mm) and minor quartz (0.3-1.0 mm) is present around clinopyroxene. On the other hand, coarse-grained brownish amphibole (0.5-9.0 mm) is associated with coarse-grained plagioclase (1.0 mm to 2.1 cm) (Fig. 20b), forming coarse-grained amphibole + plagioclase domains. Ilmenite (0.1-1.3 mm) is also present around the coarse-grained amphibole. Such coarse-grained brownish amphibole is partially modified to bluish amphibole and rare biotite, particularly along cleavage and/or crack of the host minerals (see Fig. 20b). Plagioclase is slightly altered and contains fine-grained secondary minerals (e.g., sericite), which is obviously different from un-altered perthite around clinopyroxene. Zircon is very rare and, if present, shows composite zonings composed of several domains (Fig. 20c). The outermost portion of such composite zircons is often intergrown with secondary amphibole.

4.3.2. Leucocratic quartzo-feldspathic rock

The leucocratic quartzo-feldspathic rock (sample KR22-1A) is mostly composed of perthite

(70-80 %) and quartz (20-30%) (Fig. 20d) with accessory ilmenite and apatite. Both perthite (1.9-9.2 mm) and quartz (1.3 mm to 1.1 cm) are coarse-grained and subidioblastic to xenoblastic. Thin myrmekite is formed along grain boundaries of the minerals.

4.3.3. Calc-silicate rock

Mineral assemblages and color of a calc-silicate rock shown in Figure 20e gradually change from white to dark grayish to brownish. Thus each lithology/assemblage are numbered from the center of the calc-silicate rock (white) toward the outside (brownish) as calc-silicate 1 to 5 (samples KR22-1D1 to KR22-1D5).

Calc-silicate 1 (sample KR22-1D1), which corresponds to the central portion of the calc-silicate rock, is composed of scapolite (50-60 %), wollastonite (20-30 %), and clinopyroxene (15-20 %) with accessory calcite and titanite (Fig. 20f). Although the protolith of the rock might be limestone, its primary textures are considered to have been completely modified by high-grade metamorphism. Scapolite (0.8-5.3 mm), wollastonite (1.5-4.8 mm), and clinopyroxene (2.4-3.8 mm) are coarse-grained and show granoblastic texture. Wollastonite has exsolution lamellae composed of clinopyroxene, iron-wollastonite, apatite, and quartz. The wollastonite is sometimes surrounded by thin clinopyroxene which is considered to be related to later overprinting. Rare quartz is present with calcite, which is interpreted as a product of a retrograde reaction related to breakdown of wollastonite.

Calc-silicate 2 (sample KR22-1D2) is composed of scapolite (30-40 %), clinopyroxene (25-35 %), quartz (25-35 %), and titanite (2-3 %) with accessory calcite and K-feldspar (Fig. 20g). Scapolite (0.1-1.5 mm) and quartz (0.2-1.3 mm) are medium-grained and xenoblastic. The scapolite is characterized by numerous inclusions of fine-grained and rounded quartz. Scapolite

also occurs as rare fine-grained phase associated with quartz, forming scapolite + quartz symplectite (Fig. 20h). Such a texture could have been formed by a reaction with melt phase because K-feldspar associated with the symplectite shows high BaO content as discussed in later chapters. Clinopyroxene (0.1-1.5 mm) sometimes fills grain boundaries of coarse-grained scapolite and quartz.

Calc-silicate 3 (sample KR22-1D3) is composed of clinopyroxene (25-35 %), plagioclase (20-30 %), quartz (20-30 %), scapolite (10-15 %), K-feldspar (4-5 %), amphibole (3-4 %), and titanite (2-3 %) with accessory apatite, ilmenite, and zircon (Fig. 20i). Clinopyroxene (0.3-3.1 mm) is partially replaced by greenish amphibole (0.1-1.5 mm) of retrograde origin. Plagioclase (0.3-3.3 mm) and quartz (0.3-4.1 mm) are coarse-grained and scattered in matrix. Scapolite (0.3-5.0 mm) is often altered along cleavage. K-feldspar (0.1-0.8 mm) and titanite (0.1-0.7 mm) are relatively small, and subidioblastic to xenoblastic. Bluish amphibole is finer than the greenish amphibole around clinopyroxene, and is considered to have been formed at a later stage. Apatite and titanite sometimes show compositional zoning composed of several discrete domains (Fig. 20j and 20k).

Calc-silicate 4 (sample KR22-1D4) is composed of quartz (40-50 %), plagioclase (20-30 %), clinopyroxene (20-30 %), K-feldspar (2-3 %), titanite (2-3 %), and amphibole (1-2 %) with accessory apatite, zircon, and ilmenite (Fig. 20l). Quartz (0.2-2.0 mm), clinopyroxene (0.1-1.5 mm), titanite (0.2-1.0 mm) is scattered in matrix, although K-feldspar (0.1-0.6 mm) is mainly present along grain boundaries. Amphibole (0.1-0.4 mm) partially replaces clinopyroxene probably related to retrograde hydration. Plagioclase (0.2-2.6 mm) shows a characteristic occurrence with abunant myrmekite.

Calc-silicate 5 (sample KR22-1D5) is composed of perthite (55-65 %), clinopyroxene (15-20 %), quartz (10-15 %), amphibole (2-3 %), and titanite (1-2 %) with accessory apatite,

zircon, and ilmenite (Fig. 20m). Most feldspars occur as perthite (0.6-4.0 mm) similar to the texture of the host quartzo-feldspathic rock in which K-feldspar and plagioclase are present only along grain boundaries. Clinopyroxene (0.4-2.5 mm), quartz (0.4-2.6 mm), and titanite (0.3-1.5 mm) are scattered in matrix. Amphibole (0.1-2.0 mm) is present in matrix, and partially replaces clinopyroxene. Apatite shows complex compositional zoning similar to that in calc-silicate 3.

It has to be noted that calc-silicate rocks are sometimes affected by strong local-scale alteration, where xenomorphic graphite commonly occurs as grains with lint-like shape (Fig. 20n). It is generally known that formation of graphite associated with marbles is related with either decarbonation during high-grade metamorphism, or reduction and precipitation from CO_2-rich fluid. The formation of graphite in this case is considered to have been related to hydrothermal alteration during a retrograde stage on the basis of its occurrence.

4.4. Mineral chemistry

Mineral chemical analyses were carried out using an electron microprobe analyzer (JEOL JXA8530F) at the Chemical Analysis Division of the Research Facility Center for Science and Technology, the University of Tsukuba. The analyses were performed under conditions of 15 kV accelerating voltage and 10 nA sample current, and the data were regressed using an oxide-ZAF correction program supplied by JEOL. Representative compositions of minerals in the analyzed samples are given in Tables 7 to 11.

4.4.1. Calcic amphibole

Brownish amphibole in greenish quartzo-feldspathic rock (sample KR22-1A) is Fe-rich (X_{Mg} =

0.29-0.30), characterized by the highest TiO_2 content (2.27-2.78 wt.% correspond to 0.27-0.33 pfu) and the lowest $X\mathrm{Fe}^{3+}$ (=$\mathrm{Fe}^{3+}/(\mathrm{Fe}^{2+}+\mathrm{Fe}^{3+})$ in mole) of 0-0.05, and classified as ferro-pargasite based on the classification of Leake et al. (1997). Its fluorine and chlorine contents are 0.50-0.65 wt.% and 1.19-1.34 wt.%, respectively. On the other hand, bluish amphibole partially replacing brownish amphibole shows lower TiO_2 content (0.49-0.78 wt.%) and higher $X\mathrm{Fe}^{3+}$ (0.12-0.14) and chlorine content (2.15-2.73 wt.%), whereas its X_{Mg} and fluorine content (0.27-0.29 and 0.44-0.63 wt.%, respectively) are similar to those of brownish amphibole. Such compositional variations as well as the exsolution of ilmenite within the brownish amphibole suggest temperature decrease and formation of late-stage bluish amphibole. Amphiboles of other occurrences (Figs. 20a and 20c) show clearly different compositions with intermediate TiO_2 and chlorine content (0.97-1.75 wt.% and 1.31-1.58 wt.%, respectively) and scattered X_{Mg} (0.24-0.28) from the above two types of amphibole.

Amphiboles in calc-silicates 3, 4, and 5 (samples KR22-1D3, 4, and 5) are either greenish or bluish. The greenish amphiboles is Fe-rich, and its Mg content increases from the internal portion toward the margin of the calc-silicate enclave as X_{Mg} = 0.15 (calc-silicate 3) to 0.28 (calc-silicate 5). Its fluorine, chlorine, and TiO_2 contents show relatively scattered values as 0.173-0.461 wt.%, 0.047-1.448 wt.%, and 0.300-1.183 wt.%, respectively. Fe^{3+} content is low, $X\mathrm{Fe}^{3+}$ = 0.11-0.21. On the other hand, bluish amphibole shows lower TiO_2 (0.061-0.163 wt.%) and chlorine (0.016-0.235 wt.%) contents and slightly higher $X\mathrm{Fe}^{3+}$ (0.20-0.22) than those of greenish amphibole, whereas its fluorine content (0.217-0.409 wt.%) is similar to that of greenish amphibole. Its X_{Mg} shows a broad range of 0.26-0.36.

4.4.2. Clinopyroxene

Clinopyroxene occurs in a greenish quartzo-feldspathic rock (sample KR22-1A) and in all calc-silicate rocks 1 to 5 (samples KR22-1D1, 2, 3, 4, and 5). Clinopyroxene in the greenish quartzo-feldspathic rock (sample KR22-1A) is Fe-rich as X_{Mg} = 0.35, which corresponds to the highest value among the examined samples from this quarry. There is no compositional zoning in the clinopyroxene. Clinopyroxene in the matrix of calc-silicate 1 also shows Fe-rich composition as X_{Mg} = 0.19-0.22. Exsolution lamella of clinopyroxene in wollastonite in the same sample is Mg-poor as X_{Mg} = 0.07-0.08, whereas clinopyroxene rimming wollastonite and rim of clinopyroxene in contact with wollastonite have intermediate values as X_{Mg} = 0.12-0.19. Magnesium content of clinopyroxenes in calc-silicates 2, 3, 4, and 5 increases from the interior toward the margin of the calc-silicate enclave as X_{Mg} = 0.19 (calc-silicate 2) to 0.26 (calc-silicate 5), although compositional zoning is absent in single clinopyroxene grains.

Wollastonite in calc-silicate 1 shows pure Mg-end member composition of $Ca_5MgSi_6O_{18}$, possibly purified by later exsolution of other components. The composition of iron-wollastonite present as exolution lamellae in wollastonite is close to $Ca_5FeSi_6O_{18}$, which is a common composition of wollastonite in skarn.

4.4.3. Scapolite

Scapolite is present in calc-silicates 1, 2, and 3 (samples KR22-1D1, 2, and 3). Scapolite in calc-silicate 1 shows meionite-rich composition as 72-73%. Its equivalent anorthite (Eq_{An}) value based on EPMA analyses normalized with Si + Al = 12 (Evans et al., 1969) is 59-61. Chlorine content of scapolite in calc-silicate 1 is low, 0.551-0.723 wt.%. Scapolite in the matrix of calc-silicate 2 shows slightly lower meionite content (65-69%) and Eq_{An} value (58-59), and higher chlorine content (0.648-0.782 wt.%). Composition of scapolite comprising scapolite +

quartz symplectite (Fig. 20h) is similar to that of matrix phase, particularly in meionite (66%) and chlorine content (0.634 wt.%), although its Eq_{An} value is clearly low as 44. Scapolite in calc-silicate 3 shows compositional zoning with decreasing meionite content and Eq_{An} value from core toward rim. Meionite content and EqAn value also decrease from center (calc-silicates 1) toward margin (calc-silicate 3) of the calc-silicate enclave as 35 to 70% and 33 to 60, respectively. In contrast, chlorine content (0.781-2.672) increases from center (0.781) toward margin (2.672) of the enclave. In addition, scapolite is partly modified along cleavage, which is characterized by local decreasing in meionite content (35-61%) and Eq_{An} value (33-55), and increasing chlorine content (1.014-2.672 wt.%).

4.4.4. Feldspars

K-feldspar occurs in greenish quartzo-feldspathic rock (sample KR22-1A), leucocratic quartzo-feldspathic rock (sample KR22-1B), and calc-silicate 2, 3, 4, and 5 (samples KR22-1D2, 3, 4, and 5). Most K-feldspars show similar orthoclase-rich compositions as Or_{87-94}. K-feldspar in greenish quartzo-feldspathic rock filling grain boundaries of quartz and plagioclase are slightly orthoclase-rich (Or_{97}). BaO content of K-feldspar in greenish and leucocratic quartzo-feldspathic rocks is low as 0-0.129 wt.%. Matrix K-feldspar in calc-sdilicate 2 is also depleted in BaO (0.046-0.164 wt.%). In contrast, K-feldspar with scapolite + quartz symplectite is BaO-rich as 1.44 wt.%. K-feldspar in calc-silicate 3, 4, and 5 show the highest and scattered BaO contents of 0.276-2.460 wt.%.

Plagioclase is present in greenish quartzo-feldspathic rock, leucocratic quartzo-feldspathic rock, and calc-silicate 3, 4, and 5. In the greenish quartzo-feldspathic rock, plagioclase occurring as exsolution lamellas in perthite shows uniform albite-rich compositions of

$An_{22-23}Ab_{76-77}Or_1$. On the other hand, plagioclase around amphibole is slightly anorthite- and orthoclase-rich as $An_{24-28}Ab_{70-75}Or_{2-3}$. The higher orthoclase content of the latter plagioclase is probably due to its close association with K-feldspar (Kroll et al., 1993). In the leucocratic quartzo-feldspathic rock, plagioclase occurring as exsolution lamellae in perthite is albite-rich as $An_{15-19}Ab_{80-84}Or_1$., whereas that forming grain-boundary myrmekite shows a broad compositional range of $An_{13-23}Ab_{76-82}Or_{0-1}$. Plagioclases in calc-silicate 3, 4, and 5 are also Ab-rich as An_{27-35}, An_{26-29}, and An_{5-21}, respectively. Some of plagioclases in calc-silicate 5 might have been modified by later infiltration of aqueous fluids because of its extremely high albite contents.

4.5. Geothermometry

4.5.1. Ternary feldspar geothermometry

Metamorphic temperature was estimated by using ternary feldspar geothermometry of perthites in greenish quartzo-feldspathic rock (sample KR22-1B) and leucocratic quartzo-feldspathic rock (sample KR22-1A) based on the technique described in Hokada (2001) and the thermodynamic model of Fuhrman and Lindsley (1988). Other geothermobarometric methods cannot be applied because of lack of appropriate mineral assemblages suitable for *P–T* calculations. Thus metamorphic pressure was assumed as 5 and 10 kbar for the temperature calculations in order to cover the range of inferred peak pressures of the Trivandrum Block reported in previous study (~ 10 kbar, Tadokoro et al., 2008). The integrated compositions of ternary feldspars were calculated based on the volume proportion of host domains and lamellae and calibrated densities

of K-feldspar and plagioclase (2.56 and 2.66 g/cm^3, respectively). Figure 21 shows the ternary plot of host-K-feldspar, lamella-plagioclase, and integrated-feldspar compositions for the perthites in greenish and leucocratic quartzo-feldspathic rocks (samples KR22-1B and KR22-1A). The estimated temperatures are around 900°C at both 5 and 10 kbar, which is close to the peak condition of the Trivandrum Block.

4.5.2. Crystallinity of graphite

Previous mineralogical and petrological investigations of graphite indicate that crystallinity of graphite changes irreversibly with increasing metamorphic temperature, threfore correlations of its crystallinity and temperature have been argued on various techniques (e.g., French 1964; Kisch 1980; Buseck and Huang 1985). Kouketsu et al. (2014) evaluated Raman spectra of graphite and metamorphic temperatures of the host metasedimentary rocks, and constructed a geothermometer for low-grade metamorphic rocks. Figure 22 shows a laser Raman spectrum of graphite from locally altered domain in the calc-silicate rock (sample KR22-1D3). Well-crystalized graphite formed at upper amphibolite to granulite-facies metamorphism is completely crystalized and generally shows single peak on Raman spectroscopy, whereas the crystallinity showing three peaks in this study is low and probably corresponds to a condition less than 400°C. The estimated temperature is clearly lower than the peak metamorphism of the Trivandrum Block (~900°C).

4.6. Fluid inclusions

This study performed petrographic, microthermometric, and laser Raman spectroscopic studies

of fluid inclusions in leucocratic quartzo-feldspathic rock (sample KR22-1A). The heating and cooling experiments of fluid inclusions have been done using an optical microscope and a Linkam heating/freezing system at the University of Tsukuba following the technique described in Ohyama et al. (2008) and Tsunogae et al. (2008a). Heating rates of the samaples are 1°C/min for the measurements of melting temperatures (*Tm*) and 5°C/min for the homogenization temperatures (*Th*). Repeated microthermometric measurements indicate that the precision of microthermometric results reported in this study is within ±0.1°C for *Tm* and ±0.2°C for *Th*. Laser Raman spectroscopy was carried out at room temperature and multi-phase inclusion is analyzed at both of vapor and liquid respectively. In this study, fluid inclusions in quartz within leucocratic quartzo-feldspathic rock (sample KR22-1A) were analyzed because the mineral contains numerous fluid inclusions. In contrast, other minerals are not suitable for the analysis because of the presence of exsolution lamellae in feldspars and intense alteration in scapolite.

The analysis revealed the presence of various types of fluids. CO_2-rich secondary fluid inclusions are ovoid and irregular in shape. Their homogenization temperatures are around 20°C suggesting its low density. Figures 23a and 24a are a photograph of an analyzed CO_2-rich fluid inclusion and its representative spectrum, respectively. Laser Raman spectroscopy analysis detected two types of CO_2-rich fluid inclusions: pure CO_2 and CO_2-N_2-CH_4 fluids. H_2O-rich secondary fluid inclusions show irregular shape. Their melting temperatures are more than –6.8°C, which implies that its salinity is not so high. Figures 23b and 24b show a texture of representative H_2O-rich fluid inclusion and their spectrum, respectively. The laser Raman spectroscopy traced four types of H_2O-rich fluid (H_2O, H_2O-CO_2, H_2O-CO_2-N_2, H_2O-N_2-CH_4). N_2-rich fluid inclusions show ordinary polyhedral shape. Arrays of such N_2-rich fluid inclusions are sometimes cut by those of H_2O-rich fluid inclusions, which suggests the N_2-rich fluid inclusions were trapped at earlier stage than the H_2O-rich fluid inclusions. The

microthermometry of N_2-rich inclusions indicates their homogenization temperatures are ~–156°C. Figures 23c and 24c are a representative fluid inclusion photograph and its spectrum, respectively, which suggests N_2-rich fluid inclusion is composed of N_2 and CH_4. Totally seven different types of fluid inclusions were detected in this study.

4.7. Discussion

4.7.1. Petrography and mineral chemistry

The studied quarry is composed of greenish quartzo-feldspathic rock, leucocratic quartzo-feldspathic rock, and calc-silicate enclaves. Clinopyroxene and amphiboles in the greenish quartzo-feldspathic rock show characteristic occurrences; (1) clinopyroxene is partially replaced by amphibole and (2) coarse-grained brownish amphibole is retrogressed to secondary bluish amphibole along cleavage and cracks. Zircon in greenish quartzo-feldspathic rock intergrowths with amphibole and shows domain-like zoning (Fig. 20c). Similar compositional zonings are also found in apatite and titanite in calc-silicate rocks (Figs. 20j and 20k). Graphite occurs in intensely altered calc-silicate rock.

Bluish amphibole in greenish quartzo-feldspathic rock is enriched in chlorine (2.15-2.73 wt.%) than brownish amphibole (1.19-1.34 wt.%) in the same rock, suggesting two discrete events of fluid infiltration took place to from the amphiboles. This two-stage infiltration of the aqueous fluid might be supported by complex compositional zonings recorded in zircon, apatite, and titanite. Fluorine contents of brownish (0.50-0.65 wt.%) and bluish (0.44-0.63 wt.%) amphiboles are similar, although fluorine content of amphibole is generally controlled by its X_{Mg} rather than the condition of fluid infiltration (e.g., Tsunogae et al., 2003a).

4.7.2. Fluid inclusions

Fluid inclusion study of the quartzo-feldspathic rock reveals the presence of CO_2-rich, H_2O-rich, and N_2-rich fluids. Petrographical observations of the inclusions suggest that array of H_2O-rich fluid inclusions cuts that of N_2-rich fluid inclusions, suggesting that N_2-rich fluid was trapped before the H_2O-rich fluid. This is consistent with the ordinary negative-crystal shape of the N_2-rich fluid inclusions, which is obviously different from irregular-shape H_2O-rich fluid inclusions. On the other hand, the relations between CO_2-rich fluid and other fluids are unclear. However, CO_2-rich fluid might have been trapped during prograde, peak, and retrograde stages because CO_2-rich fluid can be derived both from decarbonation of carbonates during high-grade metamorphism and from external sources. In addition, the various components in the fluids imply presence of various fluids possibly derived from several sources and trapped at different stages.

In this quarry, carbonic fluid could have played an important role because of the precipitation of graphite. A clearly lower-temperature condition obtained for the graphite (<400°C based on Kouketsu et al., 2013) than the peak condition inferred from ternary-feldspar geothermometer (~900°C) suggests that the graphite was not derived from carbon in the protolith (carbonates) but precipitated from a retrograde fluid. Such a very low-temperature condition of graphite also suggests the graphite formation is not directly related to the formation of the incipient charnockite of Nuliyam area. Huizenga and Touret (2012) argued that precipitation of graphite from fluid phases generally takes place at granulite-facies peak metamorphism and also during retrograde stage, and showed that interpreting the presence or absence of graphite requires detailed information of pressure-temperature-oxygen fugacity

condition, a relative amount of CO_2, and whether H_2O is present or not. Although precipitation process of graphite in this locality is still unknown because the stage of graphite formation is still ambiguous, increasing Fe^{3+} in secondary bluish amphibole may imply that the fomation of graphite is resulted from the progress of reduction reactions of carbonic fluid related to oxidation of Fe^{2+} in other minerals.

4.7.3. Petrogenesis of Nuliyam area

Jackson and Santosh (1992) and Harley and Santosh (1995) reported that the dominant lithologies in Nuliyam area are calc-silicate rocks (Qtz+Cpx+Cal+Gr) with wollastonite-rich seams and veins (Wo+Scp+Cc+Cpx or Wo+Scp+Qtz+Cpx) and amphibolite-facies garnet-biotite gneiss (Grt+Bt+Fsp+Qtz). Incipient charnockite occurs in the garnet-biotite gneiss closely associated with the calc-silicate rock. The calc-silicate rock shows reaction textures of polygonal calcite-quartz mosaics formed by break down of wollastonite, and symplectite of scapolite + quartz resulted from a reaction containing fluid phase ($Wo+Kfs+Na^+(fluid)+CO_2=Scp+Qtz+K^+(fluid)$). Jackson and Santosh (1992) carried out carbon isotope study of CO_2-rich fluid inclusions and graphites, and proposed dehydration-reaction fronts and carbon-isotope fronts between the incipient charnockite and host amphibolite-facies garnet-biotite gneiss because the incipient charnockite contains heavier carbon than the host gneiss. They further argued decarbonation of calc-silicate rocks provides a sufficient source of fluid triggering the formation of the incipient charnockite. On the other hand, Harley and Santosh (1995) reexamined the detailed field occurrence and distribution of the incipient charnockite, and evaluated the stability field of wollastonite-bearing mineral assemblage coexisting with CO_2-rich fluid, which implies infiltrated CO_2-rich fluid was derived from

external sources rather than decarbonation of in-situ calc-silicate rocks. They further suggested the calc-silicate rocks acted as a relatively unreactive and impermeable barrier to fluid transport, and heavier carbon isotope near the calc-silicate rocks is derived from fluid ponds formed by structural trap.

In this study, two-stage infiltrations of fluorine and chlorine-bearing hydrous fluid are suggested. The rocks investigated in this study and previous two studies from the same locality are considered to have a similar *P-T* path and fluid history, and such fluorine and chlorine-bearing high solubility hydrous fluids may be suitable for the formation symplectite of scapolite + quartz indicated by Harley and Santosh (1995). On the other hand, very low-temperature condition of the graphite formation inferred in this study implies that the graphite formation is not directly related to the formation of incipient charnockite. The formation of incipient charnockite triggered by decarbonation in Madagascar, discussed in Chapter 3, suggests carbonic fluid of decarbonation origin is usually released around peak metamorphism or slightly post-peak decompression stage under granulite-facies condition. The metamorphic condition of the Trivandrum Block is higher than the Ikalamavony sub-domain in Madagascar, therefore the *P-T* condition of incipient-charnockite formation in southern India is generally lower than the regional peak metamorphism. Therefore, charnockitization caused by infiltration of carbonic fluid derived from adjacent calc-silicate rock may not be suitable in this case of southern India. It is important to note that the central part of a large calc-silicate enclave in this quarry is not completely altered, which is different from petrographical observations of other lithologies. This confirms that calc-silicate rocks acted as an impermeable barrier to fluid transport and forms fluid ponds as suggested by Harley and Santosh (1995). The various types of fluid inclusions reported in this locality also support the role of calc-silicates as impervious cap rocks. Therefore, the result of this study support the model of Harley and Santosh (1995)

that the formation of incipient charnockite in the Nuliyam area was caused by infiltration of carbonic fluid of external sources. The cap rocks of calc-silicate rocks are also considered to have kept capturing fluids infiltrated through multi-stage fluid infiltration. The incipient charnockite formed just beneath calc-silicate rocks may reflect significant effect of such structure-controlled CO_2-rich fluids released during prograde to peak stage, which has given rise to relatively lower $a(H_2O)$ condition than the surrounding hydrated rocks and restricted progress of retrograde hydration reactions.

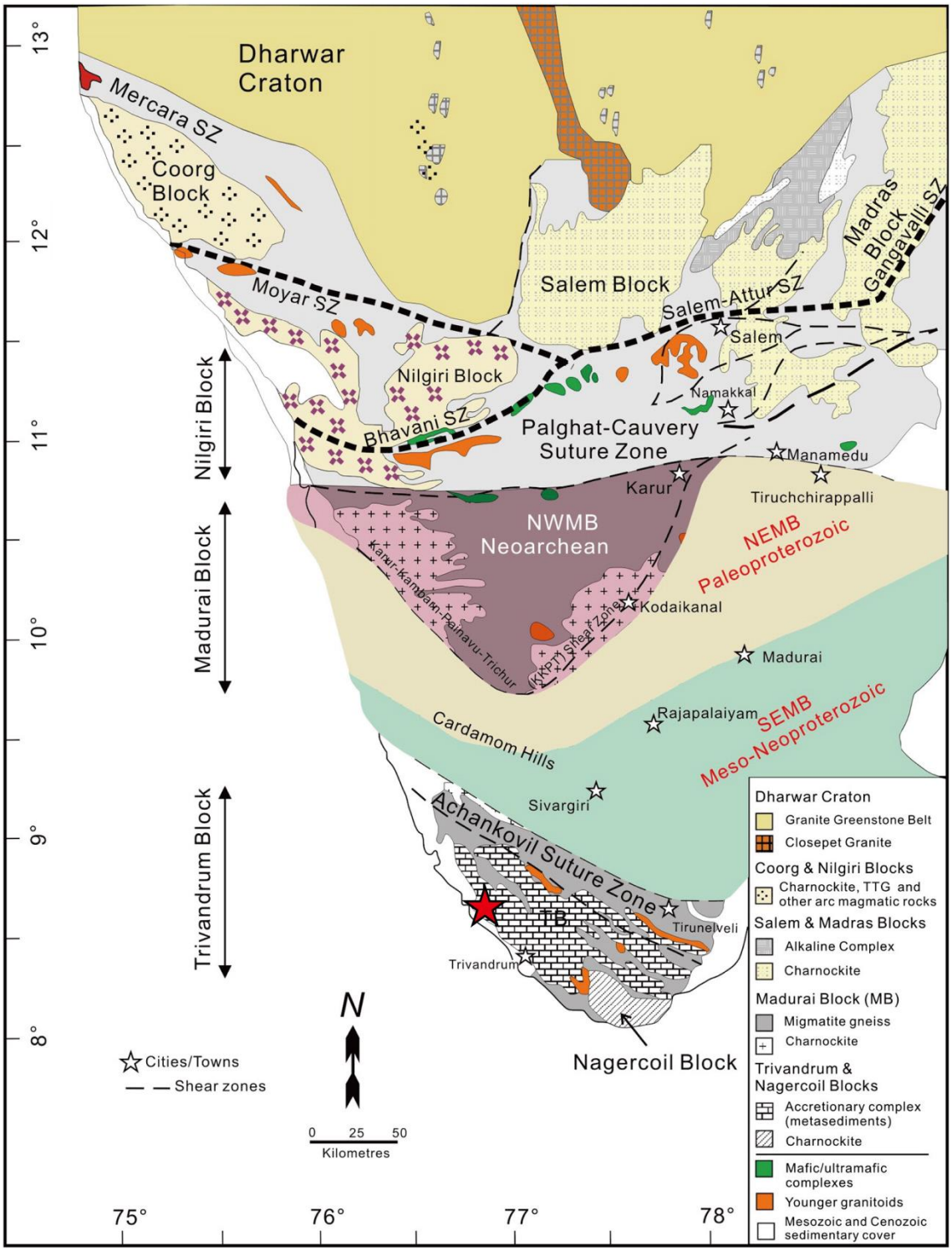

Fig. 18. Generalized geological map of southern India showing major crustal blocks with the locality of samples (star) discussed in this study (modified after Santosh et al., 2015).

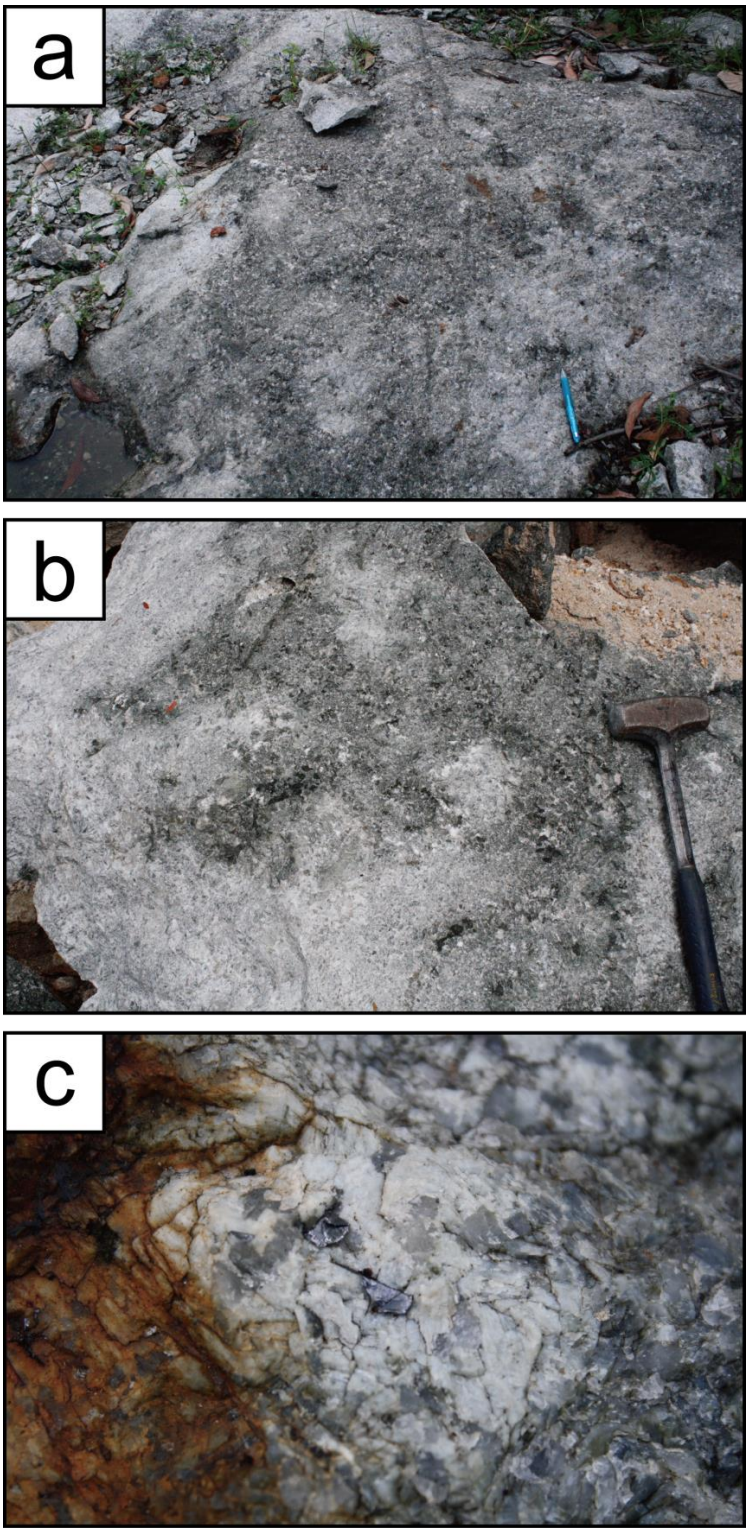

Fig. 19. Field photographs of the studied quarry from Nuliyam in the Trivandrum Block. (a) An overview of greenish and leucocratic quartzo-feldspathic rocks. (b) Enlarged photograph of greenish quartzo-feldspathic rock containing coarse-grained amphibole. (c) Enlarged photograph of graphite flake.

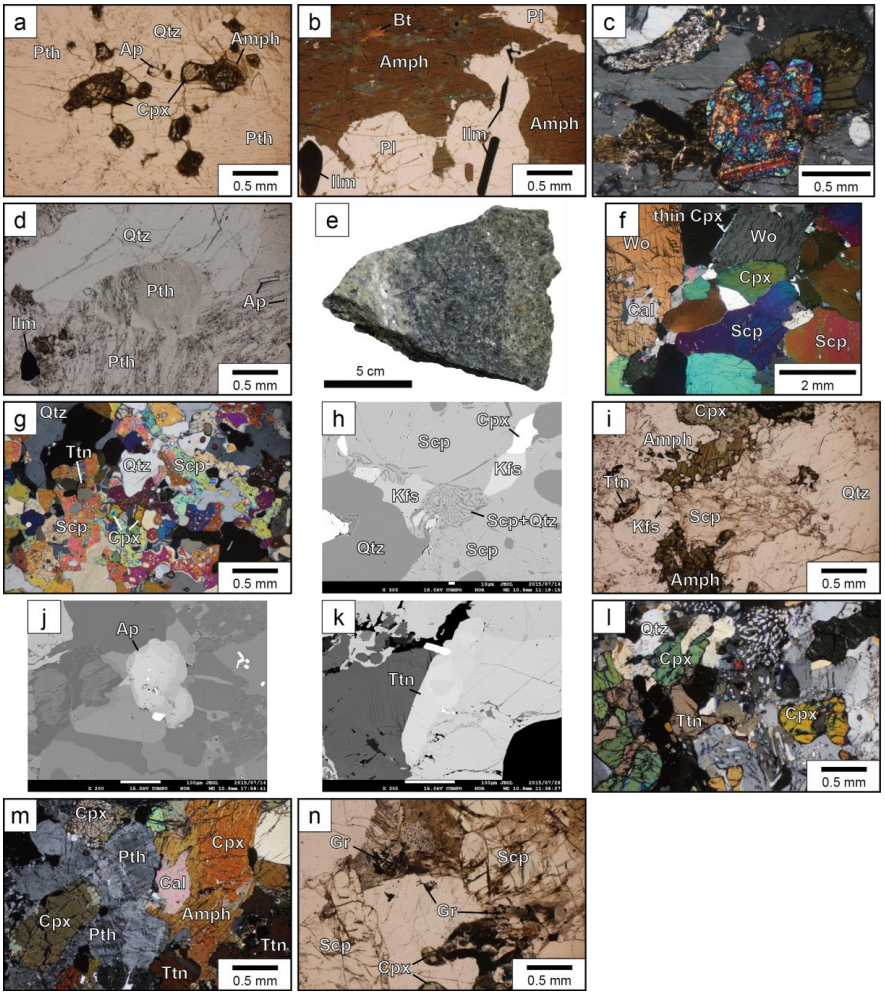

Fig. 20. Photomicrographs showing representative textures of samples and a hand sample of calc-silicate rock discussed in this study. (a) Fresh clinopyroxene with amphibole and perthite in greenish quartzo-feldspathic rock (sample KR22-1B). (b) Coarse-grained brownish amphibole partially replaced by secondary bluish amphibole and plagioclase in greenish quartzo-feldspathic rock. (c) Intergrowth of amphibole and zircon showing zoning in greenish quartzo-feldspathic rock. (d) Coarse-grained quartz and perthite in leucocratic quartzo-feldspathic rock (sample KR22-1A). (e) Hand sample of calc-silicate rock. (f) Scapolite, wollastonite, and clinopyroxene in calc-silicate 1 (sample KR22-1D1). (g) Scapolite and quartz in calc-silicate 2 (sample KR22-1D2). (h) BSE image of scapolite + quartz symplectite in calc-silicate 2. (i) Clinopyroxene replaced by amphibole and slightly altered scapolite in calc-silicate 3 (sample KR22-1D3). (j) BSE image of apatite showing compositional zoning in calc-silicate 3. (k) BSE image of titanite showing compositional zoning in calc-silicate 3. (l) Abundant myrmekite in calc-silicate 4 (sample KR22-1D4). (m) Clinopyroxene, amphibole, quartz, and perthite in calc-silicate 5 (sample KR22-1D5). (n) Xenoblastic graphite and intense alteration in calc-silicate 3.

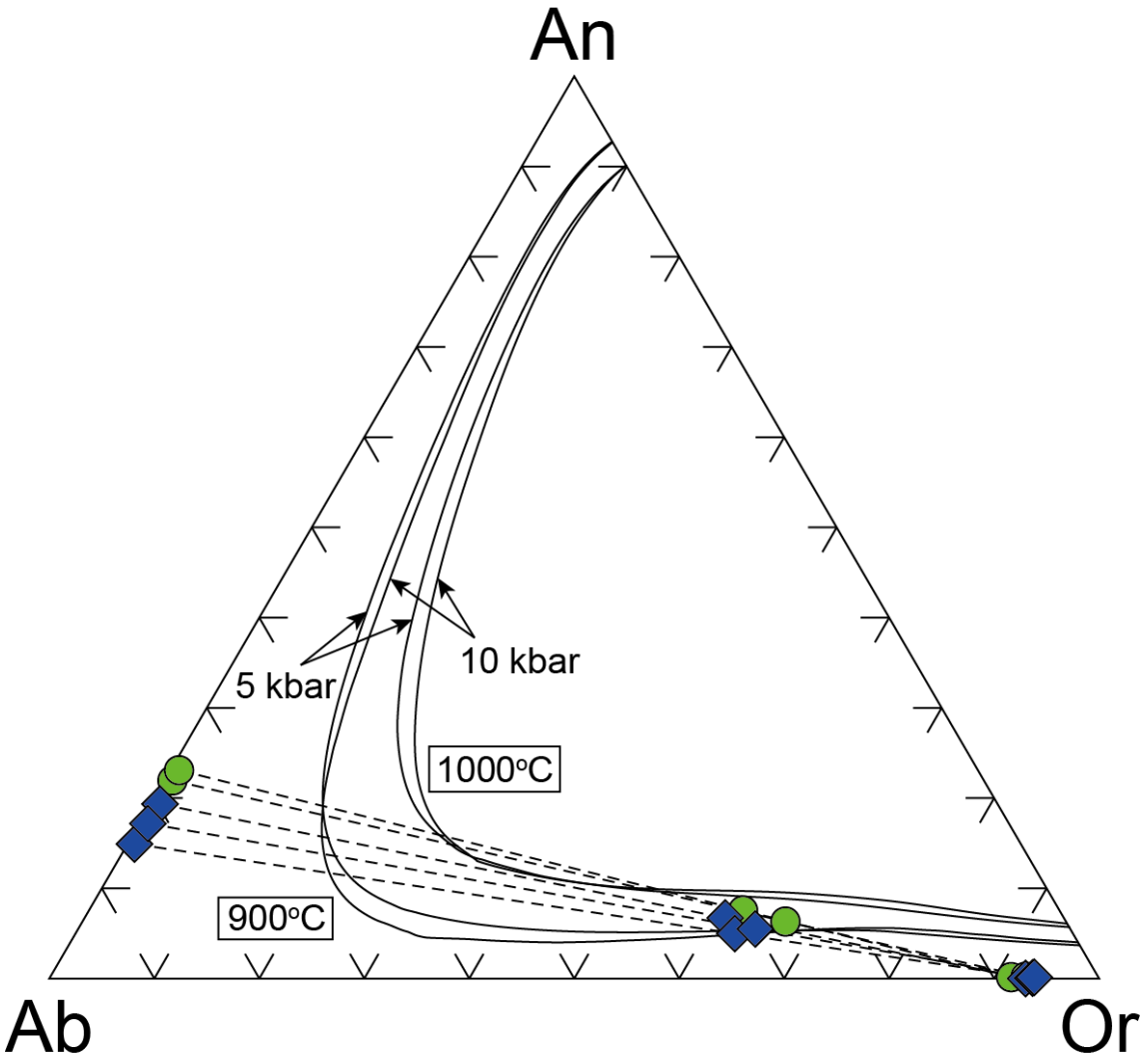

Fig. 21. Ternary plot of integrated feldspar compositions of greenish and leucocratic quartzo-feldspathic rocks (samples KR22-1B and KR22-1A). Symbols of circle and square indicate data of greenish quartzo-feldspathic rock and leucocratic quartzo-feldspathic rock, respectively. Isothermal curves at 900 and 1000°C and 5 and 10 kbar are based on the thermodynamic model of Fuhrman and Lindsley (1988).

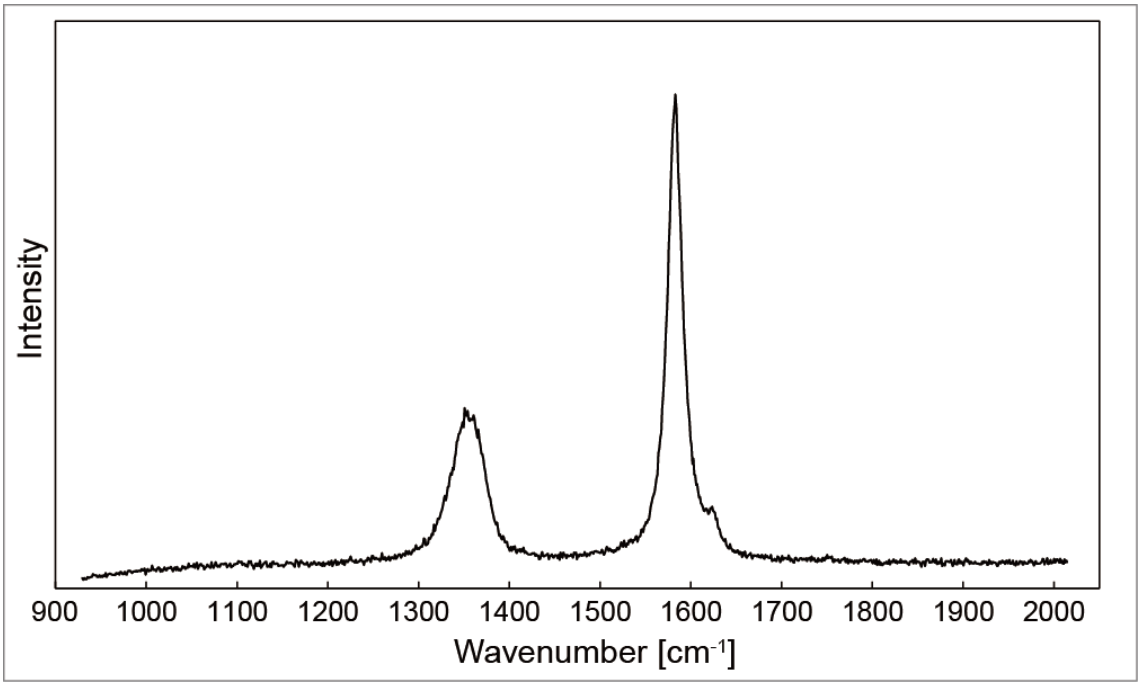

Fig. 22. Laser Raman spectrum of graphite from locally altered domain in calc-silicate rock (sample KR22-1D3). Although well-crystalized graphite formed at >~650°C has only one peak around 1600 cm^{-1}, graphite in this study shows three peaks, which indicates the graphite did not undergo granulite-facies metamorphism.

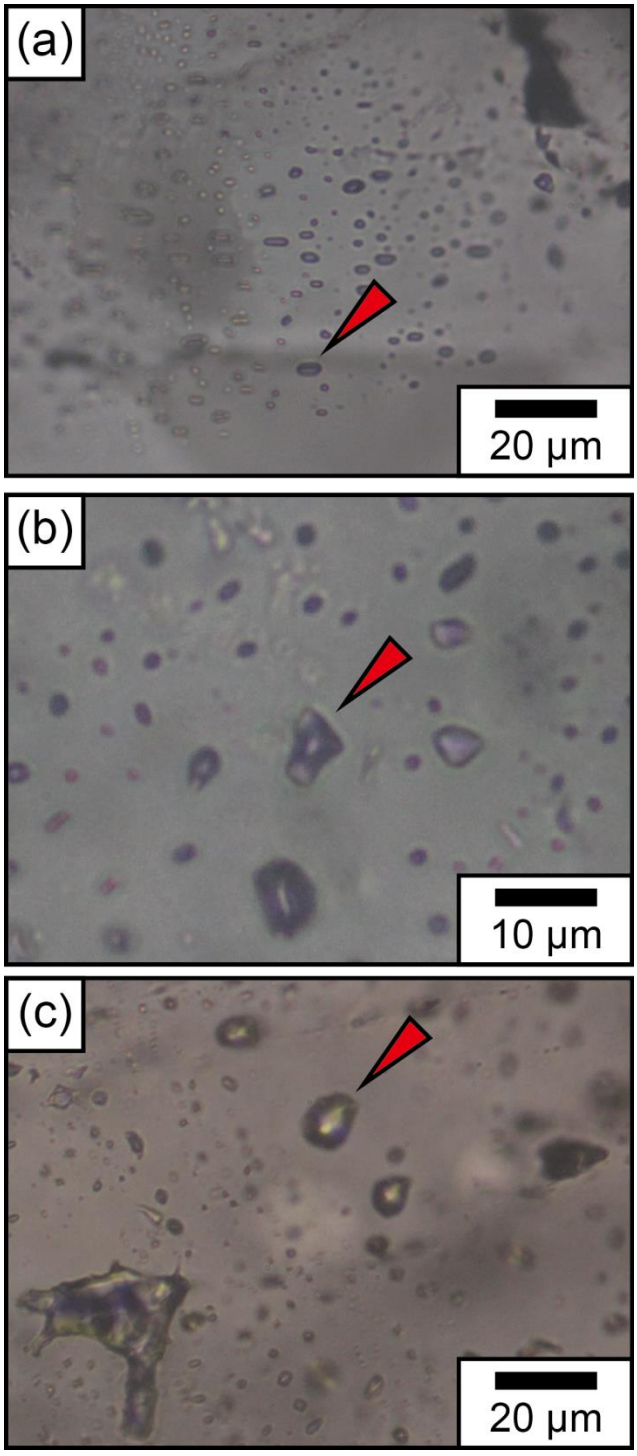

Fig. 23. Photomicrographs of representative fluid inclusions in quartz discussed in this study. (a) CO_2-rich fluid inclusion. (b) H_2O-rich fluid inclusions. (c) N_2-rich fluid inclusions. Arrows indicate the inclusions analyzed by laser Raman spectroscopy (see Figure 24).

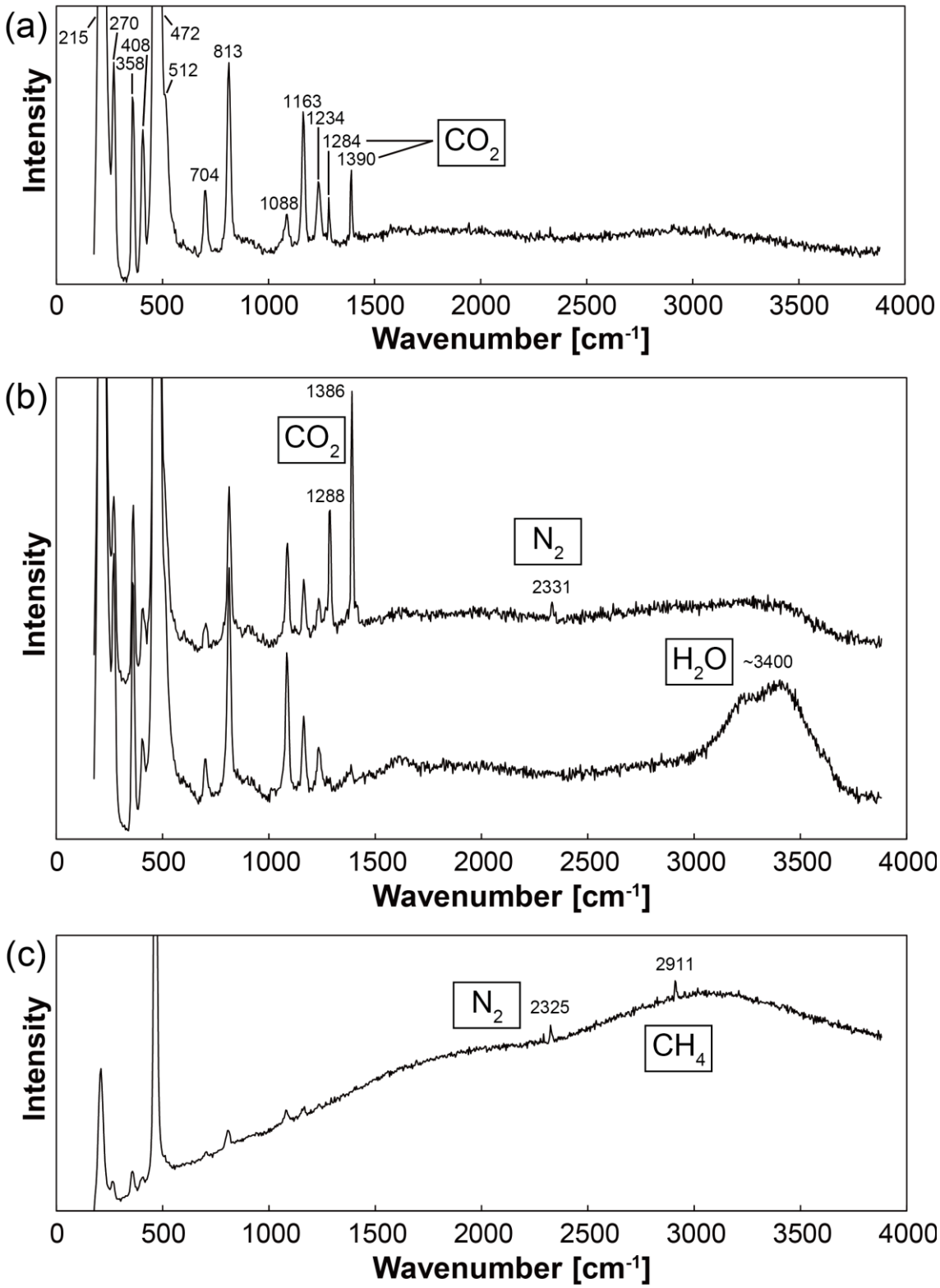

Fig. 24. Raman spectra of representative fluid inclusions marked in Fig. 23. (a) CO_2-rich fluid inclusion. (b) H_2O-rich fluid inclusion. (c) N_2-rich fluid inclusion.

Table 7. Representative electron microprobe analyses of amphiboles (O=23) from Nuliyam area in the Trivandrum Block.

Sample No.*	GF				CS3	CS5	
Remarks	Brownish	Bluish	Replacing Cpx	With Zrn	Core	Core	Bluish
SiO_2	39.86	38.99	38.97	40.16	38.57	42.64	43.91
Al_2O_3	10.17	10.36	10.53	9.14	10.44	8.00	8.07
TiO_2	2.59	0.53	0.97	1.75	1.12	0.92	0.06
Cr_2O_3	0.00	0.01	0.00	0.03	0.00	0.00	0.01
Fe_2O_3	1.00	3.76	4.30	2.54	3.97	5.58	6.63
FeO	23.12	22.79	23.17	23.39	25.75	22.63	21.35
MnO	0.03	0.06	0.05	0.02	0.16	0.21	0.22
MgO	5.70	4.67	4.15	4.99	2.53	4.70	5.19
CaO	11.38	11.39	11.38	11.18	11.05	10.96	11.09
Na_2O	1.76	1.44	1.12	1.44	1.55	1.30	1.11
K_2O	2.06	2.21	2.28	1.95	1.93	1.12	0.91
F	0.52	0.44	0.30	0.47	0.26	0.38	0.41
=O(F)	-0.22	-0.19	-0.13	-0.20	-0.11	-0.16	-0.17
Cl	1.23	2.63	1.58	1.31	1.23	0.28	0.02
=O(Cl)	-0.28	-0.59	-0.36	-0.30	-0.28	-0.06	0.00
Total	98.93	98.49	98.32	97.86	98.16	98.49	98.80
Si	6.289	6.297	6.259	6.432	6.258	6.674	6.778
Al^{iv}	1.711	1.703	1.741	1.568	1.742	1.326	1.222
Sum T	8.000	8.000	8.000	8.000	8.000	8.000	8.000
Al^{vi}	0.180	0.268	0.252	0.157	0.254	0.151	0.246
Ti	0.307	0.064	0.118	0.211	0.137	0.108	0.007
Cr	0.000	0.002	0.000	0.004	0.000	0.000	0.001
Fe^{3+}	0.119	0.457	0.519	0.306	0.484	0.657	0.770
Fe^{2+}	3.049	3.078	3.112	3.131	3.493	2.962	2.755
Mn	0.004	0.008	0.007	0.002	0.021	0.028	0.029
Mg	1.340	1.124	0.992	1.190	0.610	1.095	1.192
Sum C	5.000	5.000	5.000	5.000	5.000	5.000	5.000
Ca	1.923	1.969	1.957	1.917	1.919	1.837	1.833
Na(B)	0.077	0.031	0.043	0.083	0.081	0.163	0.167
Sum(B)	2.000	2.000	2.000	2.000	2.000	2.000	2.000
Na(A)	0.459	0.420	0.304	0.364	0.407	0.232	0.166
K	0.415	0.455	0.468	0.398	0.398	0.224	0.179
Sum(A)	0.874	0.875	0.771	0.761	0.805	0.456	0.345
Total	15.874	15.875	15.771	15.761	15.805	15.456	15.345
X_{Mg}	0.305	0.268	0.242	0.275	0.149	0.270	0.302
XFe^{3+}	0.037	0.129	0.143	0.089	0.122	0.181	0.218
Al^{vi}/Al^{iv}	0.105	0.158	0.145	0.100	0.146	0.114	0.201

* GF: greenish quartzo-feldspathic rock (sample KR22-1B), CS3: calc-silicate 3 (sample KR22-1D3), CS5: calc-silicate 5 (sample KR22-1D5)

Table 8. Representative electron microprobe analyses of clinopyroxene (O=6) from Nuliyam area in the Trivandrum Block.

Sample No.*	GF	CS1			CS2		CS3	CS4	CS5
Remarks	Matrix	Core	Grain boundary	Lamella	Core	Grain boundary	Rim	Rim	Rim
SiO_2	49.51	49.57	49.21	49.35	49.34	49.41	49.05	49.76	49.44
Al_2O_3	0.99	0.88	0.40	0.01	0.69	0.80	0.70	0.57	0.68
TiO_2	0.34	0.04	0.00	0.01	0.08	0.09	0.12	0.12	0.29
Cr_2O_3	0.02	0.07	0.03	0.00	0.05	0.00	0.00	0.00	0.04
FeO**	21.26	23.27	25.40	26.90	23.47	25.55	23.89	22.95	23.02
MnO	0.09	0.18	0.00	0.18	0.27	0.16	0.27	0.31	0.33
MgO	6.30	3.25	1.93	1.14	3.44	2.13	3.20	4.06	4.34
CaO	21.30	22.73	22.84	23.00	23.16	22.23	22.61	22.65	21.84
Na_2O	0.42	0.17	0.12	0.06	0.18	0.15	0.23	0.23	0.31
K_2O	0.00	0.00	0.01	0.00	0.01	0.02	0.01	0.00	0.00
Total	100.23	100.15	99.94	100.65	100.69	100.53	100.08	100.64	100.29
Si	1.958	1.986	1.997	2.004	1.973	1.990	1.976	1.981	1.974
Al	0.046	0.041	0.019	0.001	0.033	0.038	0.033	0.027	0.032
Ti	0.010	0.001	0.000	0.000	0.002	0.003	0.004	0.004	0.009
Cr	0.001	0.002	0.001	0.000	0.002	0.000	0.000	0.000	0.001
Fe^{2+}	0.703	0.779	0.862	0.913	0.785	0.860	0.805	0.764	0.769
Mn	0.003	0.006	0.000	0.006	0.009	0.006	0.009	0.010	0.011
Mg	0.371	0.194	0.117	0.069	0.205	0.128	0.192	0.241	0.258
Ca	0.902	0.975	0.992	1.000	0.992	0.959	0.976	0.966	0.934
Na	0.032	0.013	0.009	0.005	0.014	0.012	0.018	0.017	0.024
K	0.000	0.000	0.000	0.000	0.000	0.001	0.000	0.000	0.000
Total	4.025	3.998	3.998	3.998	4.015	3.995	4.013	4.010	4.013
X_{Mg}	0.35	0.20	0.12	0.07	0.21	0.13	0.19	0.24	0.25

* GF: greenish quartzo-feldspathic rock (sample KR22-1B), CS1: calc-silicate 1 (sample KR22-1D1), CS2: calc-silicate 2 (sample KR22-1D2) CS3: calc-silicate 3 (sample KR22-1D3),CS4: calc-silicate 4 (sample KR22-1D4), CS5: calc-silicate 5 (sample KR22-1D5)

** Total Fe as FeO

Table 9. Representative electron microprobe analyses of scapolite from Nuliyam area in the Trivandrum Block.

Sample No.*	CS1	CS2		CS3					
Remarks	Core	Matrix	Symp.	Core	Rim	Core	Rim	Core	Rim
SiO_2	46.82	47.16	51.31	47.75	49.34	49.22	51.47	54.04	52.37
Al_2O_3	26.50	26.23	24.41	26.58	25.60	25.86	24.03	23.12	23.87
TiO_2	0.00	0.01	0.00	0.00	0.00	0.00	0.00	0.00	0.00
Cr_2O_3	0.00	0.00	0.01	0.01	0.00	0.00	0.02	0.00	0.01
FeO**	0.47	0.29	0.08	0.12	0.09	0.08	0.14	0.13	0.19
MnO	0.15	0.01	0.02	0.00	0.00	0.00	0.02	0.02	0.00
MgO	0.00	0.00	0.00	0.00	0.00	0.00	0.00	0.00	0.00
CaO	16.87	16.60	14.83	15.55	14.09	14.21	11.42	9.08	10.49
Na_2O	3.25	4.00	4.10	4.48	5.36	5.25	7.10	8.34	7.30
K_2O	0.49	0.32	0.26	0.46	0.43	0.60	0.56	0.67	0.60
F	0.01	0.00	0.01	0.00	0.03	0.02	0.00	0.00	0.00
-O	0.00	0.00	0.00	0.00	-0.01	-0.01	0.00	0.00	0.00
Cl	0.55	0.68	0.63	0.97	1.21	1.34	1.83	2.43	2.07
-O	-0.12	-0.15	-0.14	-0.22	-0.27	-0.30	-0.41	-0.55	-0.47
Total	94.99	95.15	95.51	95.71	95.87	96.27	96.17	97.28	96.45
Si+Al=12									
Si	7.198	7.249	7.690	7.246	7.447	7.412	7.742	7.978	7.807
Al	4.802	4.751	4.310	4.754	4.553	4.588	4.258	4.022	4.193
Ti	0.000	0.002	0.000	0.000	0.000	0.000	0.000	0.000	0.000
Cr	0.000	0.000	0.001	0.001	0.000	0.000	0.002	0.000	0.001
Fe^{2+}	0.060	0.037	0.010	0.015	0.011	0.010	0.017	0.016	0.024
Mn	0.020	0.001	0.002	0.000	0.000	0.000	0.003	0.002	0.000
Mg	0.000	0.000	0.000	0.000	0.000	0.000	0.000	0.000	0.000
Ca	2.777	2.733	2.381	2.528	2.278	2.292	1.839	1.436	1.675
Na	0.969	1.192	1.191	1.318	1.568	1.532	2.069	2.386	2.109
K	0.096	0.062	0.049	0.090	0.083	0.116	0.108	0.126	0.115
Total	15.923	16.026	15.635	15.952	15.941	15.950	16.038	15.966	15.923
Me	73	69	66	64	58	58	46	37	43
EqAn***	60	58	44	58	52	53	42	34	40

* CS1: calc-silicate 1 (sample KR22-1D1), CS2: calc-silicate 2 (sample KR22-1D2), CS3: calc-silicate 3 (sample KR22-1D3)

** Total Fe as FeO

*** EqAn = 100*(Al-3)/3

Table 10. Representative electron microprobe analyses of K-feldspar (O=8) from Nuliyam area in the Trivandrum Block.

Sample No.*	GF		LF	CS2		CS3		CS4		CS5
Remarks	Pth	Matrix	Pth	Matrix	with Symp.	Matrix	Matrix	Matrix	Pth	Pth
SiO_2	64.52	64.63	64.56	65.89	64.98	65.64	65.04	63.62	62.79	64.39
Al_2O_3	18.22	18.50	18.27	18.55	18.69	18.68	18.20	18.77	18.88	18.60
TiO_2	0.00	0.00	0.00	0.04	0.00	0.00	0.00	0.07	0.03	0.01
FeO*	0.01	0.19	0.01	0.02	0.01	0.04	0.04	0.12	0.01	0.03
MgO	0.00	0.00	0.00	0.00	0.00	0.00	0.00	0.00	0.00	0.00
CaO	0.03	0.02	0.03	0.00	0.03	0.02	0.01	0.03	0.01	0.02
Na_2O	0.92	0.36	0.68	1.09	0.92	0.92	0.83	0.87	1.33	0.74
K_2O	15.49	16.28	15.73	14.91	14.79	15.18	14.89	14.07	14.32	15.61
BaO	0.13	0.05	0.11	0.05	1.44	0.22	0.43	2.46	1.74	0.41
Total	99.32	100.03	99.37	100.55	100.86	100.70	99.44	100.00	99.11	99.80
Si	2.999	2.991	3.000	3.008	2.989	3.001	3.012	2.969	2.953	2.986
Al	0.998	1.009	1.000	0.998	1.013	1.006	0.993	1.032	1.046	1.016
Ti	0.000	0.000	0.000	0.001	0.000	0.000	0.000	0.002	0.001	0.000
Fe^{2+}	0.000	0.007	0.000	0.001	0.001	0.002	0.002	0.005	0.000	0.001
Mg	0.000	0.000	0.000	0.000	0.000	0.000	0.000	0.000	0.000	0.000
Ca	0.002	0.001	0.001	0.000	0.001	0.001	0.000	0.002	0.000	0.001
Na	0.083	0.032	0.061	0.096	0.082	0.081	0.075	0.079	0.121	0.066
K	0.918	0.961	0.932	0.868	0.867	0.885	0.879	0.837	0.859	0.923
Ba	0.002	0.001	0.002	0.001	0.026	0.004	0.008	0.045	0.032	0.007
Total	5.002	5.001	4.996	4.973	4.979	4.979	4.969	4.971	5.013	5.001
An (mol.%)	0.2	0.1	0.1	0.0	0.1	0.1	0.0	0.2	0.0	0.1
Ab (mol.%)	8.3	3.3	6.1	9.9	8.4	8.4	7.8	8.2	12.0	6.7
Or (mol.%)	91.3	96.6	93.6	90.0	88.8	91.1	91.4	87.0	84.8	92.5
Cel (mol.%)	0.2	0.1	0.2	0.1	2.7	0.4	0.8	4.7	3.2	0.7

* GF: greenish quarzo-feldspathic rock (sample KR22-1B), LF: lucocratic quartzo-feldspathic rock (sample KR22-1A), CS2: calc-silicate 2 (sample KR22-1D2) CS3: calc-silicate 3 (sample KR22-1D3), CS4: calc-silicate 4 (sample KR22-1D4), CS5: calc-silicate 5 (sample KR22-1D5)

** Total Fe as FeO

Table 11. Representative electron microprobe analyses of plagioclase (O=8) from Nuliyam area in the Trivandrum Block.

Sample No.	GF		LF		CS3		CS4	CS5			
Remarks	Pth	Matrix	Pth	myrmekite	Matrix	Lamella	Matrix	Pth	Pth	Matrix	Matrix
SiO_2	62.97	62.02	62.96	61.60	59.93	69.16	60.52	68.14	67.82	63.36	67.53
Al_2O_3	23.24	23.13	22.71	22.88	25.40	19.72	24.43	21.61	19.55	23.58	20.47
TiO_2	0.00	0.00	0.00	0.00	0.00	0.00	0.00	0.00	0.00	0.00	0.03
FeO*	0.07	0.10	0.03	0.03	0.04	0.06	0.17	0.06	0.06	0.04	0.12
MgO	0.00	0.00	0.00	0.00	0.00	0.00	0.00	0.00	0.00	0.00	0.00
CaO	4.65	4.96	4.04	4.83	7.29	0.06	5.87	2.24	0.16	4.68	1.06
Na_2O	9.05	8.68	9.21	8.90	7.47	11.39	8.04	9.22	9.26	9.06	11.36
K_2O	0.13	0.34	0.15	0.18	0.25	0.27	0.21	0.54	4.63	0.18	0.17
BaO	0.01	0.06	0.01	0.04	0.00	0.00	0.03	0.00	0.19	0.04	0.00
Total	100.12	99.28	99.12	98.46	100.38	100.66	99.26	101.82	101.67	100.94	100.74
Si	2.784	2.772	2.807	2.775	2.664	2.999	2.711	2.927	2.974	2.780	2.942
Al	1.211	1.218	1.193	1.215	1.330	1.007	1.289	1.094	1.010	1.219	1.051
Ti	0.000	0.000	0.000	0.000	0.000	0.000	0.000	0.000	0.000	0.000	0.001
Fe^{2+}	0.003	0.004	0.001	0.001	0.001	0.002	0.006	0.002	0.002	0.001	0.004
Mg	0.000	0.000	0.000	0.000	0.000	0.000	0.000	0.000	0.000	0.000	0.000
Ca	0.220	0.238	0.193	0.233	0.347	0.003	0.282	0.103	0.007	0.220	0.050
Na	0.775	0.752	0.795	0.776	0.644	0.957	0.698	0.768	0.787	0.770	0.959
K	0.007	0.019	0.009	0.010	0.014	0.015	0.012	0.030	0.259	0.010	0.009
Ba	0.000	0.001	0.000	0.001	0.000	0.000	0.000	0.000	0.003	0.001	0.000
Total	5.001	5.004	4.998	5.011	5.000	4.984	4.999	4.924	5.043	5.001	5.016
An (mol.%)	22.0	23.6	19.3	22.9	34.5	0.3	28.4	11.5	0.7	22.0	4.9
Ab (mol.%)	77.3	74.5	79.8	76.1	64.0	98.2	70.4	85.3	74.7	77.0	94.2
Or (mol.%)	0.7	1.9	0.9	1.0	1.4	1.5	1.2	3.3	24.6	1.0	0.9

* GF: greenish quarzo-feldspathic rock (sample KR22-1B), LF: lucocratic quartzo-feldspathic rock (sample KR22-1A), CS2: calc-silicate 2 (sample KR22-1D2) CS3: calc-silicate 3 (sample KR22-1D3), CS4: calc-silicate 4 (sample KR22-1D4), CS5: calc-silicate 5 (sample KR22-1D5)

** Total Fe as FeO

CHAPTER 5
Concluding remarks

(1) The studied quarry in Ginikarawa near Kurunegala in the Wanni Complex, Sri Lanka, is composed of dark brownish to grayish irregular patches of incipient charnockite and orthopyroxene-free leucocratic biotite ± hornblende orthogneiss. Phase equilibrium modeling on the orthopyroxene-bearing mineral assemblage within charnockite constrained the conditions of incipient-charnockite formation at 3.0-3.7 kbar and 740-790°C under relatively low $a(H_2O)$ condition of 0.46, which is consistent with the available model of incipient-charnockite formation related to local decrease in $a(H_2O)$ within hydrous biotite gneiss and the progress of dehydration reactions. The estimated *P–T* condition is lower than the available peak metamorphic conditions reported for typical granulites from the Wanni Complex (~850°C and ~7 kbar), which confirmed that incipient-charnockite formation is a post-peak retrograde event possibly related to local infiltration of low-$a(H_2O)$ and CO_2-bearing fluid.

(2) Incipient charnockite from Ambodin Ifandana area in the Ikalamavony Sub-domain of south-central Madagascar occurs as patches, lenses, and layers in migmatitic biotite gneiss. Lenses and layers of calc-silicate rocks are closely associated with the charnockite. The application of mineral equilibrium modeling and fluid inclusion study on charnockite to constrain the conditions of incipient-charnockite formation define a *P-T* range of 840°C/4.5 kbar to 880°C/10.5 kbar, which is nearly consistent with the inferred *P-T* condition of the Ikalamavony Sub-domain. The modeling also demonstrated that charnockite is stable under relatively low $a(H_2O)$ condition of 0.42-0.43 similar to that of Ginikarawa from Sri Lanka. The dominant occurrence of CO_2-rich fluid inclusions in the contact charnockite suggests that the dehydration was caused by decarbonation of calc-silicate rocks during the initial stage of decompression slightly after the peak metamorphism. The calc-silicate rocks might have also behaved as a cap rock that trapped CO_2 infiltrated from external sources.

'CO_2-rich fluid ponds' formed beneath calc-silicate layers could have produced layers of coarse-grained charnockite adjacent to calc-silicate layers.

(3) The dominant lithologies of the studied locality in Nuliyam from the Trivandrum Block, southern India, are greenish quartzo-feldspathic rock, leucocratic quartzo-feldspathic rock, and calc-silicate enclaves with precipitation of graphite. Amphibolite-facies garnet-biotite gneiss and incipient charnockite are also reported in previous studies, and they are closely associated with calc-silicate rock. The peak condition of ~900°C and the graphite precipitated at <400°C were obtained in this study. The petrography and mineral chemistry of clinopyroxenes and amphiboles suggest two-stage infiltrations of fluorine and chlorine-bearing hydrous fluid. The fluid inclusion study reveals presence of various types of fluid composed of H_2O, CO_2, N_2, and CH_4, which also implies several different sources of the fluids. Various types of fluid inclusions and unaltered calc-silicate enclave support the role of calc-silicate rocks as impervious cap rock against CO_2, which was first discussed by Harley and Santosh (1995). The incipient-charnockite formation of Nuliyam area is therefore related to infiltration of carbonic fluid from external sources.

(4) The results of this study suggest that metamorphic fluids played an important role on the stability of minerals during prograde to retrograde stages in all the studied localities from the Gondwana collisional orogeny. This is consistent with abundant occurrences of incipient charnockite throughout this region, which is one of the unique characters of this orogen. Santosh and Omori (2008) argued an important role of CO_2 flushing on the formation of high- and ultrahigh-temperature granulite and charnockite derived from both decarbonation of calc-silicates and degassing of sub-lithospheric mantle. Complex subduction of oceanic plates and accretion of sediments and sea mounts during Gondwana amalgamation possibly brought large amount of limestones to the lower crust, which could have given rise to

decarbonation and production of CO_2-bearing fluid. Alternatively, post-peak slab break-off and delamination could have brought about asthenosphere upwelling and release of CO_2. The Gondwana collisional orogen is therefore considered to have experienced significant effect of CO_2-bearing metamorphism and dehydration throughout burial and exhumation stages of the orogeny.

ACKNOWLEDGEMENTS

I would like to express my gratitude to supervisor, Prof. T. Tsunogae at the Faculty of Life and Environmental Sciences, University of Tsukuba for all his support. This work would not be accomplished without his continuous guidance and critical reading of manuscript. Prof. M. Santosh at China University of Geosciences Beijing is specially thanked for his supported and guidance. I also wish to acknowledge to Prof. Yoji Arakawa, Prof. Ken-ichiro Hayashi, and Dr. Masanori Kurosawa for their helpful discussion and encouragement.

I am deeply indebted to Dr. N. Nishida and Dr. N. Chino at the Chemical Analysis Division of the Research Facility Center for Science and Technology, University of Tsukuba for their kind assistance in the microprobe analysis.

I also thank Dr. H. Shimizu, Dr. Y. Saitoh, Mr. T. Koizumi, Mr. Emmanuel N. Ugwuonah, Mr. Li Tang, Ms. M. Iinuma, Ms. A. Kobayashi, Mr. Y. Takamura, Ms. Meng Pan of metamorphic petrology laboratory for their support and help.

REFERENCES

Andriamarofahatra, J., de la Boisse, H., Nicollet, C., 1990. Datation U-Pb sur monazites et zircons du dernier épisode tectono-métamorphique granulitique majeur dans le Sud-Est de Madagascar. C. R. Acad. Sci. II, 310, 1643–1648.

Baur, N., Kröner, A., Todt, W., Liew, T.C., Hofman, A.W., 1991. U–Pb isotopic systematics of zircons from prograde and retrograde transition zones in high grade orthogneisses, Sri Lanka. Journal of Geology 99, 527–545.

Berkesi, M., Hidas, K., Guzmics, T., Dubessy, J., Bodnar, R.J., Szabó, C., Vajna, B., Tsunogae, T., 2009. Detection of small amounts of H_2O in CO_2-rich fluid inclusions using Raman spectroscopy. Journal of Raman Spectroscopy 40, 1461–1463.

Bhattacharya, S., Sen, S.K., 2000. New insights into the origin of charnockites, Kabbaldurga, Karnataka, South India. Gondwana Research 3, 489-506.

Burton, K.W., O'Nions, R.K., 1990. The timescale and mechanism of granulite formation at Kurunegala, Sri Lanka. Contributions to Mineralogy and Petrology 106, 66-89.

Braun, I., Kriegsman, L.M., 2003. Proterozoic crustal evolution of southernmost India and Sri Lanka. M. Yoshida, Windley, B., Dasgupta, S. (eds.) Proterozoic East Gondwana: Supercontinent Assembly and Breakup, Special Publication, Geological Society of London, pp. 169–202.

Braun, I., Montel, J.M., Nicollet, C., 1998. Electron microprobe dating monazites from high-grade gneisses and pegmatites of the Kerala Khondalite Belt, southern India. Chemical Geology 146, 65-85.

Brown, P.E., Hagemann, S.G., 1994. MacFlinCor: a computer program for fluid inclusion data reduction and manipulation. In: DeVivo, B., Frezzotti, M.L. (Eds.), Fluid Inclusions in Minerals: Methods and Applications. Short Course of the International Mineralogical

Association Working Group ‘‘Inclusions in Minerals.’’ Blacksburg, Virginia Polytechnic Institute Press, pp. 231–250.

Brown, P.E., Lamb, W.M., 1989. *P–V–T* properties of fluids in the system $H_2O \pm CO_2 \pm$ NaCl: new graphical presentations and implications for fluid inclusion studies. Geochimica Cosmochimica Acta 53, 1209–1221.

Buseck, P.R., Huang, B.J., 1985. Conversion of carbonaceous material to graphite during metamorphism. Geochimica et Cosmochimica Acta 49, 2003–2016.

Chacko, T., Kumar, G.R.R., Newton, R.C., 1987. Metamorphic *P-T* conditions of the Kerala (South India) Khondalite belt: a granulite-facies supracrustal terrain. Journal of Geology 96, 343-358.

Chacko, T., Lamb, M., Farquhar, J., 1996. Ultra high temperature metamorphism in the Kerala Khondalite Belt. Gondwana Research Group Memoir 3, 157-165.

Coggon, R., Holland, T.J.B., 2002. Mixing properties of phengitic micas and revised garnet-phengite thermobarometers. Journal of Metamorphic Geology 20, 683-696.

Collins, A.S., 2006. Madagascar and the amalgamation of central Gondwana. Gondwana Research 9, 3–16.

Collins, A.S., Pisarevsky, S.A., 2005. Amalgamating eastern Gondwana: The evolution of the Circum-Indian Orogens. Earth-Science Reviews 71, 229-270.

Collins, A.S., Windley, B.F., 2002. The tectonic evolution of central and northern Madagascar and its place in the final assembly of Gondwana. Journal of Geology 110, 325-340.

Collins, A.S., Clark, C., Sajeev, K., Santosh, M., Kelsey, D.E., Hand, M., 2007a. Passage through India: The Mozambique ocean suture, high-pressure granulites and the Palghat-Cauvery Shear System. Terra Nova 19, 141-147.

Collins, A.S., Santosh, M., Braun, I., Clark, C., 2007b. Age and sedimentary provenance of the

Southern Granulites, South India: U-Th-Pb SHRIMP secondary ion mass spectrometry. Precambrian Research 155, 125-138.

Connolly, J.A.D., Petrini, K., 2002. An automated strategy for calculation of phase diagram sections and retrieval of rock properties as a function of physical conditions. Journal of Metamorphic Geology 20, 697-708.

Cooray, P.G., 1962. Charnockites and their associated gneisses in the Precambrian of Ceylon. Journal of the Geological Society of London 118, 239–273.

Cooray, P.G., 1984. An introduction to the geology of Sri Lanka. National Museum Sri Lanka Publication, 340.

Cooray, P.G., 1994. The Precambrian of Sri Lanka: a historic review. Precambrian Research 66, 3–18.

de Capitani, C., Petrakakis, K., 2010. The computation of equilibrium assemblage diagrams with Theriak/Domino software. American Mineralogist 95, 1006-1016.

Devaraju, T.C., Sadashivaiah, M.S., 1969. The charnockites of Satnur-Halaguru area, Mysore State. Indian Mineralogist 10, 67-88.

Dharmapriya, P.L., Malaviarachchi, S.P.K., Santosh, M., Tang, L., Sajeev, K., 2015. Late-Neoproterozoic ultrahigh-temperature metamorphism in the Highland Complex, Sri Lanka. Precambrian Research 271, 311-333.

Diener J.F.A., Powell R., 2012 Revised activity–composition models for clinopyroxene and amphibole. Journal of Metamorphic Geology 30, 131-142.

Endo, T., Tsunogae, T., Santosh, M., Shaji, E., 2012. Phase equilibrium modeling of incipient charnockite formation in NCKFMASHTO and MnNCKFMASHTO systems: A case study from Rajapalaiyam, Madurai Block, southern India. Geoscience Frontiers 3, 801–811.

Endo, T., Tsunogae, T., Santosh, M., Shimizu, H., Shaji, E., 2013. Granulite formation in a

Gondwana fragment: petrology and mineral equilibrium modeling of incipient charnockite from Mavadi, southern India. Mineralogy and Petrology 107, 727–738.

Evans, B.W., Shaw, D.M., Haughton, D.R., 1969. Scapolite stoichiometry. Contributions to Mineralogy and Petrology 24,293-305.

Faulhaber, S., Raith, M., 1991. Geothermometry and geobarometry of high grade rocks: a case study on garnet pyroxene granulites in southern Sri Lanka. Mineralogical Magazine 55, 33–56.

French, B.M., 1964. Graphitization of organic material in a progressively metamorphosed Precambrian iron formation. Science 146, 917–918.

Fuhrman, M.L., Lindsley, D.H., 1988. Ternary-feldspar modeling and thermometry. American Mineralogist 73, 201–215.

Green, E.C.R., Holland, T.J.B., Powell, R., 2007. An order-disorder model for omphacitic pyroxenes in the system jadeite-diopside-hedenbergite-acmite, with applications to eclogite rocks. American Mineralogist 92, 1181-1189.

Hansen, E.C., Newton, R.C., Janardhan, A.S., 1984. Fluid inclusions in rocks from the amphibolite-facies gneiss to charnockite progression in southern Karnataka, India: direct evidence concerning the fluids of granulite metamorphism. Journal of Metamorphic Geology 2, 249–264.

Hansen, E.C., Janardhan, A.S., Newton, R.C., Prame, W.K.B.N., Kumar, G.R.R., 1987. Arrested charnockite formation in southern India and Sri Lanka. Contributions to Mineralogy and Petrology 96, 225–244.

Harley, S.L., 1989. The origins of granulites: a metamorphic perspective. Geological Magazine 126, 215-247.

Harley, S.L., Santosh, M., 1995. Wollastonite at Nuliyam, Kerala, southern India: a

reassessment of CO_2 infiltration and charnockite formation at a classic locality. Contributions to Mineralogy and Petrology 120, 83–94.

Harlov, D.E., Hansen, E.C., Bigler, C., 1998. Petrologic evidence for K-feldspar metasomatism in granulite facies rocks. Chemical Geology 151, 373-386.

He, X.-F., Santosh, M., Tsunogae, T., Malaviarachchi, S.P.K., 2016a. Early to late Neoproterozoic magmatism and magma mixing - mingling in Sri Lanka: implications for convergent margin processes during Gondwana assembly. Gondwana Research 32, 151-180.

He, X.-F., Santosh, M., Tsunogae, T., Malaviarachchi, S.P.K., Dharmapriya, P.L., 2016b. Neoproterozoic arc accretion along the 'eastern suture' in Sri Lanka during Gondwana assembly. Precambrian Research 279, 57-80.

Hiroi, Y., Asami, M., Cooray, P.G., Fernando, M.R.D., Jayatileke, J.M.S., Kagami, H., Mathavan, V., Matsueda, H., Motoyoshi, Y., Ogo, Y., Osanai, Y., Owada, M., Perera, L.R.K., Prame, K.B.N., Ranasinghe, N.S., Shiraishi, K., Vitanage, P.W., Yoshida, M., 1990. Arrested charnockite formation in Sri Lanka: field and petrographical evidence for low-pressure conditions. Proceedings of the NIPR Symposium on Antarctic Geosciences 4, 213-230.

Hokada, T., 2001. Feldspar thermometry in ultrahigh-temperature metamorphic rocks: Evidence of crustalmetamorphism attaining ~1100 °C in the Archean Napier Complex, East Antarctica. American Mineralogist 86, 932-938.

Holland, T.H., 1900. The charnockite series, a group of Archaean hypersthenic rocks in peninsular India. Memoir of the Geological Survey of India 28, 192–249.

Holland, T., Blundy, J., 1994. Non-ideal interactions in calcic amphiboles and their bearing on amphibole-plagioclase thermometry. Contributions to Mineralogy and Petrology 116, 433-447.

Holland, T.J.B., Powell, R., 1998a. An enlarged and update internally consistent thermodynamic

dataset with uncertainties and correlations: the system K_2O–Na_2O–CaO–MgO–MnO–FeO–Fe_2O_3–Al_2O_3–TiO_2–SiO_2–C–H_2–O_2. Journal of Metamorphic Geology 8, 89–124.

Holland, T.J.B., Powell, R., 1998b. An internally consistent thermodynamic dataset for phases of petrological interest. Journal of Metamorphic Geology 16, 309-343.

Holland, T.J.B., Powell, R., 2003. Activity–composition relations for phases in petrological calculations: an asymmetric multicomponent formulation. Contributions to Mineralogy and Petrology 145, 492–501.

Holland, T.J.B., Babu, E.V.S.S.K, Waters, D.J., 1996. Phase relations of Osumilite and dehydration melting in pelitic rocks: a simple thermodynamic model for the KFMASH system. Contributions to Mineralogy and Petrology 124, 383-394.

Hölzl, S., Köhler, H., Kröner, A., Jaeckel, P., Liew, T.C., 1991. Geochronology of the Sri Lankan basement. Geological Survey Department, Sri Lanka, Professional Paper, 5, 237-257.

Hopgood, A.M., Bowes, D.R., 1990. Contrasting structural features in the granulite-gneiss-charnockite-granite complex, Lake Baikal, USSR: evidence for diverse geotectonic regimes in early Proterozoic times. Tectonophysics 174, 279-299.

Hottin, G., 1976. Présentation et essai d'interprétation du Précambrien de Madagascar. Bull. Bureau Recherches Géol. Minière 2, 117–153.

Huizenga, J.M., Touret, J.L.R., 2012. Granulites, CO_2 and graphite. Gondwana Research 22, 799-809.

Jackson, D.H., Santosh, M., 1992. Dehydration reaction and isotope front transport induced by CO_2 infiltration at Nuliyam, South India. Journal of Metamorphic Geology 10, 365–382.

Jackson, D.H., Mattey, D.P., Harris, N.B.W., 1988. Carbon isotope compositions of fluid inclusions in charnockites from southern India. Nature 333, 167-170.

Jacobs, J., Thomas, R.J., 2004. Himalayan-type indenter-escape tectonics model for the southern part of the late Neoproterozoic-early Paleozoic East African-Antarctic orogen. Geology 32, 721-724.

Janardhan, A.S., Newton, R.C., Smith, J.V., 1979. Ancient crustal metamorphism at low p_{H2O}: charnockite formation at Kabbaldurga, south India. Nature 278, 511–514.

Janardhan, A.S., Newton, R.C., Hansen, E.C., 1982. The transformation of amphibolite facies gneiss to charnockite in southern Karnataka and northern Tamil Nadu, India. Contributions to Mineralogy and Petrology 79, 130-149.

Janecke, S.U., Evans, J.P., 1988. Feldspar-influenced rock rheologies. Geology, 16:1064–1067.

Jöns, N., Schenk, V., 2011. The ultrahigh temperature granulites of southern Madagascar in a polymetamorphic context: implications for the amalgamation of the Gondwana supercontinent. European Journal of Mineralogy 23, 127-156.

Kehelpannala, K.V.W., 1997. Deformation of a high-grade Gondwana fragment, Sri Lanka. Gondwana Research 1, 47–68.

Kehelpannala, K.V.W., 1999. Shear-zone controlled arrested charnockitization, retrogression and metasomatism of high-grade rocks. Gondwana Research 2, 573–577.

Kelsey, D.E., 2008. On ultrahigh-temperature crustal metamorphism. Gondwana Research 13, 1-29.

Kisch, H.J., 1980. Incipient metamorphism of Cambro-Silurian clastic rocks from the Jåmtland Supergroup, Central Scandinavian Caledonides,Western Sweden: Illite crystallinity and 'vitrinite' reflectance. Journal of the Geological Society 137, 271–288.

Kleinschrodt, R., 1994. Large-scale thrusting in the lower crustal basement of Sri Lanka. Precambrian Research 66, 39-57.

Kleinschrodt, R., Voll, G., Kehelpannala, W., 1991. A layered basic intrusion, deformed and

metamorphosed in granulite facies of the Sri Lanka basement. Geologische Rundschau 80, 779-800.

Knudsen, T.L., Lidwin, A., 1996. Magmatic CO_2, brine and nitrogen inclusions in Sveconorwegian enderbitic dehydration veins and a gabbro from the Bamble Sector, southern Norway. European Journal of Mineralogy 8, 1041-1063.

Kouketsu, Y., Mizukami, T., Mori, H., Endo, S., Aoya, M., 2014. A new approach to develop the Raman carbonaceous material geothermometer for low-grade metamorphism using peak width. Island Arc 23, 33-50.

Kretz, R., 1983. Symbols for rock-forming minerals. American Mineralogist 68, 277-279.

Kriegsman, L., 1995. The Pan-African events in East Antarctica: a review from Sri Lanka and the Mozambique Belt. Precambrian Research 75, 263–277.

Kriegsman, L.M., Schumacher, J.C., 1999. Petrology of sapphirine-bearing and associated granulites from central Sri Lanka. Journal of Petrology 40, 1211–1239.

Kroll, H., Evangelakakis, C., Voll, G., 1993. Two-feldspar geothermometry: a review and revision for slowly cooled rocks. Contributions to Mineralogy and Petrology 114, 510-518.

Kröner, A., Braun, I., Jaeckel, P., 1996. Zircon geochronology of anatectic melts and residues from a high grade pelitic assemblage at Ihosy, southern Madagascar: evidence for Pan-African granulite metamorphism. Geological Magazine 133, 311-323.

Kröner, A., Cooray, P.G., Vitanage, P.W., 1991. Lithotectonic subdivision of the Precambrian basement in Sri Lanka. Geological Survey Department, Sri Lanka, Professional Paper, 5, 5-21.

Kröner, A., Hegner, E., Collins, A.S., Windley, B.F., Brewer, T.S., Razakamanana, T., Pidgeon, R.T., 2000. Age and magmatic history of the Antananarivo Block, central Madagascar, as

derived from zircon geochronology and Nd isotopic systematics. American Journal of Science 200, 251-288.

Kröner, A., Kehelpannala, K.V.W., Hegner, A., 2003. Ca. 750–1100 Ma magmatic events and Grenville-age deformation in Sri Lanka: relevance for Rodinia supercontinent formation and dispersal, and Gondwana amalgamation. Journal of Asian Earth Sciences 22, 279–300.

Kröner, A., Rojas-Agramonte, Y., Kehelpannala, K. V. W., Zack, T., Hegner, E., Geng, H. Y., Wong, J., Barth, M., 2013. Age, Nd–Hf isotopes, and geochemistry of the Vijayan Complex of eastern and southern Sri Lanka: A Grenville-age magmatic arc of unknown derivation, Precambrian Research 234, 288-321.

Leake, B.E., Woolley, A.R., Arps, C.E.S., Birch, W.D., Gilbert, M.C., Grice, J.D., Hawthorne, F.C., Kato, A., Kisch, H.J., Krivovichev, V.G., Linthout, K., Laird, J., Mandarino, J.A., Maresch, W.V., Nickel, E.H., Rock, N.M.S., Schumacher, J.C., Smith, D.C., Stephenson, N.C.N., Ungaretti, L., Whittaker, E.J.W., Youzhi, G., 1997. Nomenclature of amphiboles: report of the subcommittee on amphiboles of the International Mineralogical Association, commission on new minerals and mineral names. American Mineralogist 82, 1019–1037.

Madugalla, T.B.N.S., Pitawala, H.M.T.G.A., Karunaratne, D.G.G.P., 2014. Use of Carbonatites in the Production of Precipitated Calcium Carbonate: A Case Study from Eppawala, Sri Lanka. Natural Resources Research 23, 217–229.

Mathavan, V., Fernando, G.W.A.R., 2001. Reactions and textures in grossular-wollastonite-scapolite calc-silicate granulites from Maligawila, Sri Lanka. Lithos 59, 217-232.

Mathavan, V.W.K.B.N., Prame, W.K.B.N., Cooray, P.G., 1999. Geology of the high grade Proterozoic terrains of Sri Lanka and the assembly of Gondwana: an update on recent developments. Gondwana Research 2, 237–250.

McGregor, V.R., Friend, C.R.L., 1992. Late-Archean prograde amphibolite- to granulite-facies relations in the Fiskenaesset region, southern West Greenland. Journal of Geology 100, 201-226.

Meert, J.G., Voo, R.V.D., 1997. The assembly of Gondwana 800-550 Ma. Journal of Geodynamics 23, 223-235.

Milisenda, C.C., Leiw, T.C., Hofmann, A.W., Kröner, A., 1988. Isotopic mapping of age provinces in Precambrian high grade terrains: Sri Lanka. Journal of Geology 96, 608–615.

Milisenda, C.C., Pohl, J.R., Hofmann, A.W., 1991. Charnockite formation at Kurunegala, Sri Lanka. Sri Lanka Geological Survey Department, Professional Paper, 5, 141-149.

Milisenda, C.C., Leiw, T.C., Hofmann, A.W., Köhler, H., 1994. Nd isotopic mapping of the Sri Lanka basement: update, and additional constraints from Sr isotopes. Precambrian Research 66, 95–110.

Montel, J.-M., Foret, S., Veschambre, M., Nicollet, C., Provost, A., 1996. Electron microprobe dating of monazite. Chemical Geology 131, 37-53.

Morimoto, T., Santosh, M., Tsunogae, T., Yoshimura, Y., 2004. Spinel + quartz association from the Kerala khondalites, southern India: evidence for ultrahigh temperature metamorphism. Journal of Mineralogical and Petrological Science 99, 257-278.

Nandakumar, V., Harley, S.L., 2000. A reappraisal of the pressure-temperature path of granulites from the Kerala Khondalite Belt, Southern India. Journal of Geology 108, 687-703.

Nédélec, A., Guillaume, D., Cournède, C., Duran, C., Macouin, M., Rakotondrazafy, M., Giuliani, G., 2014. Incipient charnockitisation due to carbonic fluid transfer related to late Pan-African transcurrent tectonics in Madagascar; implications for mobility of Fe, Ti, REE and other elements. Journal of African Earth Sciences 94, 86-99.

Newton, R.C., 1992. Charnockitic alteration: evidence for CO_2 infiltration in granulite facies metamorphism. Journal of Metamorphic Geology 10, 383–400.

Newton, R.C., Manning, C.E., 2010. Role of saline fluids in deep-crustal and upper-mantle metasomatism; insights from experimental studies. Geofluids 10, 58-72.

Newton, R.C., Tsunogae, T., 2014. Incipient charnockite: Characterization at the type localities. Precambrian Research 253, 38-49.

Newton, R.C., Smith, J.V., Windley, B.F., 1980. Carbonic metamorphism, granulites and crustal growth. Nature 288, 45–50.

Nicollet, C., Montel, J. M., Foret, S., Martelat, J. E., Rakotondrazafy, R., Lardeaux, J. M., 1997. E-Probe monazite dating in Madagascar: a good example of the usefulness of the in-situ dating method. UNESCO-IUGS-IGCP, 348(368), 65.

Nishimiya, Y., Tsunogae, T., Ssantosh, M., 2008. Petrology and fluid inclusions of garnet-clinopyroxene rocks from Paramati in the Palghat-Cauvery Shear Zone System, southern India. Journal of Mineralogical and Petrological Sciences 103, 354-360.

Ohyama, H., Tsunogae, T., Santosh, M., 2008. CO_2-rich fluid inclusions in staurolite and associated minerals in a high-pressure ultrahigh-temperature granulite from the Gondwana suture in southern India. Lithos 101, 177-190.

Osanai, Y., 1989. A preliminary report on sapphirine/kornerupine granulite from Highland series, Sri Lanka, (Extended abstract). In: Seminar on Recent Advantages in Precambrian Geology of Sri Lanka, IFS Kandy, Sri Lanka.

Osanai, Y., Ando, K.T., Miyashita, Y., Kusachi, I., Yamasaki, T., Doyama, D., Prame, W.K.B.N., Jayatilake, S., Mathavan, V., 2000. Geological field work in the South- western and central parts of the Highland Complex, Sri Lanka during 1998–1999, special reference to the highest grade metamorphic rocks. Journal of Geoscience, Osaka City University, 43, 227–

247.

Osanai, Y., Sajeev, K., Owada, M., Kehelpannala, K.V.W., Prame, W.K.B., Nakano, N., Jayatileke, S., 2006. Metamorphic evolution of ultrahigh-temperature and high-pressure granulites from Highland Complex, Sri Lanka. Journal of Asian Earth Sciences 28, 20–37.

Paquette, J.L., Nédélec, A., Moine, B., Rakotondrazafy, M., 1994. U-Pb, Single Zircon Pb-Evaporation, and Sm-Nd Isotopic Study of a Granulite Domain in SE Madagascar. Journal of Geology 102, 523-538.

Perchuk, L.L., Safonov, O.G., Gerya, T.V., Fu, B., Harlov, D.E., 2000. Mobility of components in metasomatic transformation and partial melting of gneisses; an example from Sri Lanka. Contributions to Mineralogy and Petrology 140, 212-232.

Pichamuthu, C.S., 1960. Charnockite in the making. Nature 188, 135–136.

Pitawala, A., Lottermoser, B.G., 2012. Petrogenesis of the Eppawala carbonatites, Sri Lanka: A cathodoluminescence and electron microprobe study. Mineralogy and Petrology 105, 57–70.

Pohl, J.G., Emmermann, R., 1991. Chemical composition of the Sri Lanka Precambrian Basement. Geological Survey Department, Sri Lanka, Professional Paper, 5, 94-123.

Powell, R., Holland, T.J.B., 1988. An internally consistent thermodynamic dataset with uncertainties and correlations: 3. application, methods, worked examples and a computer program. Journal of Metamorphic Geology 6, 173–204.

Raase, P., Schenk, V., 1994. Petrology of granulite-facies metapelites of the Highland Complex, Sri Lanka: implication for the metamorphic zonation and the *P-T* path. Precambrian Research 66, 265–294.

Raith, M., Srikantappa, C., 1993. Arrested charnockite formation at Kottavattam, southern India. Journal of Metamorphic Geology 11, 815-832.

Rajesh, H.M., Santosh, M., 2012. Charnockites and *charnockites*. Geoscience Frontiers 3, 737–

744.

Rajesh, H.M., Santosh, M., Yoshikura, S., 2011. The Nagercoil charnockite: a magnesian, calcic to calc-alkalic granitoid dehydrated during a granulite-facies metamorphic event. Journal of Petrology 52, 375–400.

Rakotondrazafy, M.A.F., Nédélec, A., Giuliani, G., 2007. Incipient charnockitisation triggered by structurally-controlled CO_2 influx in central Madagascar and magnetic implications. Gondwana Research 11, 584–585.

Ramiengar, A.S., Ramakrishnan, M., Viswanatha, M.N., 1978. Charnockite-gneiss-complex relationships in southern Karnataka. Journal of the Geological Society of India, 19:411-419.

Ray, S., 1972. Charnockite of Kabbal, Mysore - a brief study. Quarterly Journal of the Indian Society of Geology, Mining and Metallurgy, 44, 163-166.

Roedder, E., 1984. Fluid inclusions. Review in Mineralogy, Mineralogical Society of America 12, 644pp.

Safonov, O.G., Kovaleva, E.I., Kosova, S.A., Rajesh, H.M., Belyanin, G.A., Golunova, M.A., van Reenen, D.D., 2012. Experimental and petrological constraints on local-scale interaction of biotite-amphibole gneiss with H_2O-CO_2-(K,Na)Cl fluids at middle-crustal conditions: Example from the Limpopo Complex, South Africa. Geoscience Frontiers 3, 829–841.

Sajeev, K., Osanai, Y., 2004a. Ultrahigh-temperature metamorphism (1150^{o}C, 12 kbar) and multistage evolution of Mg-, Al-rich granulites from the Central Highland Complex Sri Lanka. Journal of Petrology 45, 1821–1844.

Sajeev, K., Osanai, Y., 2004b. Osumilite and spinel + quartz from Sri Lanka: Implications for UHT conditions and retrograde *P-T* path. Journal of Mineralogical and Petrological Sciences 99, 320–327.

Sajeev, K., Osanai, Y., Connolly, J.A.D., Suzuki, S., Ishioka, J., Kagami, H., Rino, S., 2007. Extreme crustal metamorphism during a Neoproterozoic event in Sri Lanka: a study of dry mafic granulites. Journal of Geology 115, 563–582.

Santosh, M., 1986. Nature and evolution of metamorphic fluids in the Precambrian khondalites of Kerala, South India. Precambrian Research 33, 283-302.

Santosh, M., Omori, S., 2008. CO_2 flushing: A plate tectonic perspective. Gondwana Research 13, 86-102.

Santosh, M., Harris, N.B.W., Jackson, D.H., Mattey, D.P., 1990. Dehydration and incipient charnockite formation: a phase equilibria and fluid inclusion study from South India. Journal of Geology 98, 915–926.

Santosh, M., Jackson, D.H., Harris, N.B.W., Mattey, D.P., 1991. Carbonic fluid inclusions in South Indian granulites: evidence for entrapment during charnockite formation. Contributions to Mineralogy and Petrology 108, 318–330.

Santosh, M., Kagami, H., Yoshida, M., Nanda-Kumar, V., 1992. Pan-African charnockite formation in East Gondwana: geochronologic (Sm-Nd and Rb-Sr) and petrogenetic constraints. Bulletin of the Indian Geologists' Association, 25, 1-10.

Santosh, M., Jackson, D.H., Harris, N.B.W., 1993. The significance of channel and fluid-inclusion CO_2 in cordierite: Evidence from carbon isotopes. Journal of Petrology 34, 233-258.

Santosh, M., Wada, H., Satish-Kumar, M., Binu-Lal, S.S., 2003. Carbon isotope "stratigraphy" in a single graphite crystal: implications for crystal growth mechanism of fluid deposited graphite. American Mineralogist 88, 1689–1696.

Santosh, M., Morimoto, T., Tsutsumi, Y., 2006a. Geochronology of the khondalite belt of Trivandrum Block, southern India: electron probe ages and implications for Gondwana

tectonics. Gondwana Research 9, 261-278.

Santosh, M., Collins, A.S., Tamashiro, I., Koshimoto, S., Tsutsumi, Y., Yokoyama, K., 2006b. The timing of ultrahigh-temperature metamorphism in Southern India: U–Th–Pb electron microprobe ages from zircon and monazite in sapphirine-bearing granulites. Gondwana Research 10, 128-155.

Santosh, M., Maruyama, S., Sato, K., 2009. Anatomy of a Cambrian suture in Gondwana: Pacific-type orogeny in southern India? Gondwana Research 16, 321-341.

Santosh, M., Xiao, W.J., Tsunogae, T., Chetty, T.R.K., Yellappa, T., 2012. The Neoproterozoic subduction complex in southern India: SIMS zircon U–Pb ages and implications for Gondwana assembly. Precambrian Research 192–195, 190–208.

Santosh, M., Tsunogae, T., Malaviarachchi, S.P.K., Zhang, Z., Ding, H., Tang, L., Dharmapriya, P.L., 2014. Neoproterozoic crustal evolution in Sri Lanka: Insights from petrologic, geochemical and zircon U–Pb and Lu–Hf isotopic data and implications for Gondwana assembly. Precambrian Research 255, 1-29.

Santosh, M., Yang, Q.Y., Shaji, E., Tsunogae, T., Ram Mohan, M., Satyanarayanan, M., 2015. An exotic Mesoarchean microcontinent: The Coorg Block, southern India. Gondwana Research 27, 165-195.

Schenk, V., Raase, P., Schumacher, R., 1991. Metamorphic zonation and *P–T* history of the Highland Complex in Sri Lanka. Geological Survey Department, Sri Lanka, Professional Paper, 5, 150–163.

Schumacher, R., Faulhaber, S. 1994. Summary and discussion of *P-T* estimates from garnet-pyroxene-plagioclase-quartz bearing granulite facies rocks from Sri Lanka. Precambrian Research 66, 295–308.

Sibson, R.H., 1983. Continental fault structure and the shallow earthquake source. Journal of the

Geological Society 140, 741-767.

Spear, F.S., 1993. Metamorphic Phase Equilibria and Pressure-Temperature-Time Paths. Mineralogical Society of America, pp. 13-24.

Srikantappa, C., Raith, M., Spiering, B., 1985. Progressive charnockitization of a leptynite-khondalite suite in southern Kerala, India: evidence for formation of charnockite through a decreasing fluid pressure? Journal of Geological Society of India 26, 62–83.

Stähle, H., Raith, M., Hoernes, S., Delfs, A., 1987. Element mobility during incipient granulite formation at Kabbuldurga, southern India. Journal of Petrology 28, 803-834.

Tadokoro, H., Tsunogae, T., Santosh, M., 2008. Metamorphic *P-T* path of the eastern Trivandrum Granulite Block, southern India: implications for regional correlation of lower crustal fragments. Journal of Mineralogical and Petrological Science 103, 279-284.

Touret, J.L.R., 2001. Fluids in metamorphic rocks. Lithos 55, 1-26.

Touret, J.L.R., Huizenga, J.M., 2011. Fluids in granulites. Geological Society of America Memoirs 207, 25-37.

Touret, J.L.R., Huizenga, J.M., 2012. Fluid-assisted granulite metamorphism: A continental journey. Gondwana Research 21, 224–235.

Tsunogae, T., Santosh, M., 2003. A new incipient charnockite locality from Nanguneri, Trivandrum Granulite Block, Southern India. Annual report of the Institute of Geoscience, the University of Tsukuba 29, 37-41.

Tsunogae, T., Santosh, M., 2011. Fluids in high- to ultrahigh-temperature metamorphism along collisional sutures: Record from fluid inclusions. Journal of Asian Earth Sciences 42, 330–340.

Tsunogae, T., van Reenen, D.D., 2007. Carbonic fluid inclusions in sapphirine + quartz bearing garnet granulite from the Limpopo Belt, southern Africa. Journal of Mineralogical and

Petrological Sciences 102, 57-60.

Tsunogae, T., van Reenen, D.D., 2014. High- to ultrahigh-temperature metasomatism related to brine infiltration in the Neoarchean Limpopo Complex: Petrology and phase equilibrium modeling. Precambrian Research 253, 157-170.

Tsunogae, T., Osanai, Y., Owada, M., Toyoshima, T., Hokada, T., Crowe, W.A., 2003a. High fluorine pargasites in ultrahigh temperature granulites from Tonagh Island in the Archean Napier Complex, East Antarctica. Lithos 70, 21-38.

Tsunogae, T., Santosh, M., Osanai, Y., Owada, M., Toyoshima, T., Hokada, T., Crowe, W.A., 2003b. Fluid inclusions in an osumilite-bearing granulite from Bunt Island in the Archean Napier Complex, East Antarctica: implications for a decompressional *P-T* path? Polar Geoscience 16, 61-75.

Tsunogae, T., Santosh, M., Dubessy, J., 2008a. Fluid characteristics of high- to ultrahigh-temperature metamorphism in southern India: A quantitative Raman spectroscopic study. Precambrian Research 162, 198-211.

Tsunogae, T., Santosh, M., Dubessy, J., Osanai, Y., Owada, M., Hokada, T., Toyoshima, T., 2008b. Carbonic fluids in ultrahigh-temperature metamorphism: evidence from Raman spectroscopic study of fluid inclusions in granulites from the Napier Complex, East Antarctica. Geol Soc London, Special Publication 308, 317-332.

Tsunogae, T., Endo, T., Santosh, M., Rakotonandrasana, N.O.T., Shaji, E., Rambeloson R.A., 2013. Phase equilibrium modeling of Pan-African incipient charnockite from southern Madagascar. Geophysical Research Abstracts 15, EGU2013-14087.

Tsunogae, T., Yang, Q.Y., Santosh, M., 2015. Early Neoproterozoic arc magmatism in the Lützow-Holm Complex, East Antarctica: Petrology, geochemistry, zircon U-Pb geochronology and Lu-Hf isotopes and tectonic implications. Precambrian Research 266,

467-489.

Tucker, R.D., Kusky, T.M., Buchwaldt, R., Handke, M.J., 2007. Neoproterozoic nappes and superposed folding of the Itremo Group, west-central Madagascar. Gondwana Research 12, 356–379.

Tucker, R.D, Roig, J.Y., Macey, P.H., Delor, C., Amelin, Y., Armstrong, R.A., Rabarimanana, M.H., Ralison, A.V., 2011. A new geological framework for south-central Madagascar, and its relevance to the "out-of-Africa" hypothesis. Precambrian Research 185, 109–130.

Van den Kerkhof, A.M., Hein, U.F., 2001. Fluid inclusion petrography. Lithos 55, 27-47.

van Reenen, D.D., Roering, C., Smit, C.A., Van Schalkwyk, J.F., Barton, J.M., Jr., 1988. Evolution of the northern high-grade margin of the Kaapvaal Craton, South Africa. Journal of Geology 90, 549-560.

Voll, G., Kleinschrodt, R., 1991. Sri Lanka: Structural, magmatic and metamorphic development of a Gondwana fragment. Geological Survey Department, Sri Lanka, Professional Paper, 5, 22-52.

Watson, E.B., Brenan, J.M., 1987. Fluids in lithosphere, 1. Experimentally determined wetting characteristics of CO_2-H_2O fluids and their implications for fluid transport, host-rock physical properties and fluid inclusion formation. Earth and Planetary Science Letters, 85, 594–615.

Weerakoon, M.W.K., Miyazaki, T., Shuto, K., Kagamil, H., 2001. Rb-Sr and Sm-Nd geochronology of the Eppawala metamorphic rocks and carbonatite, Wanni Complex, Sri Lanka. Gondwana Research 4, 409–420.

White, R.W., Powell, R., Holland, T.J.B., Worley, B.A., 2000. The effect of TiO_2 and Fe_2O_3 on metapelitic assemblages at greenschist and amphibolite facies conditions: mineral equilibria calculations in the system K_2O–FeO–MgO–Al_2O_3–SiO_2–H_2O–TiO_2–Fe_2O_3. Journal of

Metamorphic Geology 18, 497–511.

White, R.W., Powell, R., Clarke, G.L., 2002. The interpretation of reaction textures in Fe-rich metapelitic granulites of the Musgrave Block, central Australia: constraints from mineral equilibria calculations in the system K_2O-FeO-MgO-Al_2O_3- SiO_2-H_2O-TiO_2-Fe_2O_3. Journal of Metamorphic Geology 20, 41-55.

White, R. W., Powell, R., Phillips, G. N., 2003. A mineral equilibria study of the hydrothermal alteration in mafic greenschist facies rocks at Kalgoorlie, Western Australia. Journal of Metamorphic Geology 21, 455–468.

White, R.W., Powell, R., Holland, T.J.B., 2007. Progress relating to calculation of partial melting equilibria for metapelites. Journal of Metamorphic Geology 25, 511–527.

Willbold, M., Hegner, E., Kleinschrodt, R., Stosch, H.-G., Kehelpannala, K.V.W., Dulski, P., 2004. Geochemical evidence for a Neoproterozoic magmatic continental margin in Sri Lanka-relevance for the Rodinia-Gondwana supercontinental cycle. Precambrian Research 130, 185–198.

Windley, B.F., Razafiniparany, A., Razakamanana, T., Ackermand, D., 1994. Tectonic framework of the Precambrian of Madagascar and its Gondwana connections: a review and reappraisal. International Journal of Earth Sciences 83, 642-659.

Yang, Q.Y., Santosh, M., Tsunogae, T., 2014. First report of Paleoproterozoic incipient charnockite from the North China Craton: implications for ultrahigh-temperature metasomatism. Precambrian Research 243, 168-180.

Yoshida, M., Santosh, M., 1994. A tectonic perspective of incipient charnockites in East Gondwana. Precambrian Research 66, 379-392.

Yoshida, M., Santosh, M., Shirahata, H., 1991. Geochemistry of Gneiss-Granulite transformation in the “incipient charnockite” zones of southern India. Mineralogy and

Petrology 45, 69–83.